DESIGN AND DEVELOPMENT OF NOVEL ALGORITHM FOR MAMMOGRAM CLASSIFICATION FOR BREAST CANCER DETECTION

A Thesis

Submitted in partial fulfilment of the requirements for the award of the degree of

DOCTOR OF PHILOSOPHY

in

COMPUTER SCIENCE AND ENGINEERING

By

Shivaji D. Pawar

41800386

Supervised By

Kamal Kr. Sharma
Professor, School of Electronics and Electrical Engineering, Lovely Professional University, Jalandhar (P.B.), India.

Co-Supervised By

Suhas G. Sapate
Professor, Department of Computer Science and Engineering, Annasaheb Dange College of Engineering and Technology, Ashta, Sangli (M.H.), India.

LOVELY PROFESSIONAL UNIVERSITY
PUNJAB
2021

Declaration

I hereby declare that the thesis entitled "DESIGN AND DEVELOPMENT OF NOVEL ALGORITHM FOR MAMMOGRAM CLASSIFICATION FOR BREAST CANCER DETECTION" submitted by me for the Degree of Doctor of Philosophy in Computer Science and Engineering is the result of my original and independent research work carried out under the guidance of Supervisors Dr. Kamal Kr. Sharma and Dr. Suhas G Sapate, and it has not been submitted to any university or institute for the award of any degree or diploma.

Place: Phagwara
Date: 21/2/2022

Signature
Shivaji D. Pawar
Registration No.41800386

Certificate

This is to certify that the thesis entitled "DESIGN AND DEVELOPMENT OF NOVEL ALGORITHM FOR MAMMOGRAM CLASSIFICATION FOR BREAST CANCER DETECTION" submitted by Shivaji D. Pawar for the award of the degree of the Doctor of Philosophy in Computer Science and Engineering, Lovely Professional University Punjab, India is entirely based on the work carried out by him under our supervision and guidance, The work recorded, embodies the original work of the candidate and has not been submitted for the award of any degree, or diploma of any university and institute, according to the best of our knowledge.

Signature of Guide with Date & UID
Dr. Kamal Kr. Sharma

Signature of Co-Guide
Dr. Suhas G. Sapate

Place: Phagwara
Date:

DESIGN AND DEVELOPMENT OF NOVEL ALGORITHM FOR MAMMOGRAM CLASSIFICATION FOR BREAST CANCER DETECTION

EXECUTIVE SUMMARY

According to the National Center for Health Statistics, in 2021, 18.96 million new cancer cases and nearly 6 million cancer deaths are forecasted to happen in the United States. Less advanced personalized approaches in breast cancer screening are the fundamental cause of delay in breast cancer diagnosis. Hence there is a social need to have an advanced personalized computer-aided tool for breast cancer detection and classification. Mammography (also called mastography) uses low-energy X-rays (usually around 30 kVp) to examine the human breast for diagnosis and screening. The goal of mammography is the early detection of breast cancer, typically through detection of characteristic masses or microcalcifications and mammographic breast density (MBD). Mammography images consist of 4 diagnosis views known as Left MLO, Right MLO, Left CC, and Right CC.

The term Mammographic breast density (MBD), which appears in white on the mammogram, acts as a fibro-glandular tissue in the breast and a biomarker for the detection of breast cancer. In a considerably dense breast, the sensitivity of mammography decreases by 48% in the dense breast compared to 98% in a fatty breast; hence every second or third cancer may miss a prediction that will cause life-threatening and increase the treatment cost. Therefore, MBD calculation from mammography is an important and complex task in breast cancer prevention and treatment. Currently, MBD assessment is done subjectively with the help of expert radiologists as per BIRADS guidelines. Still, most recent studies show that MBD assessment has limitations regarding interobserver variability between the radiologist's assessments.

This proposed research work addresses the automated classification of Mammographic breast density, which can be further used for breast cancer detection. Mammographic breast density itself is an independent risk factor for breast cancer. However, the degree to which it is an independent risk factor is

debated among experts and is highly controversial. Breast density as a risk factor seems intuitive because density refers to the amount of epithelial and stromal elements of the breast. Breast cancers most commonly arise in epithelial cells. A more significant amount of epithelial tissue in the breast indicates a greater chance of cancer in one of the epithelial cells. Some researchers propose that breast density may increase the risk for breast cancer by up to six times, and breast density is often reported to cause a fourfold increase in the risk for breast cancer in women with dense breasts. In a meta-analysis of studies that evaluated breast density as an independent risk factor for breast cancer, the relative risk associated with dense breasts was 2.92 for 50%–74% dense and 4.64 for 75% or denser breasts. An increasing linear trend in the relative risk for breast cancer concerning increased tissue density has been noted when density is measured quantitatively.

Women with dense breast tissue have a higher risk of breast cancer than women with less dense breast tissue. Dense breast tissue also makes it harder for radiologists to see cancer. On mammograms, dense breast tissue looks white. Breast masses or tumors also look white so that the dense tissue can hide tumors. Hence it is essential to classify mammographic breast density to avoid the risk of masking breast cancer. Mammographic breast density is rapidly becoming a hot topic in both the medical and scientific literature. Having dense breast tissue increases one’s chances of developing breast cancer and makes cancers that do develop more challenging to detect. Mammographic breast density is one of the most vital independent risk factors for subsequent breast cancer, stronger than even age or family history. Hence it acts as one of the hot topics in the field of medical research. Breast cancer detection and prevention is a significant field of research. We focus on automated mammographic breast density classification for a standardized, reproducible way to measure and report breast density.

Many commercial applications are available for MBD classification but do not consist of accuracy and consistency, hence lack of flexibility and robustness. Therefore there is still an unmet social and clinical need to have precise and accurate breast density assessment. Thus, our fundamental objective behind this research topic is to "***Design and Development of Novel Algorithm for Mammogram Classification for Breast Cancer Detection.***" Basic problem

definition has the following **specific objectives**, which are the direction of our proposed research work.

1. Analysis of Existing Algorithms for Mammogram Density Measurement
2. Study and analysis on different pre-processing and classification algorithms.
3. To propose a novel algorithm for mammogram classification.
4. Comparison of the proposed method with other existing techniques.

The proposed research will be a one-step-ahead towards the classification of breast density. It will be helpful for the radiologists as the second opinion and women to know about their mammographic breast density and associated risk factors. The proposed work utilizes one publicly available dataset from Digital Database for Scanning of Mammography (DDSM), consisting of 2620 cases of different categories classified as normal, benign, and malignant cases with verified pathology information. This database consists of each patient case with MLO, LMO, Left CC, and Right CC. The proposed algorithm uses 1338 MLO and 1337 LMO views from normal, benign, and malignant cases. The team of three expert radiologists manually draws the boundaries of the pectoral muscle of each MLO and LMO view individually to develop good quality ground truth of the pectoral muscle. These manual contours are further used as ground truth for the proposed study. The proposed multi-channel architecture uses pre-processed and pectoral muscle segmented 200 MLO, 200 LMO, 200 R_CC, and 200 L_CC views from normal, benign, and malignant cases. Total 800 mammograms are used in the proposed study and divided into four BIRADS density classes.

The proposed methodology is implemented into two steps 1. **Pre-processing and segmentation of digital mammograms**, and 2. **A novel algorithm for MBD classification.**

In the first step, the primary focus is on pre-processing and segmentation of digital mammograms as breast density is estimated based on the opacity of fibro-glandular tissue displayed on digital mammograms involving the whole area of the breast. The ambiguity of pectoral muscle and fibro-glandular tissue is comparable; hence, the slight appearance of the pectoral muscle in the breast region can hamper the precision of breast density classification. Successful elimination of pectoral muscle is stimulating due to changes in shape, size, and

texture of pectoral muscle in every MLO and LMO view of the mammogram. In this step, the depth-first search (DFS) algorithm with and without heuristic approach is proposed to eliminate artifacts, noise, and pectoral muscle from digital mammograms.

Highlights of the proposed DFS algorithm are as follows 1. The heuristic approach of depth first-search algorithm (DFS) for removing the pectoral muscle. 2. A novel seed selection mechanism. 3. A numerical comparison of automatic versus manual segmentation was conducted on each BIRADS density class. 4. Results are validated subjectively by expert Radiologists and objectively by Jaccard Index and Dice similarity coefficient.

The proposed pre-processing algorithm performs contrast enhancement with AGCWD (Adaptive Gamma Correction with Weighting Distribution). The fundamental merit of this method is it removes noise from the background, enhancing the visibility at the breast border, which further helps to get a delicate breast border. After breast border detection, a novel initial seed selection mechanism is proposed, and then Otsu thresholding and Depth-first search algorithm are used to identify pectoral muscle as a strong, connected component. The straight-line approximation is used to remove the pectoral muscle from the breast. This technique works well on all the images. Still, in some cases, when the selected initial seed point is a part of the breast area instead of the pectoral muscle, then the proposed algorithm will remove a significant portion of the breast area, which causes over-segmentation and reduces segmentation accuracy. To avoid this, the proposed algorithm performs additional statistical measures to overcome the problem of over-segmentation known as the Heuristic approach. This approach is used to evaluate the circumstances of individual issues to obtain the desired solution. This approach is designed on experiments in intuition. Hence, the ratio of the threshold of breast area after pectoral muscle removal and before pectoral muscle removal is calculated in successful cases and in over-segmentation images. In unsuccessful cases, it is observed as less than 0.4. If this ratio is less than 0.4, it is observed that the maximum breast area is removed, which is the primary cause of over-segmentation. In such cases, the heuristic approaches recursively modify the initial seed towards the left side of the input image until successfully removing the pectoral muscle. Therefore, this

heuristics approach provides the correct segmentation result for failed cases (over-segmentation) of DFS.

In the second step, pre-processed 800 images are further given to the novel multi-channel architecture. This research work proposes a Multi-channel Dense-Net architecture for MBD classification. The proposed architecture consists of a four-channel Dense-Net transfer learning architecture to extract significant features from a single patient's two MLO and two CC views with stochastic gradient descent (SGD) algorithms using batch sizes 4 and 30. The entire model is trained with stochastic gradient descent (SGD) algorithms using batch sizes 4 and 30 epoch on the 800 images. The initial learning rate for this model is 0.1 (default value), further divided by ten at 50% and 75% of the total training epochs. The categorical cross-entropy acts as a loss function in this model, quantifying the difference between four probability distributions. This loss function works well with the SoftMax activation function in multi-class classification.

Time complexity in the proposed algorithm is O (V) +O (E) = O (V+E), where V is vertex and E is the edge. In the proposed algorithm, it takes ***16 milliseconds*** to execute one input image. The space complexity of the proposed algorithm is O (V) which is practically very small. Finally, the DFS algorithm with and without heuristic approach segments pectoral muscle from 2675 digital mammograms. The DFS algorithm without the heuristic approach yielded a segmentation accuracy of 82.32%. A dynamic seed selection mechanism due to the heuristic approach of DFS enhances the overall segmentation accuracy up to 86.16% on all BIRADS density classes. The proposed algorithm works well on a wide range of mammograms with varying textures, sizes, and shapes. Discussion of the failure cases, which are infrequent, are provided, and the work to address failure cases is in progress. The proposed algorithm can be used in the pre-processing breast cancer detection unit and MBD classification systems used during clinical practice.

Evaluation of the classification performance of the proposed model is done in terms of precision, recall, F1-score, and classification accuracy. After training the model on the entire dataset, the proposed model performance is validated by spitting the image dataset in a ratio of 80 % as training and 20% testing. During the testing phase, the proposed model performed significantly well on all the

BIRADS density classes and recorded the best classification accuracy, 90.00%, with a validation loss of 0.3814. The number of accurate positive samples for all four BIRADS density classes are 92%, 75.5%, 92.2%, and 94.7% of their respective totals, with an overall AUC of 0.9625. Also, there is no confusion between classes A and C, B and C, and C and D. The proposed algorithm results are consistent with the results evaluated by the radiologists, which is a positive sign that indicates deep learning models are helpful for the classification of MBD. The final experimental results show that the proposed multi-channel model has achieved good performance with an accuracy of 96.67% during training and 90.06% during testing and an average AUC of 0.9625. Obtained results are also validated qualitatively with the help of a radiologist expert in the field of MBD. Proposed architecture achieved state-of-art results with a fewer number of images and with less computation power.

Due to the simplicity and encouraging results of the Depth-first search algorithm, this algorithm can improve some failed cases in under-segmentation and no segmentation categories. Future work is underway to modify the proposed algorithm to address the above issues. It can be tested on different public and clinically proven datasets to address the proposed algorithm's generalization. And in the case of multi-channel dense-net architecture has improved the classification performance of BIRADS density classes and more research is underway to increase robustness of the proposed model.

However, there are still some issues that are needed to be addressed. Firstly, this study uses a smaller amount of image data, and no image enhancement strategies are used to expand the dataset. Hence, model performance, especially stability during validation, is affected due to a small number of image data. And model found it a little confusing to classify classes A and B. Therefore, in future work, data enhancement techniques will improve the model's performance. Secondly, the proposed work address only one type of dataset; hence this approach does not address the robustness of the model. Future work will address the robustness of the model by training the model with different vendor-specific image datasets so that it can act as an automated MBD classification technique in clinical application for MBD classification for Breast cancer detection.

In this proposed research work, a novel approach of multi-channel architecture

with Dense-Net 121 and Depth-first search algorithm are proposed for the objective assessment of MBD classification.

The proposed algorithm works well on a wide range of mammograms with varying textures, sizes, and shapes. Analysis of the results suggests that the proposed model successfully distinguishes between all the BIRADS density classes but is predominantly found superior in the two most distinctive and challenging BIRADS categories: "Scattered density" and "Heterogeneously dense. Classification accuracy of the proposed model is recorded at 96.67% during training and 90.06% during testing, with an average AUC of 0.9625. The proposed work address only one type of dataset; hence this approach does not address the robustness of the model. Future work will addresses the robustness of the model by training the model with different vendor-specific image datasets. Finally, with certain modifications, the proposed architecture is suitable to use in clinical workflow in breast cancer screening for breast cancer detection and MBD classification to avoid false recalls.

ACKNOWLEDGEMENTS

First and foremost, praises and thanks to the God, the Almighty, for his showers of blessings throughout my research work to complete the research successfully. I would like to express my deep and sincere gratitude to my research supervisors ***Dr. Kamal kr. Sharma, Department of Electronics Engineering, Lovely Professional University, Punjab*** and ***Dr. Suhas G. Sapate, Department of Computer Engineering, Annasaheb Dange college of Engineering and Technology, Ashta, Sangli*** for their invaluable advice, continuous support, and patience during my Ph.D. research work. Their immense knowledge and great experience have encouraged me in my academic research.

I want to thank all the staff members of the ***Research and Development Department*** of the ***Lovely Professional University***. It was a great privilege and honor to work and study under their guidance. Their kind help and support have made my research journey in L.P.U. an excellent time to cherish. I would also like to thank ***Dr. Geetanjali Yadav***, ***Dr. Yogesh Yadav, and Dr. Atul Sawant,*** a team of expert radiologists from ***Life Care hospital Abu Dhabi, U.A.E***., for their incredible support in performing the medical imaging evaluation during this research work. I also like to thank the ***Head of the department and staff- members*** of the ***Computer science and engineering department*** for their extended support during this research journey. I am so grateful to Library ***and administrative staff*** of ***Lovely Professional University*** for providing on time and excellent library's services.

I am extremely grateful to my parents, in-laws and brothers for their love, prayers, caring and sacrifices for educating and preparing me for my future. I am very much thankful to my wife, ***Mrs. Varsha Pawar*** and my son ***Paras Pawar*** for their love, understanding, prayers and continuing support to complete this research work. Without their tremendous understanding and encouragement in the past few years, it would be impossible to complete my research work.

My Special thanks goes to my friend ***Mr Rocky Jagtyani*** for the extended support given in my research journey and towards its completion successfully.

Mr. Shivaji D. Pawar

Research Scholar

TABLE OF CONTENTS

LIST OF FIGURES

LIST OF TABLES

LIST OF ABBREVIATIONS

MRI	Magnetic resonance imaging
PET/CT	Positron Emission Tomography - Computed Tomography
DBT	Digital breast tomosynthesis
FFDM	Full Field Digital Mammography
MLO	Medio lateral oblique
LMO	Latero medial oblique
CC	Carnio caudal
MBD	Mammographic Breast density
VBD	Volumetric Breast density
BIRADS	Breast Imaging Reporting and Data systems
ACR	American College of Radiology
CNN	Convolutional Neural network
AI	Artificial intelligence
ML	Machine Learning
DL	Deep learning
DFS	Depth-first search
AUC	Area under curve
CAD	Computer Aided detection
ABDM	Automated Breast Density Measurement
FDA	Food and Drug Administration
ReLU	Rectified Linear unit
Tanh	hyperbolic tangent function,
J	Jaccard indices
CM	Completeness
ROI	Region of Interest
PTG	Probable Texture Gradient
ELU	Exponential Linear Unit
DSC	Dice similarity coefficient
IOU	Intersection over union
GAN	Generative Adversarial Networks

LSD	Local standard deviation
K	linear weighted Cohen’s kappa coefficient
USA	United states of America
WT	Wavelet transform
AHE	Adaptive histogram equalization
ACE	Adaptive contrast enhancement
AGCWD	Adaptive Gamma Correction with Weighting Distribution
AGC	Adaptive gamma correction
SCC	Strongly connected component
LIFO	Last In First Out
Dense-Net	Dense convolutional network
HE	Histogram equalization
USM	Unsharp masking method
CLAHE	Contrast Limited Adaptive Histogram Equalization
SGD	Stochastic gradient descent
ACC	Classification Accuracy
P	Precision
R	Recall
TP	True Positive
FP	False Positive
ROC	Receiver operating characteristic

CHAPTER-1

INTRODUCTION

1.1 Overview

This research work addresses the global revelatory health challenge of breast cancer. It reveals the most important factor towards the frequent malignancy in the ladies population, and it is the second largest element of cancer mortality in women after lung cancer. According to the National Center for Health Statistics, in 2021, 18.96 million new cancer cases and nearly 6 million cancer deaths are forecasted to happen in the United States [1]. Less advanced personalized approaches in breast cancer screening are the fundamental cause of delay in breast cancer diagnosis. Hence there is a social need to have an advanced personalized diagnosis tool for breast cancer detection and classification [2]. The proposed research work address the automated classification of Mammographic breast density which can be used for breast cancer detection.

1.2 Breast Cancer

The formation of Breast cancer occurs in the adult female breast, which is the composition of a billion of healthy microscopic cells. Breast tissue is fundamentally classified into fibro glandular tissues, fatty tissues and pectoral muscle. Figure- 1.1 depicts the anatomy of the breast. Healthy cells continuously divide, multiply, grow, die, and new cells replace the healthy cell in an orderly manner. The genes regulate the entire cellular phenomenon. Sometimes these cells start behaving abnormally when the change in a gene called mutation takes place [3].

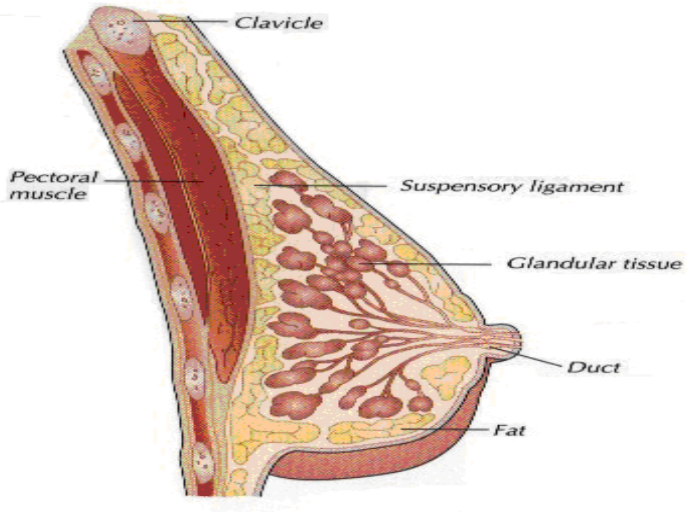

Figure -1.1. Breast anatomy

Progressive abnormal growth of cells form a tumor and it is the primary cause of breast cancer. Because of mutations, cells start dividing and multiplying in an uncontrolled and rapid manner. In the early stage, the tumor is microscopic, can't be felt, and has no symptoms [4].

1.3 Symptoms of Breast Cancer

Different patients have diverse indications of breast cancer, and few do not consist of any signs. Some of the warning symptoms are taken from [5] and listed below:

1. The recent development of thick breast tissue or lump that is different than other tissues

2. Sudden change in size, shape, and texture of the breast.

3. Swelling or Thickening of some part of the breast.

4. Nipple release, including blood in discharge.

5. Stretching of the nipple or pain in the nipple area.

1.4 Breast Cancer Imaging Modalities

In medical research, imaging modalities provides different unique tools for the detection and prevention of breast cancer. These imaging modalities are Digital mammography, Magnetic Resonance Imaging (MRI), Positron emission tomography (PET), Breast Ultrasound, and Digital breast tomosynthesis (DBT) are valuable for computer-aided detection tools of breast cancer. In addition, radiologists use the output images of these devices to diagnose breast cancer. Comparison of different breast

cancer imaging modularity are provided with Table-1.1

Table-1.1 Comparison of different breast cancer imaging modularity.

Type	Technology	Advantages	Disadvantages
Ultrasound	This technology uses a high frequency of sound waves to produce an image of organs and structures within the body	Low resolution Suitable dense breast Low sensitivity Quick and painless Low specificity, widely available	Low resolution, high operator dependency lower specificity and sensitivity.
MRI	MRI uses magnetic fields and radio waves to create detailed images of organs and tissues in the body	High sensitivity, Image in any angle, Painless	Long scan time Expensive, not easily available
Microwave Imaging	This technology uses a microwave	Non-invasive, comfortable and inexpensive	Not available in clinic or hospital
Digital mammography	This imaging uses a low-dose (ionizing radiation) X-ray system to discover inside the breast	Inexpensive, old standard and suitable for regular checkup	False negative rate is high and not convenient

Out of all, digital mammography is one of the cost-effective and commonly used imaging modality for screening breast cancer [6].

1.5 Digital Mammography

In 1950, Robert Egan manifested mammography by fusion technique of low kVp with high mA and single emulsion films for screening. After nine years, he was published his mammography method results and became the first physician to detect breast cancer

by using mammography [7]. After this success story of Robert Egan, mammography is the widely used screening technology for breast cancer. Until 2000, mammography uses screen-film cassettes. Screen-film mammography consists of certain demerits such as low spatial resolution and significantly higher cost; hence, in 2000, mammography transitioned from screen-film to digital detectors. This transition was known as Full Field Digital Mammography (FFDM) or Digital mammography, and by 2010 till date, it is the utmost popular screening tool for breast cancer [8]. Figure-1.2 depicts the breast imaging unit along with sample of digital and Film mammograms.

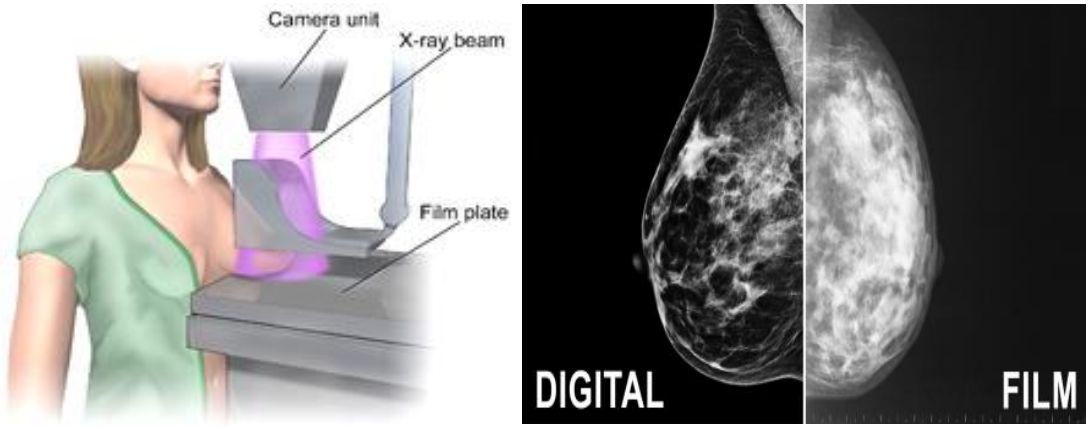

(a) (b)

Figure -1.2. (a) Breast imaging Unit and (b) View of Digital and Film Mammogram

Digital mammography uses computers and digital receptors in place of x-ray film, which enables electrical signals for reading and manipulation on the image, which is more clear and informative than film mammography. Digital mammography is also fast in diagnosis, inexpensive, acts as the gold standard for detecting masses, and is valuable for calculating mammographic breast density, which is strongly associated with the risk of breast cancer [9].

1.6 Diagnostic Views of Mammography

With the help of the mammographic unit, the different views of both left and right breast are captured. Radiologists observe two mammographic views side by side. This adjusts views of two breast of the same patient and this allows radiologists to identify any abnormal behavior in the breast [10]. Figure-1.3 depicts all the views of mammography. and a brief description of Diagnostic views of Mammography is

presented in Table-1.2.

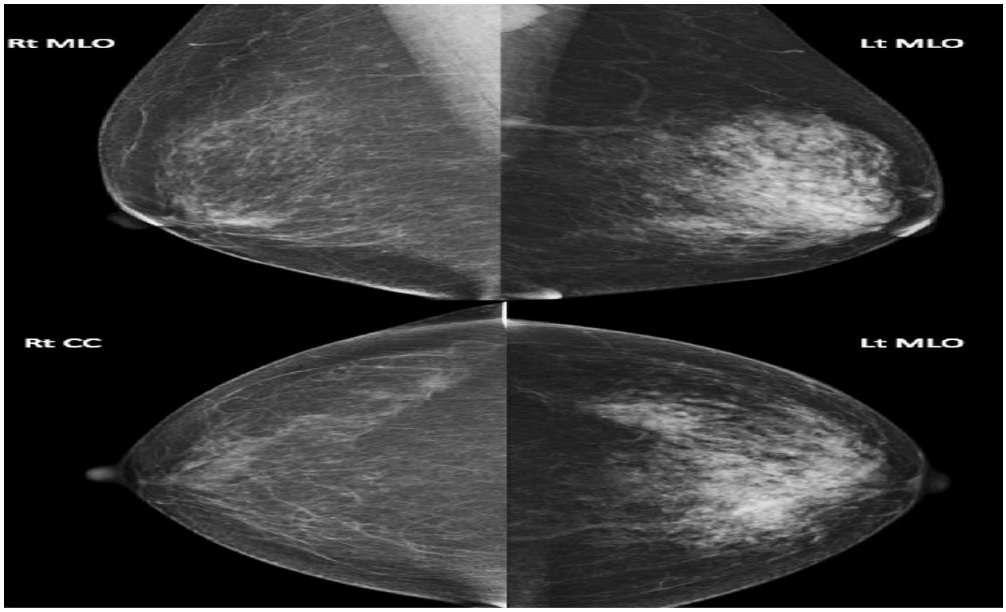

Figure-1.3. Diagnostic views of mammography

Table-1.2 Diagnostic Views of Mammography

Views of mammography	Description
Medio lateral oblique (MLO)	Taken from the mid chest to the lateral side with an angle of 45º. It is very common and clinically vital as more changes are occurring in upper quadrants during cancer growth.
Latero medial oblique (LMO)	Taken from the lateral part of the body to the mid of chest with angle of 45º. It gives best possible views including clear image of pectoral muscle and the nipple.
Carnio caudal (CC)	Taken vertically from the upper to the lower part of the breast profile including nipple.

Some of the actual merits, demerits and challenges of digital mammography used for breast cancer detection are as follows.

Merits:

1. It allows identifying small suspicious lesions showing abnormal growth.
2. It improves diagnostic accuracy
3. It offers no side effects and not harmful.

Demerits:

1. It consists of less spatial resolution and there is a requirement of ample storage space.
2. Not suitable for women aged lower than 40 years.
3. Cumulative X-ray exposures may seldom be the cause of cancers.
4. Not applicable to identify very complex lesions in women with dense breasts and women having surgical implants.
5. Poor dynamic range, low-contrast, and grainy image
6. Breast density alters sensitivity and specificity.
7. Age factor, rupture risk, and BRCA1/2 mutations.

1.7 Motivation

Mammographic breast density classification is a long-lasting research area due to more thought-provoking and challenging image preprocessing, segmentation, and classification tasks. The proposed research work is one step towards classifying Mammographic breast density towards breast cancer risk prediction. Following are the motivational points to carry out the proposed research work.

- The current method used for assessing MBD is radiologists' visual assessment, but such assessment is prone with high variability, affecting reliability and reproducibility.
- Another option for MBD is volumetric breast density (VBD) which provides a more accurate means for MBD assessment but moderate in detecting breast cancer risk.
- The current commercial instruments are performing better for MBD assessment but need specific improvements.
- The Convolutional Neural network (CNN) has gained tremendous significance for breast histopathological image density calculations in recent years. CNN has benefits over the handcrafted feature extraction method as CNN extracts feature automatically. Even though CNN has got less attention in medical imaging due to the lack of availability of public datasets.
- There is a social need to have more accurate, reproducible, and reliable personalized MBD screening tools for breast cancer risk-stratification (preventive

and predictive).

Thus, the strong motivation behind this research is to design and develop an automatic MBD assessment algorithm for breast cancer risk prediction.

1.8 Theory of Mammographic Breast Density

The term breast density or percentage mammographic breast density (MBD), which appears in white on the mammogram, acts as a fibro-glandular tissue in the breast and a biomarker for breast cancer [11]. Figure-1.4 depicts the concept of MBD.

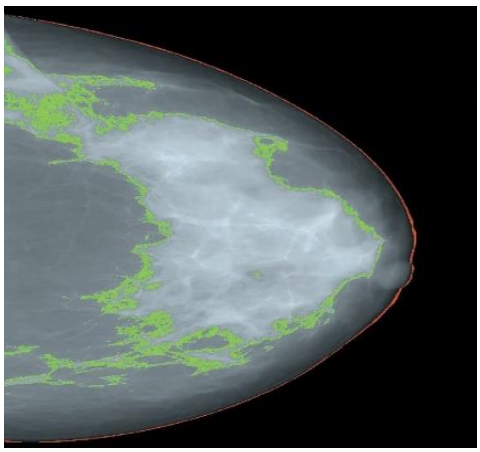

Figure- 1.4. The Concept of Mammographic Breast Density

Equation-1 and 2, mathematically defines the term of mammographic breast density

$$\text{Mammographic Breast density} = \frac{\text{Area } of\ fibro{-}gladular\ tissue}{Area\ of\ whole\ breast} * 100 \quad (1)$$

$$\text{Volumetric MBD} = \frac{\text{volume of fibograndular parenchyma}}{\text{Total breast volume.}} \quad (2)$$

Extended breast density is correlated with an increased risk of breast cancer and masking of breast lesions on mammograms, decreasing the uncertainty of early breast cancer detection and medication. In the United States, many states possess breast density advice legislation, which requires radiologists to notify women with dense breasts at mammography screening. During this investigation, the strength, as mentioned above, prompts them to undergo supplemental screening. The most usually employed breast density classification is a radiologist's visual interpretation based on

the four categories of breast imaging reporting and Data systems (BIRADS). Yet, there is a large inter-and intraradiologist variability proceeding biased density classification [12].

1.9 MBD Assessment Standard

Mammography depicts the fibro-glandular tissues that formulate breast density, grouped into four classes according to the BIRADS classification standard. The Breast Imaging Reporting and Data System (BIRADS) was originated in 1993 by the American College of Radiology (ACR) to standardize mammographic reporting to serve the following goals [13].

(i) To improve communication between radiologists.

(ii) To decrease uncertainty concerning mammographic findings.

(iii) To assist research and to expedite outcomes monitoring.

The American College of Radiology (ACR) Breast Imaging Reporting and Data System (BIRADS) classifies four important groups for classifying breast density as depicts in Figure 1.5.

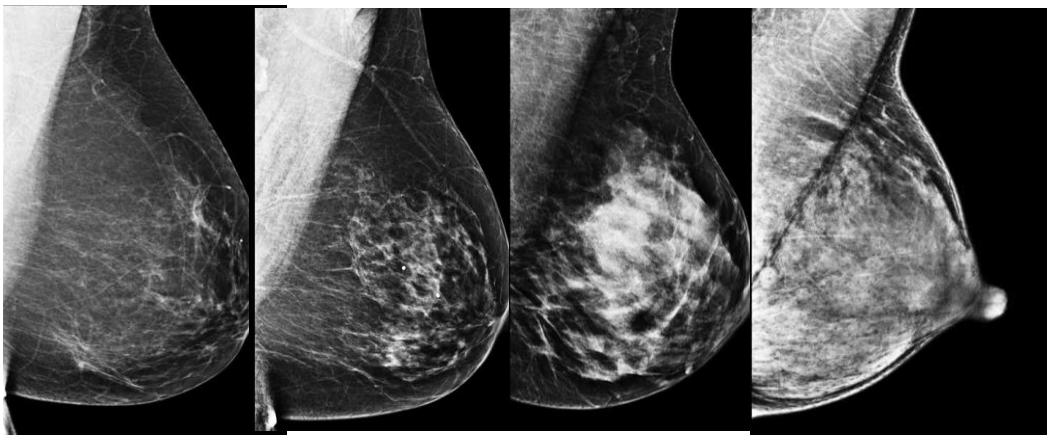

(a) BIRADS-A (b) BIRADS-B (c) BIRADS-C (d) BIRADS-D

Figure- 1.5. Edition-4 BIRADS density classes

For a radiologist, interpreting a benign mammogram is a difficult task as there exists an extended variation in the mammographic appearance of the breast. Inside the

mammogram, radiographically visible density includes ducts, lobular elements, and fibrous connective tissue. The fibrous connective tissue is of two types, interlobular or extra lobular tissue. These tissues are later seen as the prominent segment of gross density variation in mammograms [14].

1.10 Current Challenges in MBD Assessment

Even though MBD assessment is performed by BIRADS classification worldwide with expert radiologists, this subjective assessment consists of specific challenges which are listed in this section.

1.10.1 Sensitivity of Mammography

In a considerably dense breast, the sensitivity of mammography decreases by 48% in the dense breast compared to 98% in a fatty breast [15]; hence every second or third cancer may miss from a prediction which will cause life threat and will increase in the treatment cost. Therefore, MBD calculation from mammography is a complex task in breast cancer prevention and treatment. Figure-1.6 depicts the example of sensitivity of mammograms with the MBD.

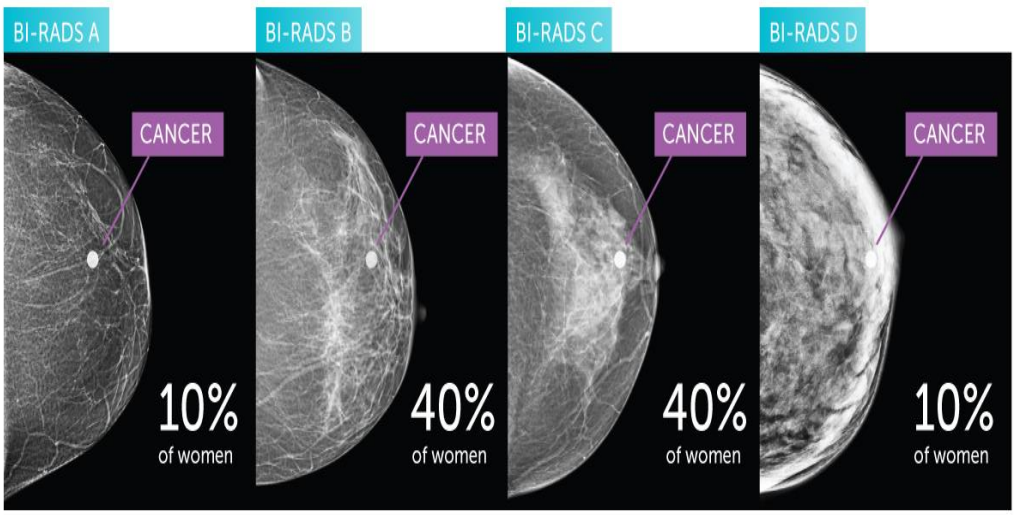

Figure- 1.6. The sensitivity of mammogram decreases as MBD increases

1.10.2 Interobserver Variability

Most of the recent studies shows that MBD assessment has other limitations regarding

interobserver variability between the radiologists. The research proposed by Ooms et al. [16] shows substantial agreements in different density classes of BIRADS. Furthermore, continuous development is needed to improve the standardization in mammographic interpretation.

1.10.3 Status of Commercial Tools Available in the Market

Currently, MBD assessment is done qualitatively by the radiologist as per the guideline of BIRADS. Commercial software is also available to measure volumetric breast density with support of mammography Known as Quanta (Hologic), Volpara (Volpara Health Technologies), Spectral Breast Density (Philips), and Insight Breast Density(Siemens Healthcare), etc. act as a merit investigation, but acceptance and approval from the international community has not been established [17].

Different commercial software is available in the market to access breast density. The most popular software used for the measurement of volumetric breast density is Volpara and Quanta. Table- 1.3 presents the technical details of different commercial software is available in the market and their methodological approach.

Table- 1.3. Commercial software is available in the market for MBD measurement

Product Name	**Name of Manufacturer**	**Methodologic Approach**	**Clinical Outputs**
Volpara Density	Volpara Health Technologies	Relative physics; is based on x-ray attenuation	Volumetric breast density expressed as Volpara Density grades.
Quantra	Hologic	Machine learning of pattern and texture analyses	Quantra density categories
Spectral Breast Density Measurement Application MicroDose	Philips Healthcare	Spectral breast density	Volumetric breast density expressed as MicroDose density scores

Insight Breast Density	Siemens Healthcare	Relative physics; is based on x-ray attenuation	Volumetric breast density expressed as density categories
PowerLook Density Assessment (formerly iReveal)	iCAD	Analyzes the structure, texture, and dispersion	Area breast density expressed as PowerLook Density Assessment density categories
DenSeeMammo	Statlife	Nearest-neighbour comparison with reference database	BIRADS 5th Edition categories

Even though there are many commercial approaches available, no application as per the literature survey is precise and accurate; hence, does not act as a supportive tool. Therefore, MBD is analyzed qualitatively by radiologists with guidelines of the BIRADS reporting system. Thus, a combined effort from the medical and researcher's community is required to design a predictive model to predict breast cancer signs early from breast density, saving many patients from the trauma of late diagnosis and course of treatments.

1.11 Outline of the Thesis

The proposed research work are combined in this dissertation such that the opening chapter highlights aspects concerning the intended field of study.

Chapter-2 entitled-"***systematic literature survey"*** discusses on diverse state-of-art techniques for classification of mammographic Breast density. This survey consists of contribution of various researchers towards the objective MBD assessment which also focus on history and background of intended area of research.

Chapter-3 entitled ***–"Problem formulation and research methodology,"*** covers the research gap identified and list out the objectives of the proposed research work. The methodology used to solve the problem is also described in detail to accomplish the desired goals.

Chapter-4 "***Preprocessing and segmentation of pectoral muscle"*** presents details about preprocessing of digital mammograms. This chapter provides a comprehensive analysis of a novel seed selection mechanism for the DFS algorithm. Further, it explains the novel heuristic approach of the DFS algorithm. This chapter also enlightens about the effect of the ablation study performed with and without a heuristic approach.

Chapter-5 "*Multichannel architecture for MBD classification"* explains the novel approach for MBD classification with Dense-Net architecture. This chapter further illustrates the evaluation of the proposed model with confusion matrix and AUC curve.
Chapter-6 ***"Results and discussion"*** presents the results of the proposed algorithm and comparison with existing state of art algorithms.

Chapter-7 "***Conclusion and future scope,"*** it summarizes the proposed research work with future scope.

CHAPTER 2

BACKGROUND AND LITERATURE SURVEY

2.1 Overview

The literature survey helps to decide the future path for research activity which is based on the existing knowledge domain. Hence, an extensive literature review is performed in the initial phase of the proposed research to understand the field subject in-depth. In this chapter, the comprehensive literature survey of proposed research work is classified into four subsections. The initial section of this chapter is dedicated to the background and historical literature review of the proposed research area. Then later sections illustrates the literature survey of preprocessing and removal of the pectoral muscle from digital mammograms, and finally, state-of-art deep and machine learning algorithms used for classification of mammographic breast density.

2.2 History and Background Intended Area of Research

Forecasting of Breast cancer is possible from mammographic breast density, and John Wolfe put forward this hypothesis in 1976. He further classified MBD into four distinct classes known as Wolfe classification (N_1, P_1, P_2, and D_y). In this classification, N_1 consists of the primary fatty breast, also called normal breast. P_1 categories consist of fatty patterns and linear densities (enlarged ducts) not occupying 25% of the breast. Further, the P2 class consists of linear densities from the enlarged ducts and occupies more than 25% breast area. They are predominant spread in the upper quadrant and scattered throughout the whole breast. Finally, the dense, radiopaque breast is called dysplasia (Dy). These density groups are classified into low risk (N1 and P1) and high-risk (P2 and Dy) [18]. Table-2.1 presents the summary of Wolfe's MBD classification.

Table- 2.1 Summary of Wolfe's MBD classification.

MBD Classes	Conditional Description	Risk categories
N_1	Primary fatty breast	Low-Risk
P_1	Linear densities from the enlarged ducts	Low-Risk
P_2	Predominant spread of density in the upper quadrant	High-Risk
D_y	Dense, radiopaque breast	High-Risk

Boyd et al. [19] proposed another alternative method for quantitative assessment of MBD in 1980. In this method, classification of MBD is done into six classes of unequal intervals. These six groupings are as follows. (i) A: 0% (ii) B: >0-10% (iii) C: >10-25% (IV) D: >25-50% (v) E: >50-75% and F: >75%. In 1980 professor Wolfe and martin Yaffe also developed Cumulus, a semiautomatic software-based density measurement tool on the 2D surface area, but results are qualitative and subjective. Table- 2.2 presents Boyd's classes of MBD.

Table- 2.2 Boyd's MBD classification guidelines

MBD Classes	Conditional Description
A	MBD= 0 %
B	MBD > 0-10 %
C	MBD > 10-25 %
D	MBD > 25-50 %
E	MBD > 50-75 %
F	MBD >75 %

Tabor et al. [20] introduced a different strategy for analysis of MBD in 1997. In this strategy, mammograms are classified into five different classes according to the histologic-mammographic correlation with the three-dimensional thick-slice technique. This classification technique depends on four building blocks: nodular densities, linear densities, homogeneous fibrous tissue, and radiolucent fat tissue. Five classification blocks are as below.

- Class I: it evenly balance all breast tissue elements with a small predominance of fibrous tissue.
- Class II: predominance of fat tissue (fat-Breast)

- Class III: predominance of fat tissue with retro areolar surplus fibrous tissue
- Class IV: predominantly nodular densities and
- Finally, class V: Predominantly fibrous tissue (dense breast).

These patterns are further classified as low-risk (I, II, III) and (IV, V) as high-risk patterns. The summary of Tabor MBD classification is shown in Table- 2.3.

Table- 2.3 Summary of Tabor MBD classification

MBD Classes	Conditional description	Risk Categories
Class I	Even balance of all elements of breast tissue	Low-Risk
Class II	Predominance of fat tissue (fat-Breast)	Low-Risk
Class III	Predominance of fat tissue with retro areolar surplus fibrous tissue	Low-Risk
Class IV	Predominantly nodular densities	High-Risk
Class V	Predominantly fibrous tissue (dense breast)	High-Risk

Mammography depicts the fibro-glandular tissues that formulate breast density, classified into four classes according to the BIRADS classification standard [21]. The Breast Imaging Reporting and Data System (BIRADS) was developed in 1993 by the American College of Radiology (ACR) to standardize mammographic reporting to satisfy the certain goals of classifying mammographic breast density. BIRADS density classification is shown in Table- 2.4.

Table- 2.4. BIRADS Edition_4 MBD classification

MBD Classes	Conditional description	Percentage Density
BIRADS-A	Breasts are almost entirely fatty	0-25%
BIRADS-B	Presence of scattered areas of fibroglandular density	25-50%
BIRADS-C	Breasts are heterogeneously dense, which may obscure small masses	50-75%
BIRADS-D	Breasts are extremely dense, which lowers the sensitivity of mammography	75- 100%

The fifth edition, released in 2013, achieves specific tasks like adding multiple new descriptors to recognize the increased risk of malignancy. Some old descriptors were

removed from this edition to evade underutilization or excessive application, and name changes to pre-existing descriptors to align descriptions across the three imaging modalities. Subsequently, images obtained directly from mammography, ultrasound, and MRI supersedes expert rendering to express pathology in the 5th edition. Also, the terms available to represent breast composition on a mammogram no longer include percentage quartiles. The fundamental reason behind this is Radiologists' evaluation of numeric quartiles has consistently do not match with automatic volume calculations. This problem significantly takes place in fibroglandular volume. Table 2.5 depicts the comparison between BIRADS' fourth and fifth editions for MBD classification.

Table- 2.5 Comparison between BIRADS 4th and 5th editions.

BIRADS 4th edition	**BIRADS 5th edition**
Formerly based on percentages	**Percentages are removed at present**
(A) Almost entirely fat (less than 25%)	(A) Breasts are almost entirely fatty
(B) Scattered fibroglandular densities (25—50%)	(B) There are scattered areas of fibroglandular density
(C) Heterogeneously dense (50—75%)	(C) Breasts are heterogeneously dense, which may obscure small masses
(D) Extremely dense (greater than 75%)	(D) Breasts are extremely dense, which lowers the sensitivity of mammography

Currently, classification of MBD is done subjectively with expert radiologists as per guidelines of BIRADS version 5 which consist of significant interobserver variation. Hence, there is a social need to have a precise and accurate software tool that can assist radiologists.

2.2.1 Expectations of Radiologists

During the proposed research work, expectation of few radiologists for automatic MBD classification system were discussed and the same of them are listed below:

1. CAD system should act as a reliable support system for radiologists for providing accurate classification of MBD.
2. Designed CAD system should consist of all the variations of imaging parameters such as pixels intensity and contrast, etc.
3. CAD system should classify breast density as per BI-RADs classification.
4. CAD system should learn from its experience so that accuracy will improve over time.

2.3 Development of Commercial Applications

Many research efforts have been taken to develop the commercial tool in this field from the last four decades listed in this section. This section is divided into two subsections as per year of implementation of commercial applications in the past and present and this section is finally ended with future scope of implementation in the field of mammographic breast density.

2.3.1 Area-Based MBD Classification

In the initial phase of computerized clinical applications, all applications use the concept of semiautomatic area-based density measurement. Boyd, Byng, and Yaffe developed the first semiautomatic clinical applications on area-based density measurement in 1994, known as “cumulus” [22-25]. This application was the gold standard for 20 years for breast density measurement. This method uses interactive thresholding, brightness variations in terms of average skewness, and the calculation of fractal dimensions of grayscale images. The fundamental limitation of this method is that the reader has to identify the threshold and boundaries of breast tissue to calculate the breast density. The user interface of Cumulus is shown in Figure-2.1(a), where edges are highlighted with red color and fibro glandular tissue with green color.

In 1998, an area-based computerized Clinical application known as “Madena,” in which Astrahan coded for measuring density patterns on a mammogram, was used for tracking the changes in density patterns with medical treatments. This application works on histogram-based thresholding. Results obtained by this method are

moderately correlated (r > 0.85) as compared with the products from the expert outlining approach [26].

In 2000, “ABDM,” another clinical application, was developed by Heine et al. [27]. This application was based on a statistical model that used Chi-Square probability to separate the fatty breast from fibro glandular tissues on a digital mammogram with the support of digital filtering. This model uses multiresolution wavelet expansion and 1/f power law analysis with parametric modeling of the mammogram. Results obtained by the ABDM are depicted in Figure- 2.1(b), in which the narrow upper curve is related to the fat area, and the lower spread out curve corresponds to the denser area.

(a) (b) (c)

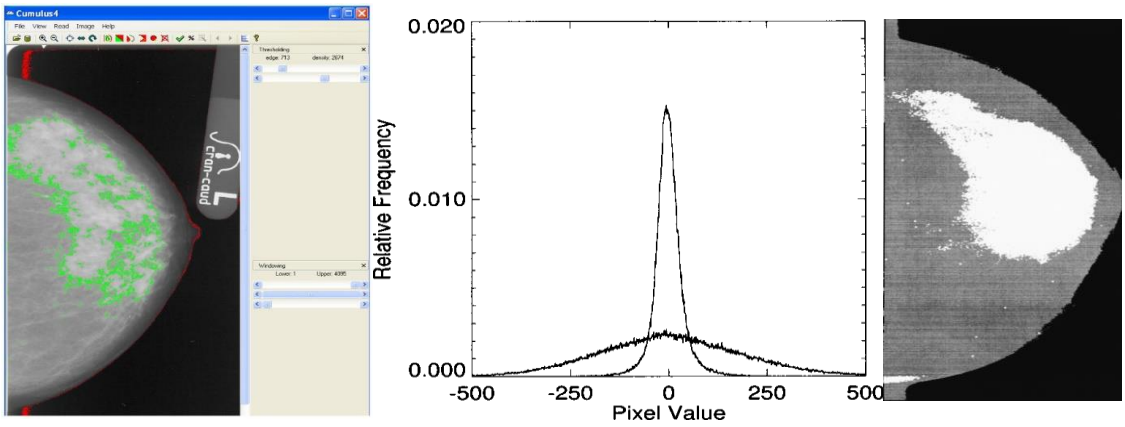

Figure- 2.1 (a) cumulus interface (b) output pixel value (c) Visualization of Breast density

In the year 2009, Automatic application is based on the concept of maximum Entropy and spatial information known as “MedDensity” developed by Tagliafico et al. [28]. This clinical application was available in semiautomatic and automatic mode. In semiautomatic mode, the quantitative assessment of MBD is performed using the thresholding and edge detection methods. The primary limitation of this method was that the radiologists identified the edges of the breast manually. Then the percentage of the dense breast is read into the black circle. In automatic mode, thresholds are adjusted automatically as shown on the left side of the computer interface in Figure-2.2. There is the mask of the breast tissue and the value of mammographic density on the right

side.

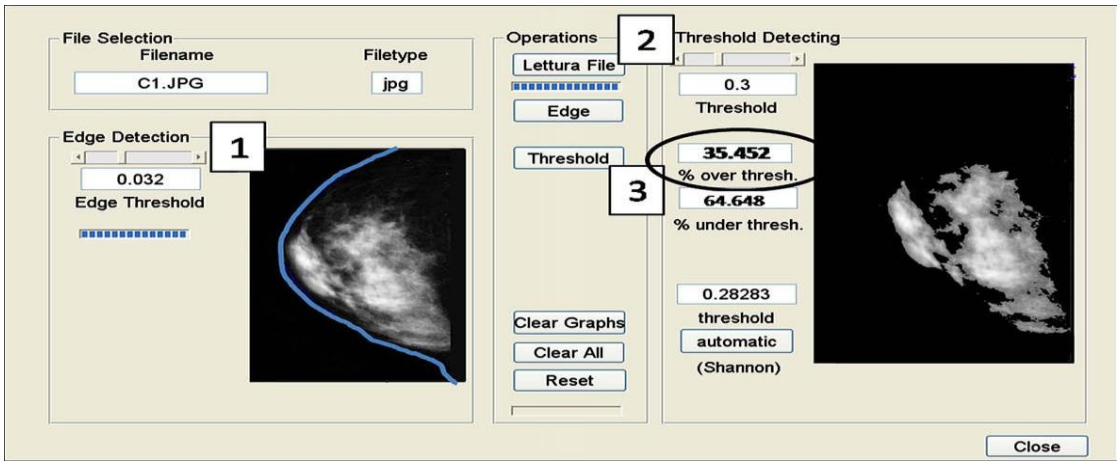

Figure- 2.2 Graphical user interface of MedDensity

2.3.2 Volumetric Breast Density Measurement

Higham et al. [29] proposed another research paradigm for three-dimensional MBD assessment instead of a two-dimensional MBD assessment as a volumetric breast density demonstrated in Higham's Ph.D. thesis. In 2003, "Cumulus" first clinical application was available in the market to measure volumetric breast density. After 16 years, it became the backbone for some commercial software approved by the FDA. In this application, the tissue-equivalent plastic object is calibrated with an imaging system with specific correction in variations in image parameters by keeping images of aluminum step-wedge placed during imaging. With the help of this information, volumetric breast density was calculated [30].

In 2008, Quantra another commercial clinical application that provides volumetric breast density analysis which is based on the physical model of the breast. In this application thickness of fibro glandular breast tissue is associated with each pixel and further aggregated to calculate the entire breast volume. The volume of fibro glandular tissue was calculated to get the value of volumetric breast density with the help of the difference in attenuation of fibro glandular tissue pixels and fatty pixels [31]. Quantified analyses of all studied clinical applications from 1990 to 2009 are presented in Table-2.6.

Table- 2.6. Quantified analysis of all clinical application in the past

Basic Approach	Implementation year	Name of clinical application	Software Algorithm used	Merits/demerit if any
Area-based Density measurement.	1994	"Cumulus"	Interactive thresholding	Semiautomatic
	1998	"Madena"	Histogram-based thresholding	Results obtained by this method are moderately correlate (r > 0.85)
	2000	"ADBM"	Multiresolution wavelet expansion and 1/f power law analysis with parametric modelling of mammogram	Frist statistical model used to calculate breast density
	2009	"MedDensity"	concept of maximum Entropy and spatial information	Available in semiautomatic and automatic mode
Volumetric Breast density	2003	"Cumulus"	Tissue equivalent plastic object is calibrated with imaging system	Frist volumetric application of breast density
	2008	"Quantra'	Works on physical model of the breast	Thickness of fibro glandular breast tissue was calculated with physical model.

2.4 Systems in the Present

This section provides an overview of different clinical applications for breast density measurement from 2010 to 2019. These applications are sub-divided into two subsections one is area while another is volumetric breast density measurement.

2.4.1 Area-Based Density Measurement

After 2010, advancements in computer vision algorithms provide an excellent platform to process digital mammograms to offer more insights into the images. In 2012, two clinical applications, "M-Vu Breast Density," worked on Computer vision algorithms

to process digital mammograms. According to the BI-RADS standard, this algorithm structural and texture difference in fatty and fibro glandular tissue is used to classify area-based mammographic breast density [32].

And another one is "ImageJ," a fully automated area-based breast density measurement tool similar to the cumulus by using penalized regression with some additional features of mammograms to predict the danger of breast cancer associated with breast density [33].

In clinical application known as "Auto density" in 2013, optimum thresholding is used to classify the object into two classes. An optimal threshold method is used to segment fibro glandular tissue from the whole breast [34]. However, after 2013, there was no application in clinical practice as the research paradigm shifted towards volumetric breast density.

2.4.2 Volumetric Density Measurement

In 2010, Volpara was another FDA-approved and the most commonly used clinical application based on the relative physics model. This model used "hint" [35] and standard mammogram form "SMF" [36]. The "Hint" method normalizes mammogram of engaging tissue by measuring anatomical information from the mammogram where each pixel represents the thickness of fibro glandular tissue during compression. This information helps to get the volume of the whole breast. "SMF" provides an estimation of fibro glandular tissue at each location of mammograms which is helpful to estimate the volume of fibro glandular tissue. This application also consists of calibrated datasets such as mAs and kVp, providing a realistic breast model [37].

In 2014, 'Philips' Spectral Breast Density Measurement was a FDA approved clinical tool [38-39], which used the concept of the difference between the energy spectrum of fatty and fibro glandular tissue. The thickness and density of each pixel are measured independently, which is further used to estimate volumetric breast density. This method does not use the information of compressed breast like Volpara, but results of this method also co-relate with BI-RADs classification. This is the first clinical application in which non-contrast spectral imaging was used to measure photons counting technology which was divided into low and high energy categories. Interface of Volpara is depicted in Figure-2.3.

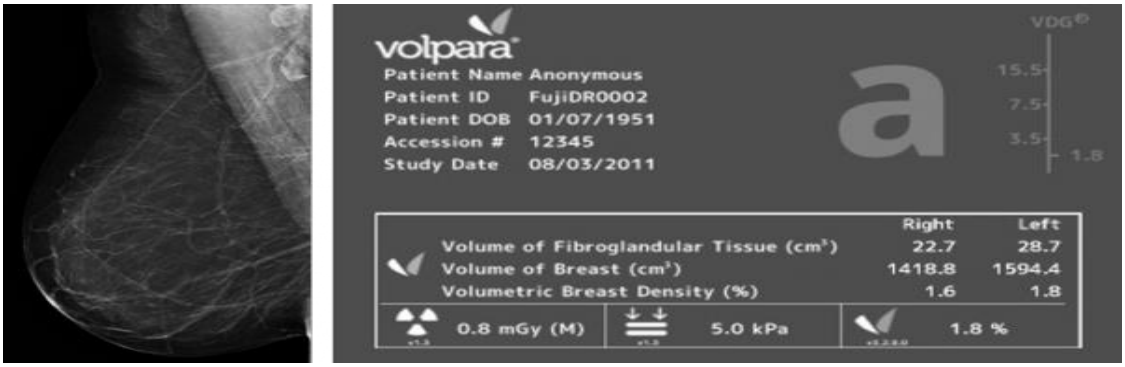

Figure 2.3 Interface of Volpara

In 2018, Siemens Healthineers had cleared FDA approval for its clinical application named "MAMMOMAT." This application performs tomosynthesis scans at different angles with a range of 500 to provide a detailed 3D view which is helpful to identify overlapping breast tissue. This application also has an additional integrated imaging tool known as InSpect, which will speed up the biopsies process and make it more comfortable with one click [40-41].From 2010, mammographic breast density measurement technique is diverted more towards volumetric than the areas-based density measurement. The quantified analysis of systems in the present is presented in Table- 2.7.

Table- 2.7 Quantified analysis of systems in present

Basic Approach	**Implementation year**	**Name of clinical application**	**Software Algorithm used**	**Merits/demerit if any**
Area-Based density measurement	2012	M-Vu Breast Density	Structural and texture difference in fatty and fibro glandular tissue	Breast density according to BI-RADS standard
	2012	"ImageJ"	Penalized regression	Uses some additional features of mammograms to predict risk of breast cancer
	2013	"Auto density'	Optimal thresholding	Provides better segmentation results
Volumetric Breast density	2010	Volpara	Relative physics model	Used calibrated parameters such as such as mAs and kVp for measurement of breast thickness.

	2014	'Philips'	Difference between energy spectrum of fatty and fibro glandular tissue	First clinical application in which non-contrast spectral imaging was used to measure photons counting technology.
	2018	"MAMMOMAT".	Performs tomosynthesis scans at different angles with range of 50^0	This technology is helpful to identify overlapping breast tissue.

2.5 Future of Commercial Application

In the United States of America, breast density notification to the individual patient after mammography screening is mandatory in 30 states [42]. In the future, it becomes the social need of all the countries to know breast density and its correlation with breast cancer risk and requires supplementary screenings. Hence, future research needs to reduce inter-reader variations and provide a more reliable and accurate clinical application to predict breast cancer in advance.

The research paradigm of breast density has changed from area to volume and is now gaining more attention towards machine and deep learning approaches. Artificial intelligence can learn complex features of objects [43-44] and it is beneficial for both volumetric and area-based density measurement. Hence, there are many deep learning and machine learning-based innovations that are under clinical trials. These models use either two-class or four-class classification by using convolutional neural networks models. The deep learning model consists of five to six convolutional layers, three connected layers, and the SoftMax function for classification. In addition, specific modification is going on in terms of RELU, hyperbolic tangent function. Simultaneously, there is yet another path for research innovations under feature extraction, segmentation, and dimension reduction for machine learning classifications. These modifications surely helps to make breast density measurement more objective than subjective. And such models can be a future for screening tool for breast cancer risk prediction [45]**.** Research development path for mammographic breast density of the last four decades is depicted in Figure 2.4.

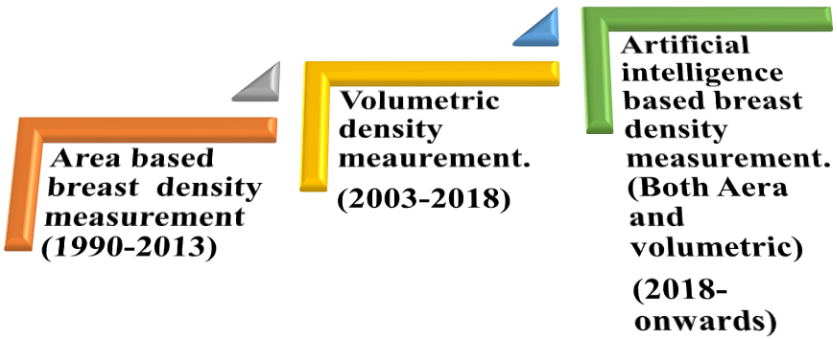

Figure- 2.4 Research development path for MBD classification

Even though there are many automated clinical applications in the market for MBD classification, these applications have advantages like faster processing speed, cost-effective, and are more objective but do not provide optimal results. Nevertheless, some observations recorded during this study may be helpful to decide the future path of research in breast density measurement.

- There are three basic approaches for breast density measurement: area-based, volumetric-based, and now deep learning.
- In all the MBD classification applications, the essential focus is to analyze the attenuation and absorption characteristics of the breast tissue and compared to the physical breast tissue.
- Different manufacturers perform digital mammograms at different clinical environments with the help of different proprietary algorithms and different imaging parameters, which will change the contrast of each mammogram, which may be one of the causes of error in breast density measurement.
- Assessment of three-dimensional breast density from two-dimension mammograms is a challenging task.
- Compression of the breast during mammography is one of the critical causes to hamper the results of area-based density.
- Volumetric breast density is another good option to increase measurement reliability, used by different manufacturers like Volpara, Quantra, etc.

- There are no external or absolute ground truth images of different countries for validations of MBD classification; hence challenging to perform a comparative analysis of obtained results.
- In the future, Artificial intelligence can learn complex features of mammograms and hence there is future research hope which will provide more reliable breast density classification tool for prediction of breast cancer.

2.6 Pre-Processing of Digital Mammograms

Digital mammography acts as a unique screening technology to protect the lives of females against breast cancer for the past few decades. Mammographic breast density is a well-known biomarker and plays a substantial role in breast cancer prediction and treatments. Breast density is calculated based on the opacity of fibro-glandular tissue on digital mammograms concerning the whole area of the breast. The opacity of pectoral muscle and fibro-glandular tissue is similar to each other; hence, the small presence of the pectoral muscle in the breast area can hamper the accuracy of breast density classification. Successful removal of pectoral muscle is challenging due to changes in shape, size, and texture of pectoral muscle in every mammogram [46]. This section will describe some of the state-of-arts methods used for pre-processing of digital mammograms. Preprocessing of digital mammogram are classified into:

1. Breast border detection
2. Pectoral muscle removal

2.6.1 Literature Survey of Breast Border Detection Methods

The main focus behind breast border detection is to separate the breast area from the background of digital mammograms. For accurate measurement of breast density, it is essential to identify tissue-air interface with breast area. Due to its in-built merits, such as ease of execution and high computational speed, thresholding is a crucial tool for image segmentation. The critical design factor in thresholding is the choice of the threshold value which will divide the image into two or more than two parts. There are different methods available in practice to select the threshold values, either manual or

automatic, with the help of mean or median value of the intensity. Details of literature survey till date are presented in Table- 2.7.

Table- 2.8 Literature survey till date on Breast border detection

Detail of the journal/ website link	**Year of Publication**	**Indexing of journal**	**Main findings relevant to proposed research work**	**Merits/demerits**
'International Conference on Biomedical Engineering and Informatics', https://doi.org/10.1109/BMEI.2010.5639662../ [47]	2011	SCOPUS	In this method, the local variances of the 5x5 neighbours are calculated on all pixels in an ROI (region of interest). The Radon transform is used on the resulting variance image to detect the most significant lines representing the edge of the muscles. The contents in the left side of the detected line are removed as the pectoral muscle	This method requires an additional tool, interactive-based screening for pectoral muscle having complicated shapes.
'Computer Methods and Programs in Biomedicine'. https://doi.org/10.1016/j.cmpb.2010.11.016. [48]	2011	SCOPUS	The proposed algorithm uses the Minimum cross-entropy thresholding for breast border detection.	The proposed method has less computational complexity and provide average accuracy but is sensitive to noise.
Medical Physics, https://doi.org/10.1118/1.4736530 [49]	2012	SCOPUS	'In this method, the body-air interface boundary is determined by a threshold based on the gray-level intensity Histogram, which is independent of any prior assumptions'.	Performance of this method found satisfactory for breast border detection.
Signal Processing. ,https://doi.org/10.1016	2013	SCOPUS	Proposed Novel k-means algorithm for	K-means algorithms with Cartesian coordinate

/j.sigpro.2012.07.026.[50]			breast boarder detection	space provides better visualization of breast border.
'Artificial Intelligence in Medicine'. 'https://doi.org/10.1016/j.artmed.2017.06.001 [51]	2017	SCOPUS	This research article provides a comparative analysis of three different breast border detection methods: the histogram-based method of Chen and Zwiggelaar, the k-means thresholding, and Otsu's thresholding.	Out of three, the Entropy-based method provides better results for breast border detection.
'International Conference on Innovations in Information, Embedded and Communication Systems', 'https://doi.org/10.1109/ICIIECS.2017.8276139' [52]	2018	SCOPUS	In this approach, binary thresholding is used for breast border detection.	This approach is quite simple to implement. However consist of limitations related noise at the breast border.

During this literature survey, we came across different thresholding algorithms for breast border detection which are depicted in Figure- 2.5.

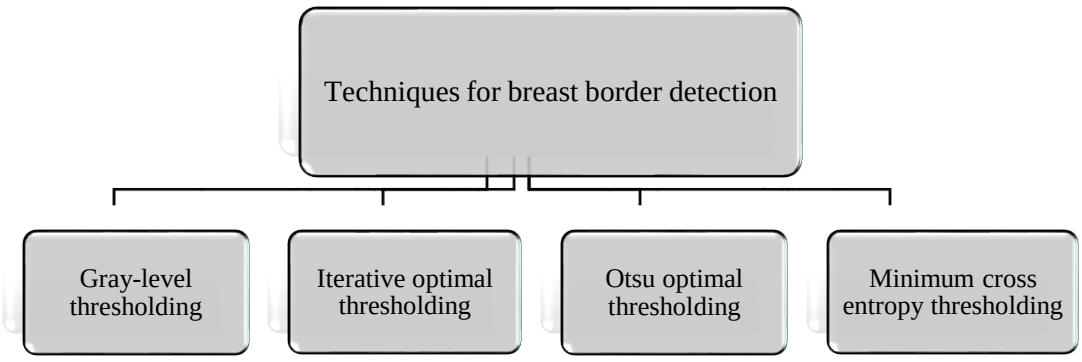

Figure 2.5 State of art algorithms for Breast border detection

2.6.2 Comparative Analysis

Table-2.9 illustrates the performance metrics of reviewed breast border detection methods.

Table-2.9.The performance metrics of reviewed breast border detection methods

Segmentation Methods	Data sets	Classification Accuracy	Implementation Accuracy	Merits and Demerits
Region growing Algorithms	88 FFDM	Moderate	87%	The accuracy of this method was affected by empirically selected wavelet, classifier, and sub-regions.
Graph cut techniques	Mini MIAS dataset	Moderate	Completeness CM=0.435	Initial seeds are marked by the user, which will affect the classification accuracy. We need to use another algorithms to mark the initial seed automatically.
Fuzzy C-Means.	160 FFDM	High.	Jaccard indices of J = 0.62±0.22	Values of k are generally found sensitive to the change in peaks or shifts in histogram construction hence shows average agreement with Radiologists prediction.
Watershed segmentation	Mini MIAS dataset	Moderate.	87.5%.	Chances of over-segmentation hence requires support of marking functions.
Otsu's optimal thresholding	Mini-MIAs dataset	High	83.3%	Histogram should be bimodal. Does not use any object structure or spatial coherence.
Physical method	Mini-MIAs dataset	High.	79.2%	It is difficult to correlate tissue compression information from the mammograms.
Fusion of K-means and Region growing Algorithms	Mini-MIAs dataset	Moderate.	92.87%	Automatic selection of k enhances the accuracy.

2.6.3 Research Gap identified

All the surveyed methods have variations in computational complexity from low to high. They consist of the drawback of unclear boundaries between Breast border and background, which will hampers segmentation accuracy. Minimum cross-entropy is found better if noise issues are correctly handled [47-52]. Hence, future research needs to refine these algorithms to reduce noise sensitivity and increase segmentation accuracy. We will try to use the refined version of either iterative optimal thresholding or Otsu thresholding for breast border detection in our proposed research work.

2.6.4 Pectoral Muscle Removal Algorithms

Pectoral muscle detection and segmentation are more thought-provoking due to the change in density, size, and shape in each case of mammogram. Pectoral muscle and fibro glandular tissue often have the same opacity, which will cause a significant impact on the accuracy of breast density measurement; hence, accurate removal of pectoral muscle is another cardinal goal of the pre-processing technique. The critical issues in automatic pectoral muscle removal are occurrence of the overlapping of glandular tissues and pectoral muscle boundary, the similarity between the pectoral and breast regions, and low difference along the skin-air border. These listed issues act as a real test for researchers working on automatic pectoral muscle boundary detection [53]. Accurate removal of the pectoral muscle and breast border detection from the digital mammogram is a thought-provoking and challenging job in front of researchers due to its change in size, shape, and position in each mammogram. For the last few decades, different researchers have proposed diverse approaches for removing pectoral muscle from the breast; this section will describe some of them.

2.6.4.1. Intensity-Based Techniques

The fundamental concept used in this approach is the intensity difference between the breast tissues and pectoral muscle. Thresholding, watershed, and region-growing are the most widely applied algorithms for pectoral muscle removal. These algorithms are based on assumptions that the intensity of pectoral muscle is higher than breast tissue. Saltanat et al. [54] used exponential scale to map existing pixel values in digital

mammograms. Then, a thresholding algorithm is applied over this mapping to extract pectoral muscle. Exponential scale mapping enhances the performance of this algorithm in terms of a lesser overflow of regions. Maitra et al. [55] introduced a dynamic seed selection mechanism to identify the pectoral muscle. Then, the region growing algorithm is used to determine the pectoral muscle in the upper side triangle. Finally, the Cartesian slope-intercept equation is used to remove the pectoral muscle from the mammograms. Automatic seed selection is the primary merit of this algorithm, but this algorithm fails to remove pectoral muscle if it is not triangular in shape.

The simple approach of local thresholding with a contrast enhancement was suggested by Vikhe et al. [22] for pectoral muscle segmentation. But results of this algorithm are mostly affected by unclear boundaries between the pectoral muscle and breast area. Local abrupt changes and discontinuities at the border can hamper the output of this algorithm. The watershed algorithm is another region-based technique that utilizes the concept of image morphology. Watershed transformation of pectoral muscle in terms of the image gradient to extract watershed region was suggested by Taifi et al. [23]. In this approach, the watershed algorithm was used to locate catchment basin boundaries at a higher gradient point to remove the pectoral muscle successfully from the breast area. Despite its merit, this algorithm consists of issues of over-segmentation in some cases. Singh et al. [24] proposed a region-growing algorithm for the removal of the pectoral muscle. In this approach, the adaptive K-mean algorithm is proposed to identify the pectoral muscle. Then with the initial seed (small threshold), the region-growing algorithm is applied to remove the pectoral muscle. Finally, the smoothing of an image is done with a median filter.

Thresholding and region-growing techniques depend on pixel values within a particular range that belongs to one class. The fundamental limitations of all the above methods include (i) they do not consist of any spatial information of the image and (ii) they do not provide better results on unclear boundaries. In contrast, region growing methods generally rely on neighboring pixels. The fundamental limitation of the intensity-based techniques is that the intensity variation between pectoral muscle and breast area is minimal; hence, either over-segmentation or under- segmentation takes place.

2.6.4.2 Edge Detection Techniques

The fundamental approach of this segmentation technique is to identify sharp brightness changes inside the image to detect the border between the objects. This method uses straight-line modeling of the pectoral muscle boundaries to segmentation pectoral muscle from the breast area. In this segmentation technique, Hough transform is used to find the peak in Hough space with the support of orientation, gradient magnitude, and projected line length.

Rampun et al. [56] proposed canny edge detection with five features to detect the edge of the pectoral muscle. This method further uses an active contour growing model for the final suppression of pectoral muscle. This method's primary limitation is that it overestimates the boundaries of pectoral muscle due to artifacts and noise, which requires further post-processing. Devi et al. [57] introduced the fusion of global thresholding, Hough transform, and connected component technique to segment pectoral muscle from 161 digital mammograms. Morphological operations are used to remove noises and artifacts inside the mammograms. And finally, polynomial curve fitting is used to suppress pectoral muscle. Liu et al. [58] proposed Randon transform technique to forecast objects in the images using a set of angles and resulting projections. These projections are used to add intensities of the pixels in all directions, which is the concept of line integral. The proposed method uses the local variance of neighbours calculated on all the pixels of ROI and finally on resulted variance image. Radon transform is implemented to identify the most significant line that represents an edge of muscles. The contents detected in the left side of the detected line are removed as the pectoral muscle.

The polynomial curve fitting techniques are used to estimate curves from a straight line that best fits the input series. The curve is calculated at fixed pixel intervals and the smooth curve determined along with the edge of the pectoral muscle in such techniques. One such method is extended by Subashini et al. [59], which is based on regression analysis with flexibility for different shapes and simple implementation. The fundamental limitation of this algorithm is that if the degree of polynomial increases, then this algorithm becomes unstable; hence there must be a proper trade-off between shape (curvature of pectoral muscle edge) and degree of the polynomial(number of the turn).

Bora et al. [60] proposed a novel method for pectoral muscle segmentation. In this method, a texture gradient-based approach is used. A straight line is used by which pectoral muscle is detected with Hough transform based on Probable Texture Gradient (PTG) map. Then block averaging approximated line is used to detect the accurate line. A soft curvature of the pectoral muscle is obtained by Euclidean distance regression and polynomial modeling techniques. This algorithm is validated with 340 MLO views from three different databases and yielded a 96.75% qualitative score index for segmentation. This method has recorded low segmentation accuracy when the pectoral muscle size is small, and contrast is low. Also, segmentation accuracy depends upon the straight-line approximation of the pectoral muscle.

Line Detection techniques consist of several merits: the ability to force specific geometric properties, good handling of noisy data, and easy adjustment to noise. This method also has few limitations, such as it requires larger storage space and high computational complexity. In each image, the pectoral muscle cannot be detected as a straight line due to overlapping boundaries between the pectoral muscle and the breast area.

2.6.4.3 Wavelet-Based Segmentation Techniques

Wavelet transform is a popular image processing technique that uses the short-term Fourier transform. In this technique, wavelets are used to identify spatial frequency information from the image. Ferrari et al. [61] proposed a wavelet-based approach to detect the edge of pectoral muscle inside the breast. Gabor wavelet filter bank is used to enhance the pectoral muscle edge, and then the hybrid method is used to obtain the delineation of the pectoral muscle. This hybrid method consists of the combination of Gabor wavelets and Hough transform. Finally, a Gaussian kernel and low pass filter are used to extract pectoral muscle from the breast area. A similar approach of wavelet decomposition and contour detection techniques was proposed by Mustra et al. [62]. The proposed method uses a Sobel filter to detect the edge in a fourth-level dyadic wavelet decomposed image. After edge detection, removing the pectoral muscle is done from the image by marking the smooth curve. In this method, fourth-level decomposition acts as an excellent option to identify and remove fine details like noise and granulation.

The primary merit of this technique lies in the edge information given by wavelet decomposition, which is sufficient to remove pectoral muscle; hence, no need to reconstruct the image. However, wavelet transform combines the infinite series expansion of image; hence high-frequency information is unavoidably lost during segmentation, which further hampers segmentation accuracy.

2.6.4.4 Deep Learning Techniques

Due to composite variations in size and shape of the pectoral muscle, hand-crafted methods possess certain limitations, and to overcome these limitations, recently, deep learning approaches are investigated by some researchers for the segmentation of pectoral muscle [63]. Successful implementation of deep learning classifiers like Google-Net, Res-Net, and VGG-Net provides new medical imaging and diagnosis expectations. To segment pectoral muscle, semantic segmentation with U-Net architecture is proposed by Wang et al. [64]. Before training the proposed model, different operations like image normalization, zero, and extrapolated padding are performed on input images. The proposed model is trained with 2000 digital mammograms, and validation results are obtained on 825 images in terms of median dice-similarity coefficient as 0.8879. A similar approach of Res U-Net is proposed by Ali et al. [65]. In this model, Gaussian and median filters are used to enhance input images. Expert radiologists involved in this study marked ground truth for validation of the model. Original images and ground truth images are given for training and validation of the proposed model. The proposed model consists of skip connections and drop-out layers in convolutional layers to solve connectivity problems and ELU activation function in the output layer, providing a final output in terms of a probability map of the pectoral muscle. Finally, to remove false positives, pectoral muscle boundaries are detected with the help of canny edge detection and a probability map of the pectoral muscle. The qualitative assessment of this algorithm shows the best score of segmentation in terms of 97 ± 1.5 mean intersection over union (IOU), 96 ± 2.57 Dice similarity coefficient (DSC), and 98 ± 0.58 segmentation accuracy. Another similar approach is suggested by Kim et al. [66], in which U-net architecture for pectoral muscle segmentation is proposed for 322 images from Mini-Mias datasets. Input images are down sampled and given to U-Net architecture, consisting of 23 layers

with a combination of coding and decoding units. The model is trained with Jaccard loss function and Adam optimizer over 300 epochs for input images. Validation of the model is performed with a mean value of the Dice coefficient and recorded 95.88% mean value.

To enhance segmentation accuracy with U-Net architecture, Guo et al. [67] proposed a two-stage framework for pectoral muscle segmentation. In the first stage, training of U-Net architecture is performed with 633 input mammograms and validated ground truth. During the training phase, the variance of each predicted snapshot of output is calculated. In the second stage, the GAN network is trained with three-channel input, consisting of breast shape, detected pectoral muscle region, and completed region indicator and distribution from the ground-truth data. Validation of proposed architecture is performed with U-Net architecture and obtained a DSC of 97.03%.

The primary limitation of this model is computational complexity (time) which is higher due to the requirement of different models for segmentation. Some of the others literature review is presented in tabular form with the help of Table- 2.10.

Table- 2.10 Literature survey till date on pectoral muscle removal.

Detail of the journal/ website link	**Year of Publication**	**Indexing of journal**	**Main findings relevant to proposed research work**	**Remarks**
International Journal of Image and Graphics. https://doi.org/10.1142/s0219467813500137 [68]	2013	SCOPUS	Seeded region growing algorithm is used on the extracted triangle to suppress the pectoral region	Cartesian slope–intercept equation for the line is chosen for seed selection.
'Journal of Digital imaging. https://doi.org/10.1007/s10278-015-9813-5' [60]	2015	SCOPUS	Texture gradient-based approach is applied over 340 datasets. The pectoral edge is initially approximated to a straight line by applying Hough transform on Probable Texture Gradient	This approach obtained Qualitatively, 96.75 % accuracy.

			(PTG) map of the mammogram followed by block averaging with the aid of approximated line	
'Procedia Computer Science, Volume 46, Elsevier https://doi.org/10.1016/j.procs.2015.02.117. [57]	2015	SCI	In this approach Edge detection processes are used to identify the edge of the full breast and connected component labelling is utilized for identify and remove the connected pixels outside the breast region.	The result shows that our approach removes Gaussian and impulse noise effectively without any loss of desired data and overall gives 90.06% accuracy.
'Procedia Computer Science Volume 79, Elsevier https://doi.org/10.1016/j.procs.2016.03.034.'[69]	2016	SCI	Performance of intensity thresholding based pectoral muscle removal is found 96.52%	This method is less utilized due to less accuracy but found good segmentation accuracy in this approach.
'IEEE Xplore. https://doi.org/10.1109/CGiV.2017.24'. [70]	2017	SCOPUS	The developed methodology is based on Morphological Watersheds based segmentation and applied on 80 digital mammograms. Marker based watershed method will be a better choice to avoid over segmentation.	All the average FN and FP pixel percentages are 3.68% and 2.98%, with the range shown from 0.90 to 0.99 for accuracy and 0.86 to 0.99 for precision rate
Journal of Digital imaging https://doi.org/10.10	2018	SCOPUS	The proposed method combines genetic algorithm and	This algorithm was applied on three different

07/s10278-018-0068-9 [71]			morphological selection algorithm, incorporating four steps: pre-processing, genetic algorithm, morphological selection, and polynomial curve fitting	datasets mini MIAS, DDSM, IN Breast with a total of 651 mammograms.
'Lecture Notes in Computer Science, vol. 11854. Springer. https://doi.org/10.1007/978-3-030-34879-3_7.' [72]	2019	SCOPUS	Proposed u-net deep learning architecture for segmenting breast area and pectoral muscle from digital mammograms	Obtained median dice-similarity coefficients of 0.8879 and 0.9919, respectively for pectoral and breast segmentations from 825 testing images
Springer Verlag https://doi.org/10.1007/978-3-319-33793-7_2. [73]	2020	SCOPUS	Got insight of different methods used for pectoral muscle removal.	Performance of the RANSAC algorithm is found 82%.

Different authors proposed different approaches for pectoral muscle removal, which is listed graphically in Figure- 2.6.

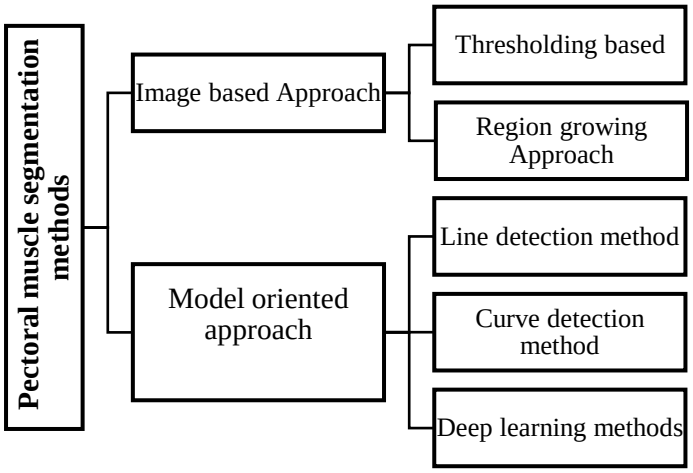

Figure- 2.6 Different surveyed algorithms for removal of pectoral muscle

2.6.5 Comparative Analysis of State-of-Art Pectoral Muscle Removal Algorithm

Performance metrics of pectoral muscle removal methods are combined together in tabular form for comparison purpose in Table- 2.11.

Table- 2.11. The Performance Parameter Analysis of Different Pectoral Muscle Extractions Techniques

Method	Operating principle	Computational complexity	Accuracy	Merits	Demerits
Hough transform	Canny edge operator	Moderate	Good	Ability to force certain geometric properties from the data. Simple to implement, Less affected by noise	Larger storage space required, Domain restrictions, Suitable for one object at a time
Randon transform	Line integral	Average	Average	Computational simplicity.	Average segmentation accuracy.
Polynomial curve fitting	Regression analysis	Moderate	Average	Moderate flexibility of shapes Computationally easy to use	Poor interpolator properties Higher degree polynomial cause poor trade-off between shape and degree
Dynamic seed region growing	Clustering approach.	Low	Good	Simple to implement. effective storage and fast retrieval	Difficulty in automating seed generation.
Deep learning Approach	Learning from the data	High	Good	Capable to learn complex hierarchical features. Provides better accuracy than hand crafted technique.	High design complexity and requires larger dataset.

Pectoral muscle detection and segmentation is more challenging as muscles' size, shape, and density vary case by case. Variations can even be seen in mammograms for the same patient obtained at different situations or time points. Sophisticated automated techniques for muscle segmentation are available in several recent studies. Other authors proposed different approaches for pectoral muscle removal, and comparative

analysis is presented in Table 2.12.

Table- 2.12 Performance parameter analysis of different Pectoral muscle extractions techniques

Comparison parameter	Image based Approach	Model based Approach
Operating Principle	Clustering or Thresholding	Mathematical analysis like Regression, Line Integral or Learning from data.
Computational complexity	Low	Moderate to High
Accuracy	82 to 95.65%	90 to 96.65%
Merit	Simple to implement. Effective storage and fast retrieval.	Ability to force certain geometric properties from the data. Capable to learn complex hierarchical features. Provides better accuracy than hand crafted technique.
Demerits	Difficulty in automating seed generation.	Larger storage space required. Domain restrictions.

2.7 Literature Survey on Mammographic Breast Density Classification

Mammographic breast density is one of the most significant risk markers, and it is assessed visually with the support of radiologists with four qualitative BIRADS categories. It is a challenging task for Radiologists to discriminate the two most variably assigned BIRADS categories, which are "Scattered density" and "Heterogeneously dense." Recently, *c*onvolution neural networks and machine learning approaches have been found superior in classification tasks due to their ability to extract local features with shared weight architecture and space invariance characteristics. Literature survey for MBD assessment is divided into two subsections

1. Machine learning approaches
2. Deep learning approaches

2.7.1 Machine Learning Approaches

Machine learning is one of the best alternative for image processing techniques recently. Many researchers have used Machine Learning (ML) techniques to avoid the

limitations of these traditional techniques such as assist physicians with a second opinion, and reduce the potential human errors which may cost the patient's life [74]. All machine learning approaches follow the image processing pipeline in which pre-processing segmentation and classification blocks are used to increase the accuracy of breast density classification. Even though all are significant innovations, there is a research gap to improve accuracy and reproducibility to make breast density classification more objective. Summary of literature review of machine learning models are presented in tabular form in Table-2.13.

Table-2.13 Summary of reviewed articles for machine learning approaches.

Details of journal/ website	**Year**	**Indexing Journal**	**Main findings relevant to proposed research work**	**Remarks**
'IEEE Transactions on Medical Imaging. https://doi.org/10.1109/42.906424' [75]	2001	SCI/ Scopus	Markov Random Field Probabilistic Approach	Semiautomatic approach
Academic Radiology https://doi.org/10.1016/S1076-6332(03)80534-2 [76]	2001	SCI	Kittler's optimal threshold	A high correlation in mammographic Breast density calculations
Medical and Biological Engineering and Computing. /https://doi.org/10.1007/BF02344714. [77]	2004	SCI	Gaussian mixture modelling and Expectation-Maximization algorithms	Accuracy can be increased if better normalization and trade-off between image resolution and sensitivity is calculated
Lecture Notes in Computer Science/ https://doi.org/10.1007/978-3-540-70538-3_2. [78]	2008	Scopus	Graph cut and Region growing algorithms	Semiautomatic
'International Conference on Computer Research and Development, https://doi.org/10.1109/ICCRD.2010.87'. [79]	2010	Scopus	Graph cut and clustering	Quantitative performance of this method is in satisfactory range
'International Conference on Biomedical Engineering and Informatics,	2011	Scopus	Region growing and SVM	High agreement rate but affected by parameter like wavelets, classifier

https://doi.org/10.1109/BMEI.2011.6098327'. [80]				structures
'Medical Physics/ https://doi.org/10.1118/1.4736530'. [81]	2012	Scopus	C-means and SVM	Novel idea of fusion of algorithm
Springer Verlag. https://doi.org/10.1007/978-3-319-41546-8_45 [82]	2016	Scopus	A multi-resolution stack representation	Shortcoming in terms of quantification of change of relative proportion of breast tissue.
International Journal of Computer Applications, https://doi.org/10.5120/ijca2017913208.[83]	2017	Scopus	Fusion of super pixels and a watershed based technique	Results shows good segmentation
International Journal of Intelligent Engineering and Systems. https://doi.org/10.22266/IJIES2019.0228.03. [84]	2019	Scopus	Two algorithms(K-mean) and fuzzy c-mean method (FCM	Provided good classification results.

2.7.2 Deep Learning Approach

Due to the shortcomings of traditional computer-aided detection (CAD), current research inclinations aim to develop novel deep learning (DL) methods for mammographic breast density measurement for early detection of breast cancer and reduce the false diagnosis of breast cancer [85]. Deep learning is the one of crucial subset of machine learning is gaining more popularity among the classification of images.

MBD classification is a long-lasting research area due to more thought-provoking and challenging image preprocessing, segmentation, and classification tasks. Successful implementation of deep learning classifiers like Google-Net, Res-Net, and VGG-Net provides new medical imaging and diagnosis expectations. In addition, these classifiers offer better results on different imaging modularity for image classification. This section describes some of such state-of-the-art methods used for MBD classification.

Intrinsically high inter-reader fluctuations are the prime problem in MBD assessment. To overwhelm this problem, Ciritsis et al. [86] suggested deep learning architecture

with 11 convolutional layers, three fully connected layers, and an output SoftMax layer to distinguish breast density into two classes and four classes. Two expert radiologists marked density ground truth during this classification task. A combination of MLO and CC (left or right) views of 20,578 digital mammograms were used to train the proposed model. During the training, to enhance the model's performance and desist over fitting, the convolutional layers are zero-padded and used dropout rate of 50%. Batch size and the highest number of epochs used during training are 40 and 120, respectively. Input data segmented as 70% for training and 30% for validation. This model is validated independently on CC and MLO views for two-class classification and achieved an overall classification accuracy of 89.9% and 86.6%.

As to predominance, fat appears darker than fibro glandular tissue in MBD assessment. Hence, the pixel intensity of the histogram act as an essential feature for classifier training. Nan Wu et al. [87] suggested this technique for MBD classification. In this method, to learn pixel intensity histograms, the SoftMax regression classifier is used. Four standard views (L-CC, R-CC, L-MLO, and R-MLO) of 2, 00,000 screening images given separately to train the model. The proposed architecture is deep and consists of 100 hidden units between input and output layers. Each hidden layer uses ReLU as an activation unit. This model is tested for two class and four class classification and achieved 81.1% and 82.5% classification accuracy. Thus, this model provides moderate classification accuracy despite an extensive dataset.

Francesca Lizzi et al. [88] proposed a Residual convolutional network for MBD classification. This architecture consists of 41 convolutional layers organized in residual blocks with 2 million learnable parameters. The input block of this architecture is made up of a convolutional layer, a batch normalization layer, a leaky ReLU as an activation function, and a 2D-max pooling. A series of four blocks consisting of 3 residual modules uses the output features of the input block. Leaky ReLU with $\alpha = 0.2$ activation functions is used to train the architecture. Categorical cross-entropy as a loss function validates the performance of the model. Maximum accuracy with four-class classification is 78%, and the two-class accuracy was 89.4%.

A comparative study for evaluating the performance of deep learning and transfer learning on a similar dataset, Mohamed et al. [89] proposed both approaches on 22000 mammographic images. In this approach, expert radiologists marked density ground

truth for the input images. Initially, the model's training starts with 500 images with an AUC of 0.942, and the final value of AUC is 0.9882 reported on the whole dataset. Then, the proposed model is cross-validated with the transfer learning (Image Net) application and obtained an overall AUC of 0.9857. Thus, this research study shows that both deep learning and transfer learning applications provide almost identical results on the equivalent dataset.

The requirement of a larger dataset for training is an essential need of deep learning architecture. To optimize deep learning performance on smaller datasets, Peng Shi et al. [90] proposed optimized lightweight deep learning architecture. This architecture combines three convolutional neural networks, one dense layer, and an output layer with the SoftMax function. Data augmentation is done with additional image processing to increase the number of the dataset. This architecture was trained and tested on a 322 Mini-Mias dataset. This architecture provides overall accuracy of 83.6 % on four-class classification. The main limitation of lightweight architecture on smaller datasets is the low stability of the network, which may occasionally cause large and significant variations in the accuracy. Data augmentation can enlarge the dataset in this method, but it is still challenging to get well-trained convolutional layers due to little diversity between the original and generated datasets. In the literature, there are two ways recorded to enhance the model performance with a smaller dataset which are Generative Adversarial Network (GAN), and another is transfer learning [91]

Recently, different researchers proposed the concept of transfer learning on a smaller dataset. For example, N. Kaiser et al. [92] proposed new architecture that can take all four views of single patients to classify MBD into two-class classification (dense and non-dense). For this purpose, the author proposed four-channel VGG-Net architecture to extract all the features with average global pooling from input mammograms. Before the classification layer, to concatenate all the input layer features, two dense layers are used. Then, the proposed model is trained with 5-fold cross-validation and recorded 88% classification accuracy with an AUC of 0.954. Finally, subjective assessment is done with a panel of 32 radiologists to compare inter-observer variability. In this approach, inter-observer variability for breast density assessment is observed even higher in two-class classification. Thus, the automated processes for MBD can help to

minimize inter-observer variability.

Despite different automated approaches, MBD assessment is subjective and consists of intra and inter-observer variations. Objective evaluation of other commercially viable methods consists of mixed evaluation results. Another fundamental limitation is that mostly all 'state-of-the-art deep learning' methods need a larger dataset and validated density ground truth; hence, data acquisition becomes difficult for researchers. In addition, mammographic images are vendor-specific, making deep learning more robust; training the deep learning model through different vendor-specific samples is required, another bottleneck in MBD classification. All the limitations are mentioned in the above result in moderate objective MBD classification accuracy.

Remaining some of the 'state-of-art deep learning' approaches are presented in tabular form with help of Table- 2.14.

Table- 2.14 Summary of literature review for deep learning modelling.

Details of journal/ website	**Year**	**Indexing Journal**	**Main findings relevant to proposed research work**	**Remarks**
Medical Image Understanding and Analysis/ http://130.203.133.150 [93]	2002	Scopus	Feed forward Artificial Neural network (ANN)	Average recognition rates on two class and four class are 96.7% and 71.4% Respectively.
'IEEE Transactions on Medical Imaging. https://doi.org/10.1002/1097-0142.' [94]	2016	SCI	Convolutional architecture and sparse auto encoder	AUC of 0.61
'Academic Radiology/ https://doi.org/10.1016/j.acra.2017.12.025'.[95]	2018	SCI	Deep CNN	Pattern Generations in texture feature map into CNN
IEEE Conference *ICCTA 2018*. https://doi.org/10.1109/CATA.2018.8398679. [96]	2018	SCI	Image features generated and which is applied to ANN	Moderate accuracy
'Medical Physics/	2018	SCI	Deep convolutional	Results as compare to

https://doi.org/10.1002/mp.12763'. [97]			neural network	existing state of art system LIBRA.
'Medical Physics/ https://doi.org/10.1002/mp.12683.' [98]	2018	SCI	Deep convolutional neural network	AUC of 0. 9421
'British Journal of Radiology https://doi.org/10.1259/bjr.20180691'. [99]	2019	SCI	Deep convolutional neural network (DCNN).	Classification accuracy of 71.7% for MLO and of 71.0% for CC.
'Journal of Digital Imaging/ https://doi.org/10.1007/s10278-019-00244-w.' [100]	2019	SCI	Deep convolutional neural network	Results of this method are not optimized level due to use of less Image dataset.
'Cancer Imaging/ https://doi.org/10.1186/s40644-019-0227-3.' [101]	2019	SCI	Transfer learning concept	AUC =0.65) and Correct Classification accuracy was 75.2%.
Academic Radiology https://doi.org/10.1016/j.acra.2018.06.020 [102]	2019	Scopus	CNN architecture	Overall accuracy of 72%
International Conference on Bioinformatics Models, Methods and Algorithms, [103]	2019	Scopus	Residual convolutional network	four standard classes accuracy =78% and two class accuracy =89.4%

2.7.3 Survey of Statistical Modelling

Even though very less research materials are available on this approach, it is also one of the significant area of research for breast density calculation. Another Approach density estimation using progressive elimination method was proposed by Indra kanta et al. [104] in which lower intensity bands in individual phase by means of well-known statistical approach known as local standard deviation (LSD) values are applied to recognize significant transition and to separate most substantial transitions. This

approach reduces computational complexity but consist of an accuracy of 73.91% and linear weighted Cohen's kappa coefficient k=.0673. Author Devi S.S. et.al. [105]. Proposed Statistical features extraction followed by SVM algorithm for classification on Mini-Mias data set ended up with an average accuracy of 89.7% which can be further enhanced by amalgamation of diverse feature extraction and classification approach. Literature review for statistical modelling is presented in Table-2.15.

Table- 2.15 Summary of literature review for Statistical modelling.

Citation number/year	**Authors**	**Statistical model**	**Accuracy**	**Merit/Demerit**
[**104**]/2013	Indra kanta et al.	local standard deviation (LSD) to isolate most significant transitions	Accuracy of 73.91% and Cohen's kappa coefficient k=.0673.	Reduces computational complexity
[**105**] /2018	Devi S.S. et.al.	Statistical features extraction followed by SVM	average accuracy of 89.7%	Further improved by combination of different feature extraction

2.8 Summary

As per the literature survey, different authors have different approaches for breast density calculation. If we compare all strategies on classification accuracy level, there are many variations in the results from 78% to 95%. Figure-2.8 depicts the classification accuracy variations of all the reviewed state-of-art methods.

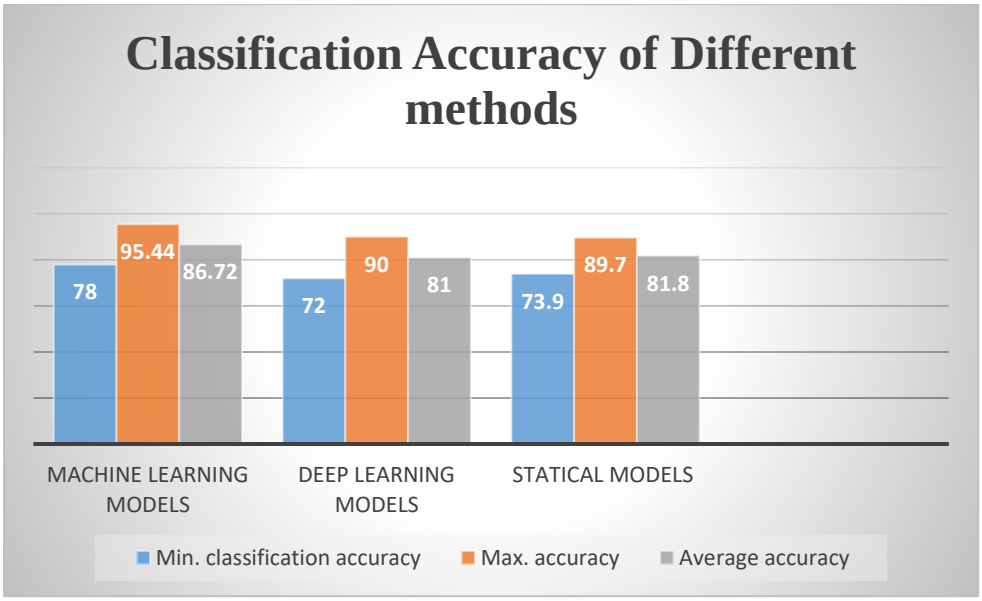

Figure- 2.7 Variation in Classification accuracy in different surveyed model

This variation in classification accuracy and status of commercial equipment shows a need for an accurate and reliable method that will be helpful for the clinical application of mammographic breast density.

In the USA, breast density notification to the individual patient after mammography screening is mandatory in 30 states [42]. In the future, it becomes the social need of all the countries to know breast density and its correlation with breast cancer risk and requires supplementary screenings. Hence, future research needs to reduce inter-reader variations and provide a most reliable and accurate clinical application to predict breast cancer in advance.

The research paradigm of breast density has changed from area to volume and it is gaining more attention towards the machine and deep learning algorithms from the last few years. Artificial intelligence can learn complex features of objects [43-44] and is beneficial for both volumetric and area-based density measurement. Hence, there are many deep learning and machine learning-based innovations that are under clinical trials. These models are use two-class or four-class classification by using convolutional neural networks models. The deep learning model consists of five to six convolutional layers, three connected layers, and the SoftMax function for classification. In addition, specific modification is going on in terms of RELU,

hyperbolic tangent function. Simultaneously, there is another path for research innovations under feature extraction, segmentation, and dimension reduction for machine learning classifications. These modifications surely will help to make breast density measurement more objective than subjective. In the future, these modifications acts as screening tools for breast cancer risk prediction [45].

Even though there are many automated clinical applications in the market for MBD classification, these applications have advantages like faster in processing, cost-effectiveness, and more objective but do not provide optimal results. Nevertheless, some effective observations recorded during this study may be helpful to decide the future path of research in breast density measurement.

1. There are three basic approaches for breast density measurement: area-based, volumetric-based, and now deep learning.
2. All the MBD assessment tools are uses the attenuation and absorption characteristics of the actual breast tissue and then compared with the physical breast tissue.
3. Different manufacturers perform digital mammograms at different clinical environments with the help of different proprietary algorithms and different imaging parameters, which will change the contrast of each mammogram, which may be one of the causes of error in breast density measurement.
4. Assessment of three-dimensional breast density from two-dimension mammograms is a challenging task.
5. Compression of the breast during mammography is one of the critical causes to hamper the results of area-based density.
6. Volumetric breast density is another good option to increase measurement reliability, used by different manufacturers like Volpara, Quantra, etc.
7. There is no external or absolute ground truth for validations and standard datasets of different countries for validations.

   In the future, Artificial intelligence can learn complex features of mammograms and will provide more reliable breast density classification tool for breast cancer prediction.

CHAPTER-3
PROBLEM FORMULATION

3.1 Overview

This chapter provides the research objectives of the proposed research work. These objectives are appropriately formed to address the research gap identified with an extensive literature survey of the intended research area. Methodological steps and work environment is also explained to achieve the proposed research objectives.

3.2 Research Gaps

Mammographic breast density has created much more interest and debate amongst breast radiologists and researchers in the past few decades. Breast density classification is an essential part of breast cancer screening. As MBD is strongly associated with increased risk of breast cancer also a dense breast involves a higher risk of masking cancer. This will be also the primary cause a reduction of mammographic sensitivity. Also, from significant and updated literature reviews, the following are the critical research gaps or issues observed in breast density classifications.

1. The current breast density classification is qualitative with the help of expert radiologists as per guidelines of BIRADS categories, which consist of limitations of substantial inter-and intra-reader variations; and hence it is subjective [106].
2. Different commercial software have been available for quantitative breast density measurement in recent years. But an additional study shows that the difference between two commonly used commercial software (Quantra and Volpara) and radiologist's assessment of BI-RADS density categories was as significant as 14% in the classification of women with dense breasts. The comprehensive agreement measured by weighted kappa statistics was moderate ($0.4 < kappa < 0.6$), even though they are standard in current clinical practice [107].
3. As per the literature review, many deep learning algorithms and handcrafted algorithms [37-58] are used for breast density classifications like

thresholding, clustering, active contour, watershed, graph-cut, etc. The primary motivation behind these algorithms is segment the fibro glandular tissue of the breast from the entire breast. Distinguishing features extracted from segmentation are either classified into two-class or Four-class classifications. But significant variations in breast density are estimated by different methods shown in the Figure-3.1 which lead to uncertainty in decision-making when density is used for risk-based cancer screening.

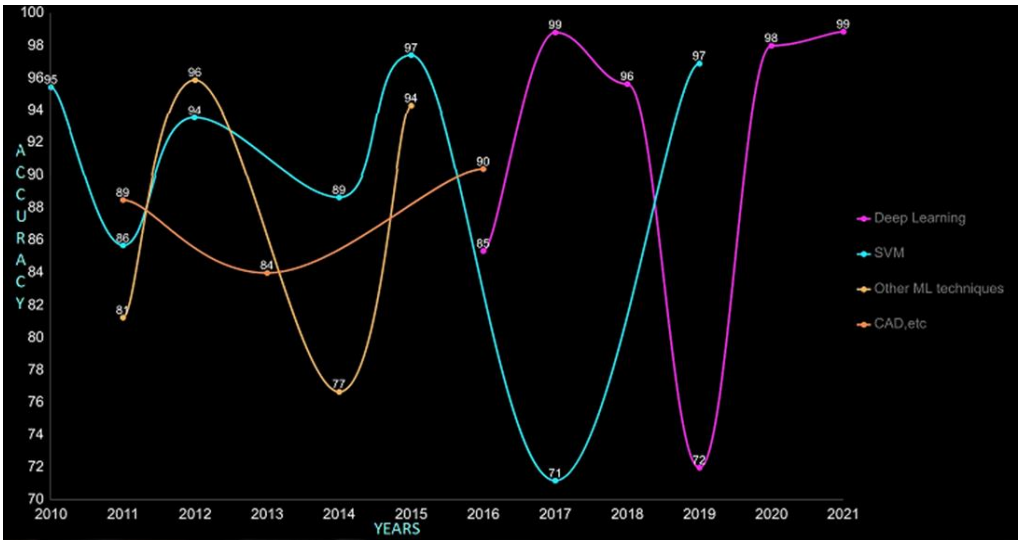

Figure- 3.1 Variation in classification accuracy of different state-of art methods

4. The Convolutional Neural network (CNN) has gained immense importance for breast histopathological image density classifications in recent years. CNN is many advantages over the handcrafted feature extraction technique. CNN extracts features automatically. Even though CNN has got less attention in medical imaging due to the lack of availability of public datasets [108].

3.3 Problem Formulation

From the substantial literature survey, we can put the hypothesis that there is still a research gap in the design and development of the system for automatic breast density classification**.** Many commercial methods are available for classifying the breast density but do not consist of a deep learning approach, hence lacking flexibility and robustness of learning models. Therefore there is still an unmet social and clinical need to have precise and accurate automated breast density assessment based on learning

directly from data. The essential focus will be an attempt to increase the accuracy and consistency of breast density classification. Hence, our basic objective behind this research topic is to

Design and Development of Novel Algorithm for Mammogram Classification for Breast Cancer Detection.

3.4 Specific Research Objectives

Basic problem definition having following specific objectives which are the direction of our proposed research work.

1. Analysis of Existing Algorithms for Mammogram Density Measurement
2. Study and analysis on different pre-processing and classification algorithms.
3. To propose a novel algorithm for mammogram classification.
4. Comparison of proposed method with other existing techniques

3.5 Research Work Plan

To carry out proposed research, work plan undertaken is divided into four subsections which are as follows:

1. Extensive literature survey
2. Implementation of some existing algorithms.
3. Design and development of novel algorithms for pectoral muscle segmentation and mammographic breast density classification.
4. Validation of proposed algorithms with existing state-of-art algorithms.

Graphical abstract of research work plan is illustrated in Figure 3.2.

Figure-3.2 Graphical abstract of proposed research work

3.6 Research Methodology

Recently, deep learning algorithms provide state-of –art solutions for various computer vision applications, hence in our proposed work, we proposed the multichannel Dense-Net architecture for classification of mammographic images into four BIRAS density class. The proposed methodology is implemented into two steps:

1. Preprocessing and segmentation of digital mammogram
2. A novel algorithm for MBD classification

Generalized block diagram of research methodology is depicted in Figure- 3.3

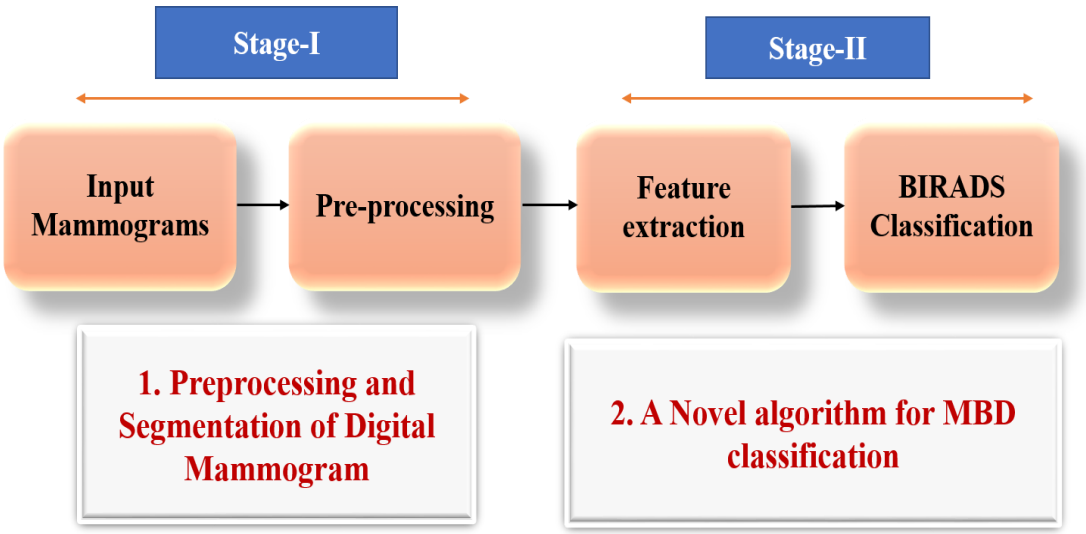

Figure-3.3.The proposed methodology to achieve specific objectives

3.6.1 Preprocessing and Segmentation of Digital Mammogram

Breast density calculations is based on the opacity of fibro-glandular tissue displayed on digital mammograms involving the whole area of the breast. The ambiguity of pectoral muscle and fibro-glandular tissue is comparable; hence, the slight appearance of the pectoral muscle in the breast region can hamper the precision of breast density classification. Successful elimination of pectoral muscle is stimulating due to changes in shape, size, and texture of pectoral muscle in every MLO and LMO view of the mammogram. In this step, the depth-first search (DFS) algorithm with and without heuristic approach is proposed to eliminate artifacts, noise and pectoral muscle from digital mammograms. Highlights of proposed DFS algorithm are as follows:

- The heuristic approach of depth first-search algorithm (DFS) for removal of the pectoral muscle.
- A novel seed selection mechanism.
- A numerical comparison of automatic versus manual segmentation conducted on each BIRADS density class.
- Results are validated subjectively by expert Radiologists and objectively by Jaccard Index and Dice similarity coefficient.

3.6.2 A Multichannel Dense-Net Architecture for MBD Classification

Mammographic breast density is one of the most significant risk markers, and it is assessed visually with the support of radiologists with four qualitative BIRADS categories. It is a challenging task for Radiologists to distinguish the two most variably assigned BIRADS categories, which are "Scattered density" and "Heterogeneously dense." Recently, *c*onvolution neural networks have been found superior in classification tasks due to their ability to extract local features with shared weight architecture and space invariance characteristics. This proposed work aims to investigate a deep learning-based density classifier for the classification of BIRADS density classes, aiming at a potential computerized tool to assist radiologists in classifying the BIRADS category in the current clinical flow. This article proposes *a* Multi-channel Dense-Net architecture for MBD classification. The proposed architecture consists of four-channel Dense-Net transfer learning architecture to extract

the significant features from two MLO and two CC view mammograms of a single patient.

Highlights of proposed multichannel architecture are as follows:

- Multi-channel Dense-Net architecture for mammographic breast density classification.
- Classifier performance is evaluated with 800 digital mammograms with different BIRADS density classes.
- Results are validated subjectively by expert Radiologists and objectively by classification accuracy and AUC.

3.6.3 Work Environment

A segmentation algorithm for pectoral muscle removal was implemented in python while the experimentally proposed multichannel architecture is trained and tested on the Pytorch framework on Google Colaboratory, which is a free online cloud-based Jupiter notebook environment.

1. Python
2. Keras
3. Tensor Flow
4. PyTorch

Work environment used for the proposed research activity is shown in Figure- 3.4.

Figure-3.4 Work environment used for the proposed methodology

3.7 Resource Datasets

The commonly used different public data set are available which are Mini-Mias and INBreast and DDSM.

3.7.1. Mini-Mias dataset

The Mammographic Image Analysis Society (MIAS) is an organization of UK research groups interested in the understanding of mammograms and has generated a database of digital mammograms. Films taken from the UK National Breast Screening Programme have been digitized to 50 micron pixel edge with a Joyce-Loebl scanning microdensitometer, a device linear in the optical density range 0-3.2 and representing each pixel with an 8-bit word. The database contains 322 digitized films and is available on 2.3GB 8mm (Exabyte) tape. It also includes radiologist's "truth"-markings on the locations of any abnormalities that may be present. The database has been reduced to a 200 micron pixel edge and padded/clipped so that all the images are 1024x1024. Mammographic images are available via the Pilot European Image Processing Archive (PEIPA) at the University of Essex.

3.7.2 AMDI-Indexed atlas of digital mammograms Dataset

AMDI provides a tool that enables the user to download cases from the mammographic database, so as to make the information available to authorized medical and research communities interested in breast cancer diagnosis. The mammographic database was projected to include cases with all of the available mammographic views, radiological findings, and diagnosis proven by biopsy, the patient's clinical history, and information regarding the life style of the patient. Each exam of each case includes four views (two views of each breast: Cranio-caudal or CC, and Medio-lateral oblique or MLO). To address the teaching and research aspects, the database links each mammogram with the contour of the breast, the boundary of the pectoral muscle (MLO views only), the contours of masses (if present), the regions of clusters of calcifications and the number of calcifications (if present), and the locations and details of any other features of interest. The mammographic database also supports the inclusion of several mammographic exams of the same patient performed at different instants of time.

3.7.3 DDSM Digital Database for Scanning of Mammography dataset

The proposed work utilizes one publicly available dataset from Digital Database for Scanning of Mammography (DDSM) [109], consists of 2620 cases of different categories classified as normal, benign, and malignant cases with verified pathology information. This database consists of each patient case with MLO, LMO, Left CC, and Right CC. The proposed algorithm uses 1338 MLO and 1337 LMO views from normal, benign, and malignant cases. To develop good quality ground truth of the pectoral muscle, the boundaries of pectoral muscle of each MLO and LMO views are manually drawn by the team of three expert radiologists individually. These manual contours are further used as a ground truth for the proposed study. Some sample copy of ground truth marking are depicted in Figure.3.5.

Ground truth is marked by using labeling software on laptop by the radiologist for faster work. These ground truth images are further divided into four BIRADS density classes as class A, B, C, and D. All LMO views are rotated such that the chest wall location, which consists of the pectoral muscle, remains on the left side of the image. The total input image samples belong to different BIRADS density classes are shown in Table-3.1.

Table- 3.1 Input dataset used for testing of the proposed algorithm

BIRADS Density Class	**Number of images**
Class-A	359
Class-B	1043
Class-C	698
Class-D	575
Total	2675

Total 2675 images are used for this study. In Table-3.1, the first column shows BIRADS density class and second column shows the number of images belongs to the respective class in each row.

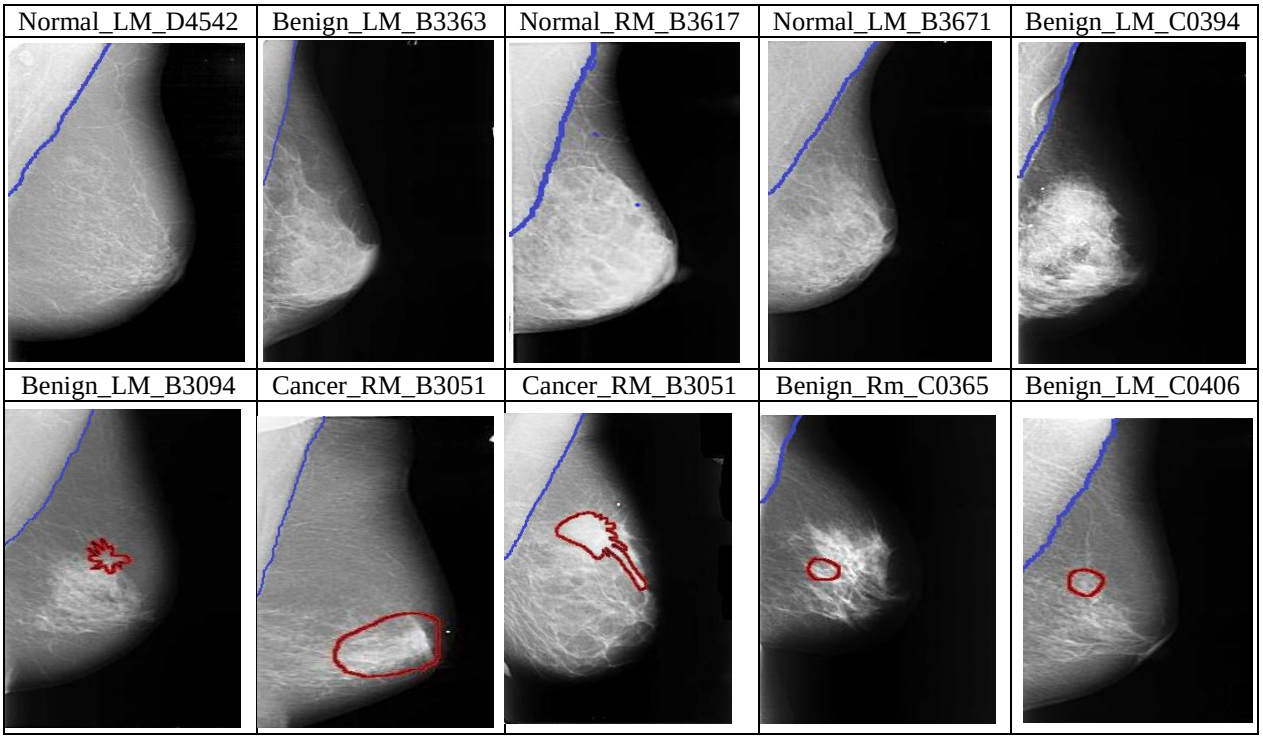

Figure- 3.5 Ground Truth marking of some input images

3.8 Dataset for Multichannel Architecture

The proposed algorithm uses 200 MLO, 200 LMO, 200 R_CC, and 200 L_CC views from normal, benign, and malignant cases. Total 800 mammograms are used in the proposed study and divided into four BIRADS density classes: class A, B, C, and D. Each density class consists of 200 cases in four images (MLO, LMO, R_CC, and L_CC). Table-3.2 presents the details of the dataset used in the proposed study.

Table- 3.2 Input dataset used for testing and validation of Multichannel algorithm

BI_RADS Density Class	**Number of images**
Class-A	200
Class-B	200
Class-C	200
Class-D	200
Total	800

The sample of Input images for preprocessing and input images used for classification algorithms are depicted in the Figure- 3.6 (a) and 3.6 (b).

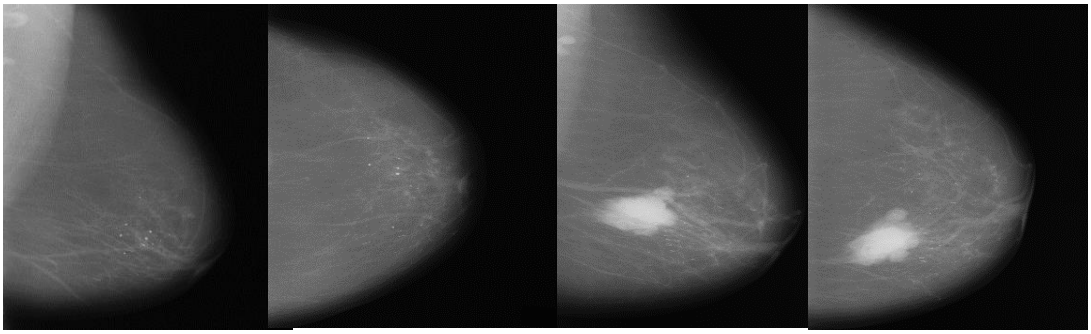

(a) (b) (c) (d)

Figure- 3.6 (a) Input raw images used for preprocessing (a) Left _MLO (b) Left_CC (c) Right_ MLO (d) Right_ CC

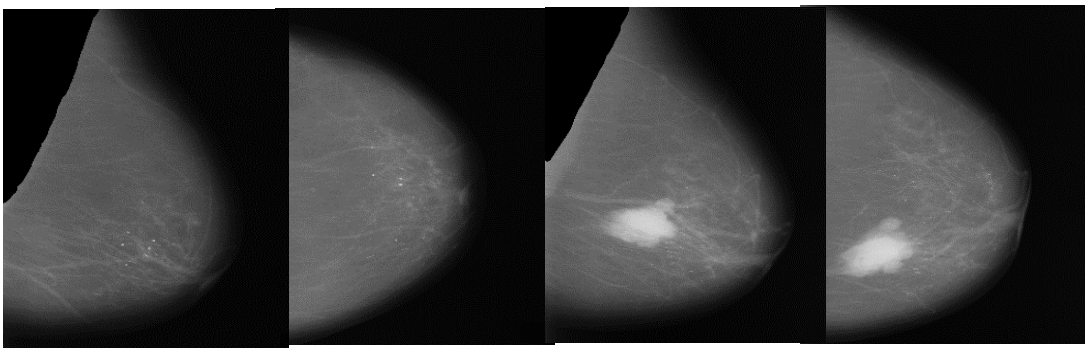

(a) (b) (c) (d)

Figure- 3.6 (b) - Output images after segmentation and cropping used as a input images for classification (a) Left_MLO (b) Left_CC (c) Right_ MLO (d) Right_ CC

CHAPTER-4

PRE-PROCESSING AND SEGMENTATION OF DIGITAL MAMMOGRAMS

4.1 Overview

This chapter describes the experimental work performed to satisfy the Preprocessing and segmentation of pectoral muscle research objectives. This chapter describes the primary purposes behind the preprocessing algorithm. This chapter describes the experimental work carried out with a Depth-first search algorithm with and without a heuristic approach. And explains the importance of seed selection mechanism and with working and computational complexity analysis of proposed algorithm.

The primary reason to use DFS algorism is that it is less utilized in state-of-art breast cancer detection and provides constant search. DFS visits all the vertices in the graph. This type of algorithm always chooses to go deeper into the graph. After DFS has visited all the reachable vertices from a particular source, it chooses one of the remaining undiscovered vertices and continues the search. DFS reminds the space limitation of breadth first search by consistently generating next a child of the deepest unexpanded nodded. This property helps find pectoral muscle as a single connected component and requires less memory space and better time complexity.

4.2 Basic Objectives behind Proposed Algorithm

The opacity of pectoral muscle and fibro-glandular tissue is almost the same, and artifacts have high-intensity marks on mammograms. The small presence of these areas in the breast can reduce the accuracy of breast density classification [110-111]. The primary objectives behind the proposed DFS algorithm undertaken are as follows.

- To remove artifacts and labels on the background region
- To detect the breast tissue region from the background
- To detect and suppress the pectoral muscle

- To test the results of DFS with some additional Heuristics
- To analyse the performance of the proposed algorithm
- To compare the results of the proposed algorithm with state-of-art methods.

Block diagram of proposed Depth-First search algorithm with heuristic approach is depicted in Figure-4.1

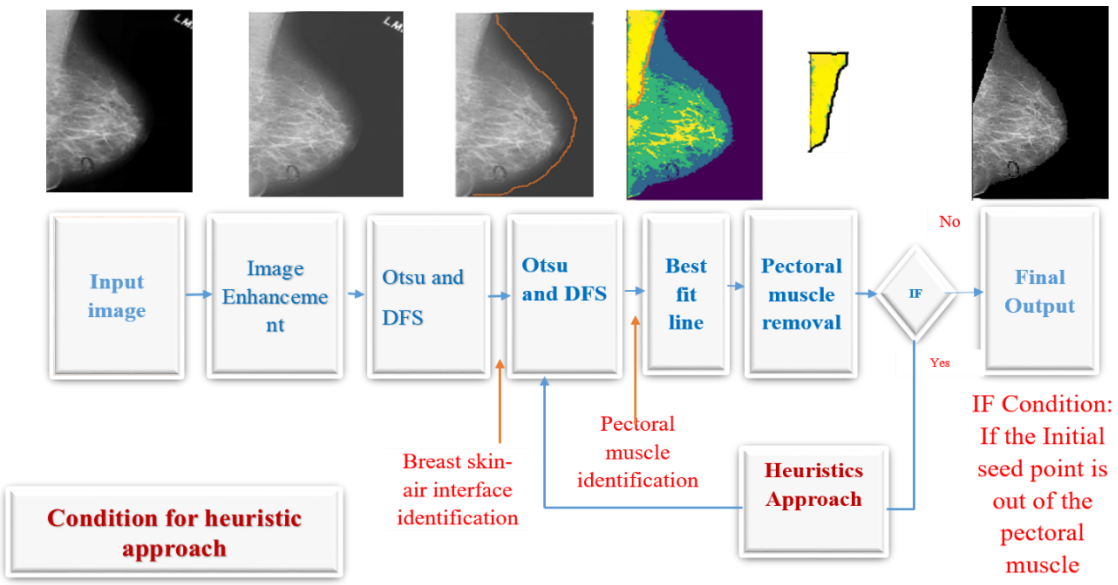

Figure- 4.1 Block diagram of Depth-first search algorithm with heuristic approach

Description of each and every block inside the proposed algorithm are described as below:

4.3 Input Resource Dataset

This algorithms uses input images of each patient case with MLO, LMO, Left CC, and Right CC. The proposed algorithm uses 1338 MLO and 1337 LMO views from normal, benign, and malignant cases. To develop good quality ground truth of the pectoral muscle, the boundaries of pectoral muscle of each MLO and LMO views are manually drawn by the team of three expert radiologists individually. These manual contours are further used as a ground truth for the proposed study. Detailed description of dataset is given in previous chapter.

4.4 Contrast Enhancement

Digital mammography acts as a unique screening technology protecting the lives of females against breast cancer for the past few decades. Digital mammography provides all the advantages of digital image processing to enhance image quality, which can be further helpful for precise breast cancer diagnosis. Many techniques are recorded for processing digital mammograms, which are useful in Computer-Aided Detection (CAD) systems. The foremost step for pre-processing is the detection of the breast border and pectoral muscle. For breast border detection, breast skin-air interface segmentation is a complex task because the intensity of the edge of the breast is similar to the background. This will cause sub-segmentation of the breast part by converting pixels near the border into the ground. Contrast enhancement of the input image should be performed to reduce the noise and enhance visibility at the breast border. There are many clinical methods recorded in the literature to improve the background quality of the medical image. Some of the recorded ways are wavelet transform (W.T.), Histogram equalization, Adaptive histogram equalization (AHE). These methods consist of limitations in terms of processing time and noise reduction [112-114]. Another approach suggested in the literature is the unsharp masking method (USM). This method limits global contrast and enhances local contrast inside the image [115]. The basic demerit of this method is that it creates artifacts inside the image, making the output image look artificial. Due to this reason, this technique is not suitable for the enhancement of medical images. Adaptive contrast enhancement (ACE) uses contrast to gain adjustment for the high-frequency component of the image, but this method takes a long time for pre-processing [116].

The proposed algorithm performs contrast enhancement with AGCWD (Adaptive Gamma Correction with Weighting Distribution) offered by [117-118]. This author provides a new technique for adjusting the histogram with a fusion of gamma correction and histogram equalization. Equation-4.1 describes gamma correction.

$$T(l) = l_{max}\left(\frac{l}{l_{max}}\right)^{\gamma} \tag{4.1}$$

Where l_{max} is max. Intensity of the input image and γ is an adaptive parameter. Intensity value l of the image becomes $T(l)$ after gamma correction, Equation-4.2 defines histogram equalization.

$$T(l) = F(l).l_{max} \tag{4.2}$$

$F(l)$ is the cumulative distribution function calculated based on the probability distribution function f, the probability density function f is defined by Equation-4.3.

$$f(l) = \frac{n_l}{n_{tot}} \tag{4.3}$$

Where n_l the number of pixels with intensity is value l and n_{tot} is the total number of pixels in the image. Equation-4.4 calculates the cumulative distribution function.

$$F(l) = \sum_{K=0}^{l} f(k) \tag{4.4}$$

Authors in [118] proposed an adaptive gamma correction (AGC) based on the modified cumulative distribution function is described by Equation-4.5

$$T(l) = l_{max}(\frac{l}{l_{max}})^{\gamma(l)} = l_{max}(\frac{l}{l_{max}})^{1-F_w(l)} \tag{4.5}$$

This technique increases the value of pixels of low intensity while avoiding significant degradation of high-intensity pixel values. The introduction of weighing distribution (W.D.) somewhat modifies the statistical histogram and reduces adverse effects. Equation-4.6 defines a weighting distribution function

$$Fw(l) = f_{max}(\frac{f_{(l)} - f_{min}}{f_{max} - f_{min}})^{\propto} \tag{4.6}$$

Where $\propto$ is the adjusted parameter, f_{max} and f_{min} are the maximum and minimum values of probability density function.

The fundamental merit of this method is that exceptionally dark and light points are not affected by mid-tones due to the non-linear function of the proposed method. Due to this, breast border pixel intensity can be identified more precisely, which further helps to widen the breast border. This method reduces the noise at the breast skin air interface and background, enhancing the visibility at the breast border, which further helps to get a delicate breast border. The contrast-enhanced version of the input image is depicted in Figure-4.2.

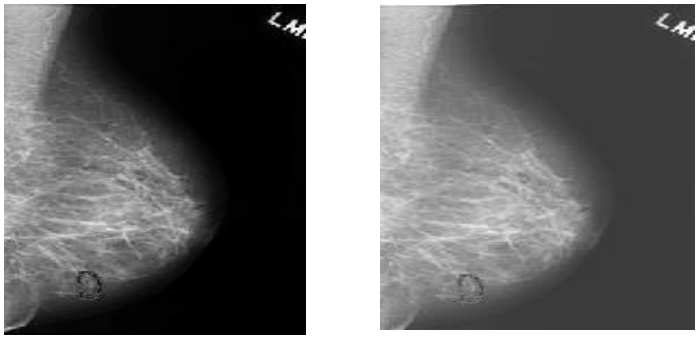

(a) (b)

Figure-4.2 Image enhancement (a) Input image (unclear breast skin air interface) (b) Enhanced image. (Enhancement in the visibility of skin air interface)

4.5 Breast Border Detection

Output Image obtained from the previous stage Figure-4.2 (b) is used for breast border detection. Local thresholding is performed with four class Multiotsu thresholding to find the initial seed for the depth search algorithm. This algorithm optimizes the variance between the classes. Each class acts as a distinct class with respect to the intensity values of their pixels. Proposed method uses four classes (C_1, C_2, C_3, and C_4) for thresholding. Equation-4.7 gives the concept of between-class variance.

$$\sigma^2{}_B = \sum_{k=1}^{K} P_k (M_k - M_G)^2 \quad (4.7)$$

$$\text{Where } P_k = \sum_{i \epsilon ck} P_i$$

$$\text{and } M_k = \sum_{i_{\epsilon ck}} iP_i$$

Where $\sigma^2 B$ variance of the class,

P_k is the probability of the class while

M_k is value of pixel in the group and

M_G is mean value of pixel in individual group

The results of thresholding are illustrated in Figure-4.4 (b). Specific observations are performed with different image samples to select the initial seed. After detailed observations, the image pixel point (150, 20) is identified as an initial seed that will always remain inside the breast and pectoral muscle.

4.6 Working of DFS Algorithm

A depth-first search algorithm is a blind search that ensures all the vertices have been visited. The essential merit of this algorithm is to find vertex or nodes that have not been visited in-depth and decomposing directed graph into the strongly connected component. The first linear-time algorithm for the connected component was proposed by Tarjan et al. [119].

In any given graph, G = (V, E), where V stands for vertices and E stands for the set of edges in the given directed graph. A vertex u ϵ V, during exploration of each vertex. There are two techniques to represent the graph which are by link list and by matrix. Link list presentation provides better space complexity than the matrix form; hence, the proposed algorithm uses a link list approach to avoid space complexity. One of the classic applications of the depth-first search algorithm is the decomposition of the directed graph into a strongly connected component. A strongly connected component of the graph consists of different classes of the object. A strongly connected component (SCC) of any graph is a maximal set of the vertices C, that is the subset of V. In other words, two vertices of the directed graph are in the same component if they can be connected to each other.

A straightforward demonstration of the execution of the depth-first algorithm on the input graph is depicted in Figure-4.3.

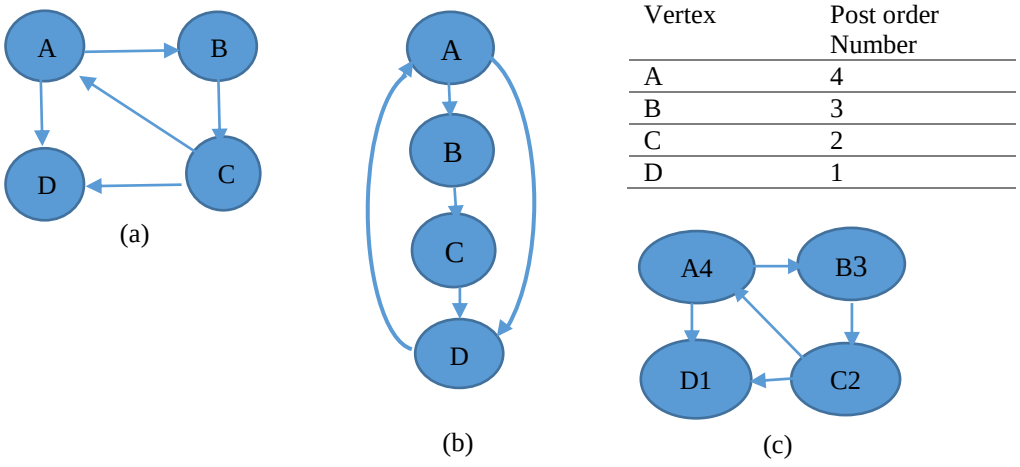

Figure- 4.3 Application of DFS towards decomposition into the single connected component. (a) Input graph (b) Depth-First search (c) Reverse Graph to identify single connected component

In the first step of execution, DFS generates a tree which is shown above in Fig.4.3 (b). Connection from C to A indicates the back edge inside the graph. During post-order traversal, this tree gives D, C, B, and A. The graph is reversed by assigning the same post-order numbering shown above in Figure- 4.3(c). When DFS is performed on a reversed graph, DFS starts with node A and then goes to node C and then B. DFS does not move ahead at position B, indicating (A, B, C) are strongly connected components, and the second DFS ends at the D node itself. Hence, single connected components on this graph are (A, B, C) and (D).

In the proposed algorithm, after initial seed selection, a depth-first search is performed from the initial seed point till the threshold value is non-zero. This procedure provides a single connected component as a breast tissue illustrated in Fig.4.4(c). After breast tissue identification, all the tags and artifacts are removed from the background to improve image quality, shown in Figure.4.4 (d).

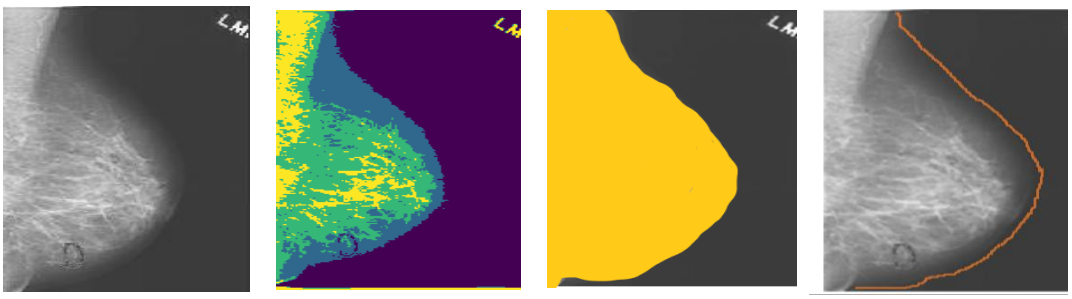

(a) (b) (c) (d)

Figure-4.4 Breast border detection (a) Input mammogram (b) Multiotsu thresholding (four class) (c) Breast as a single connected component (d) Breast border detection and artifacts removal

4.7 Initial Seed Selection

Output images from the previous stage (Figure-4.4 (d)) are used for pectoral muscle removal. Multi-Otsu thresholding is used again to identify the exact location of the pectoral muscle on the output image. In almost all the images, pectoral muscle is found in the first region of thresholding, but the range of pixel values changes in each image.

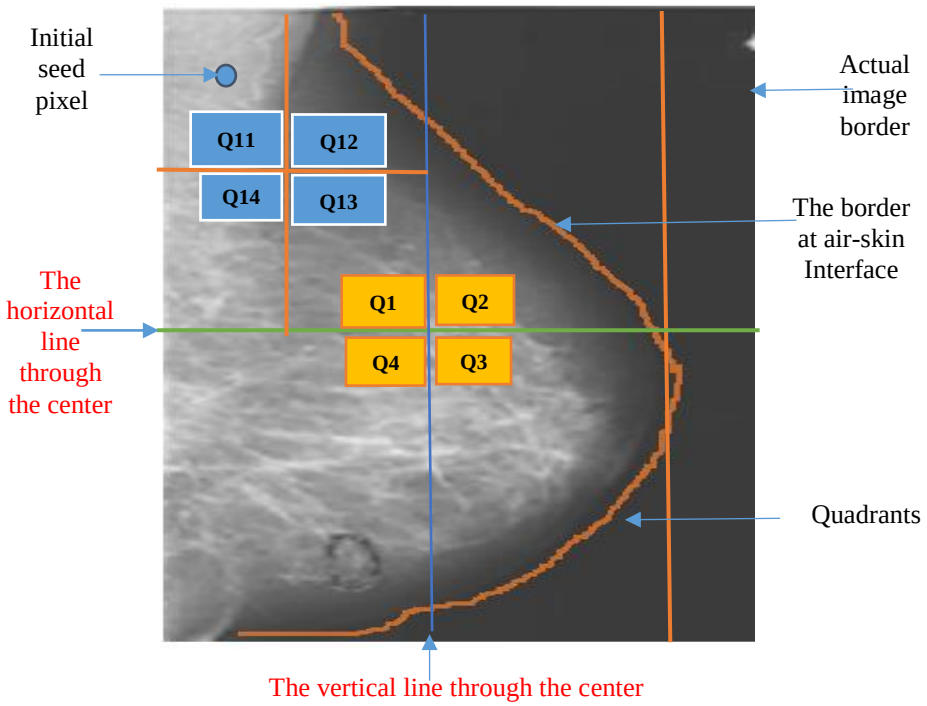

Figure- 4.5 A dynamic seed selection mechanism

In order to provide the initial range for DFS, a dynamic seed selection mechanism is incorporated in the proposed algorithm, which is described as follows.

1. Mammogram width is finalized with respect to the air-skin interface of the breast.
2. Image is divided into four quadrants as Q1, Q2, Q3, and Q4 in a clockwise manner.
3. Quarter Q1 is again divided into four quadrants as Q11, Q12, Q13, and Q14.
4. Seed pixel is selected from the midsection of the Q11 quadrant, which is depicted in Figure-4.5.

4.8 Pectoral Muscle Removal Using DFS

After dynamic seed selection, the depth-first search algorithm is applied to each sample image from different BIRADS density classes. This algorithm searches 'deeper' in the graph to find connected components in the graph. Automatically, it starts at the initial seed point and explores a similar seed point as far as possible before backtracking. Thus, the DFS algorithm can solve the most extended path search problem. The search method of the DFS algorithm is depicted in Figure-4.6.

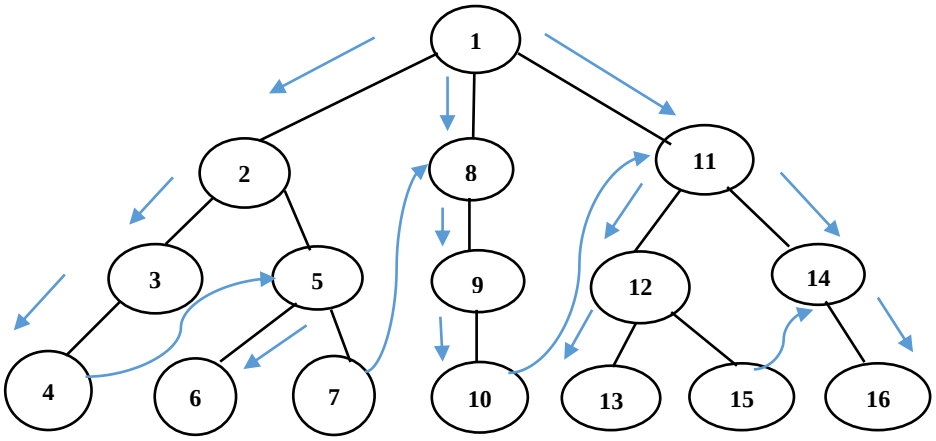

Figure- 4.6 Search method of depth-first search Algorithm

DFS starts from the initial seed point in the proposed algorithm and performs depth search to add similar neighbouring pixels as 4-connected neighbours until it fills a coherent region as a pectoral muscle. This process will run iteratively to find all the pixel points consisting of similar initial seed properties. This region growing process will produce a single part as a pectoral muscle from the whole breast area. Identification of pectoral muscle as a single connected component is illustrated in Figure-4.7 (a). The minimum threshold is selected from the identified pectoral muscle. All the pixel points above the minimum threshold value are removed as a pectoral muscle with the help of the best fit line, as shown in Figure-4.7 (b). The concept of dynamic seed selection and DFS works well on full images in all the BIRADS classes. The output of the DFS algorithm is shown in Figure-4.7(c).

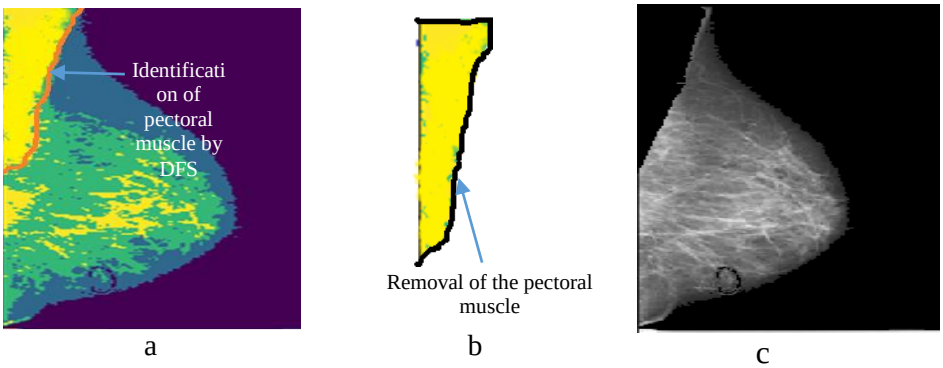

Figure-4.7 Results of DFS algorithm:)a) Identification of pectoral muscle (b) Removal of the pectoral muscle (c) Final output

4.9 DFS with the Heuristic Approach

In some cases, when the selected initial seed point is a part of the breast area instead of the pectoral muscle, then the proposed algorithm will remove a significant portion of the breast area, which causes over-segmentation and reduces segmentation accuracy, as illustrated in Figure-4.8 (b). Fundamental issues behind this over-segmentation are.

1. Absence of pectoral muscle in some input mammograms.
2. A tiny area of the pectoral muscle.
3. Overlapping boundaries between breast and pectoral muscle.

The proposed algorithm performs additional statistical measures to overcome the problem of over-segmentation known as the Heuristic approach. This approach is used to evaluate the circumstances of individual issues to obtain the desired solution. This approach is designed on experiments based on intuition. Unfortunately, the dynamic seed selection approach performs over-segmentation in some cases, reducing the proposed algorithm's segmentation accuracy. Hence, the ratio of the threshold of breast area after pectoral muscle removal and before pectoral muscle removal is calculated in successful cases and over-segmentation cases with Equation-8.

$$\frac{\text{Threshold of breast area after pectoral muscle removal}}{\text{Threshold of breast area before pectoral muscle removal}} < 0.4 \tag{4.8}$$

If this ratio is less than 0.4, then it is observed that the maximum breast area is removed and the primary cause of over-segmentation. In such cases, the heuristic approaches recursively modify the initial seed towards the left side of the input image until successfully removing the pectoral muscle. This modification in the initial seed point towards the pectoral muscle side is shown in Figure.4.8(c). Therefore, this heuristics approach provides the correct segmentation result for failure cases (over-segmentation) of DFS. The outcome of the failure case of DFS Figure.4.8 (b) is rectified by the heuristic approach of DFS, depicted in Figure-4.8 (d).

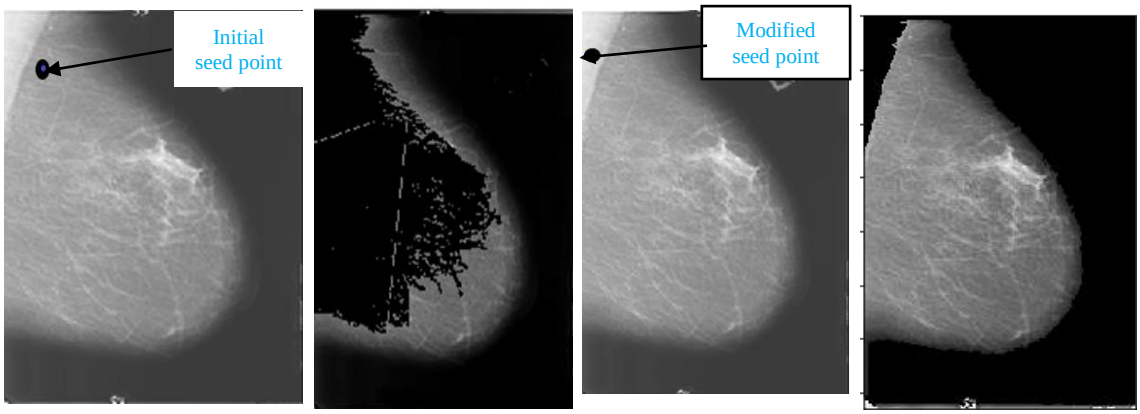

(a) (b) (c) (d)

Figure-4.8- Over segmentation problem of DFS algorithm and modification in results with heuristic approach (a)) Input image with initial seed (b) Over-segmentation of DFS (c) Input image with modified seed (d) Heuristic approach output

4.10 Complexity analysis and merits of the proposed DFS algorithm

Complexity of proposed DFS algorithms are measured in terms of Time and space complexity

A. Time complexity

Time complexity is the function that describes the amount of time taken by the algorithm to execute the given input. Time taken to execute given input by any algorithm can be measured in terms of the number of memory accesses performed, inner loop execution time, and many parameters like language, computer hardware type, programmer's proficiency, optimization in the compiler, etc. In case of the proposed DFS algorithm, the graph is represented as an adjacency list where each node maintains a list of all its adjacent edges; hence, if V is the number of nodes and E is many edges in the graph. Then for each node, we have to discover all its neighbours by traversing its adjacency list just once in linear time. For such a directed graph, the sum of sizes of the adjacency list of the nodes is E., so the time complexity in the proposed algorithm is given by Equation -4.9

$$O(V) + O(E) = O(V+E) \quad (4.9)$$

In the proposed algorithm, it takes ***16 milliseconds*** to execute one input image.

B. Space complexity

It is a function that describes the amount of memory (space) taken by the algorithm to execute the input of a given algorithm. In the case of the proposed algorithm, we are maintaining a stack to keep track of the record of the last visited node; hence in the worst-case stack could take up to the size of the nodes in the graph, so the Space complexity of the proposed algorithm is O (V) which practically is very small.

C. Merits of proposed DFS algorithm over other preprocessing algorithm

Basic reason to select the DFS algorithm for preprocessing and segmentation of proposed research work are as follows:

- No techniques in the literature were found robust for pectoral muscle removal due to wide range and texture of pectoral muscle.
- The size and shape of the pectoral muscle are not similar in each mammogram; hence no standard algorithm is suitable for removing the pectoral muscle.
- The primary limitation of the region growing algorithm is a failure in initial seed selection hence providing less segmentation accuracy
- Deep learning models can act as the best alternative, but such models consist of high computational complexity, less stability, and need a larger dataset.

Hence, the fundamental focus of this DFS algorithm is to provide another alternative in terms of the graph search method towards the improvement of segmentation accuracy of the pectoral muscle removal from digital mammograms for breast density classification.

- **Fundamentals merits of proposed algorithm is**

1. Easy to implement
2. Less space complexity.
3. Novel approach for initial seed selection.
4. Novel heuristic approach for failure case of segmentation.
5. Works well on different size and shape of pectoral muscle.

DFS is also an important type of uniform search. DFS visits all the vertices in the graph.

This type of algorithm always chooses to go deeper into the graph. After DFS visited all the reachable vertices from a particular sources vertices and it chooses one of the remaining undiscovered vertices and continues the search. DFS reminds the space limitation of breath first search by always generating next a child of the deepest unexpanded node. The data structure stack or last in first out (LIFO) is used for DFS. One interesting property of DFS is that, the discover and finish time of each vertex from a parenthesis structure. If we use one open parenthesis when a vertex is finished then the result is a properly nested set of parenthesis.

CHAPTER-5

NOVEL MULTICHANNEL ARCHITECTURE FOR MBD CLASSIFICATION

5.1 Overview

Mammographic breast density is one of the most significant risk markers, and it is assessed visually with the support of radiologists with four qualitative BIRADS categories. It is a challenging task for Radiologists to distinguish the two most variably assigned BIRADS categories: "Scattered density" and "Heterogeneously dense." Recently, convolution neural networks have been found superior in classification tasks due to their ability to extract local features with shared weight architecture and space invariance characteristics. This chapter describes the proposed architecture that aims to investigate a deep learning-based density classifier to classify BIRADS density classes, seeking a potential computerized tool to assist radiologists in organizing the BIRADS category in the current clinical flow. The proposed architecture consists of four-channel Dense-Net transfer learning architecture to extract significant features from a single patient's two MLO and two CC view mammograms. The performance of the proposed classifier is evaluated using 200 cases consisting of 800 digital mammograms of different BIRADS density classes with validated density ground truth from a team of radiologists.

5.2 Why DenseNet?

Different scientific studies have revealed that digital mammograms' sensitivity strongly depends on the density class of the breast tissue. In dense breasts, the sensitivity of mammograms is as low as 63%, while in low-density breasts, it is a dramatic rise of 87%. Hence, patients with high-density breasts have to go for additional imaging like tomosynthesis, ultrasound, or breast MR to enhance cancer detection chances [120]. There are many semiautomatic and automatic approaches for measuring breast density proposed by different researchers from the last two decades. However, mammographic breast density (MBD) assessment is subjective, which is done by expert radiologists [121].

For an automatic objective assessment of MBD classification, different research efforts are in progress for the last few decades. The initial research direction focused on image processing techniques like area-based thresholding, region growing, and clustering algorithms. A significant step forward was the emergence of machine learning algorithms based on different hand-crafted image features extracted from the histogram, texture intensities, patterns, and image acquisition parameters [122]. Nowadays, deep learning algorithms provide yet another leap forward in MBD Classification. Deep learning algorithms can go substantially deeper and discover all significant features from the image. Due to improvements in system architecture and hardware, it is possible to train deep learning architecture intensely. This improvement makes deep learning architecture an excellent tool for medical image analysis. Many deep learning architectures like Le-Net, VGG19, Highway networks, Residual networks, and Dense-Net are recorded in literature [123-124].

Whenever, any deep learning network goes more profound, a new research problem occurs, which is the "vanishing gradient problem." Dense-Net (Dense convolutional network) provides unique insight to confirm maximum information flow amongst all the layers to solve the connectivity problem. This network directly connects all the layers with matching feature map sizes in feed-forward nature; hence, individual layer receives input from all previous layers and passes its feature map to all further layers. Thus, the Dense Net concatenate feature map passes through all subsequent layers instead of summarizing features like Res-Net. This concept introduces L (L+1)/2 connection instead of L connections, identifying a dense connectivity pattern [125].

The counter-intuitive effect of this connectivity pattern in Dense-Net architecture provides the following advantages

- Effective solution for gradient disappearance
- Consolidation in feature propagation
- Provision of feature reuse
- Significant reduction in training parameters
- Easy to train and offers better parameter efficiency.

Due to these advantages, it is good to use this model, which does not require pre-training to medical image classification.

The primary objective behind this research work is to investigate the use of multichannel Dense-Net architecture for MBD classification and analyze the proposed architecture compared with other state-of-art methods.

5.3 Input Dataset

The proposed algorithm uses 200 MLO, 200 LMO, 200 R_CC, and 200 L_CC views from normal, benign, and malignant cases. Total 800 mammograms are used in the proposed study and divided into four BIRADS density classes: class A, B, C, and D. Each density class consists of 200 cases in four images (MLO, LMO, R_CC, and L_CC). The sample of input images after preprocessing used for MBD classification are depicted in Figure- 5.1.

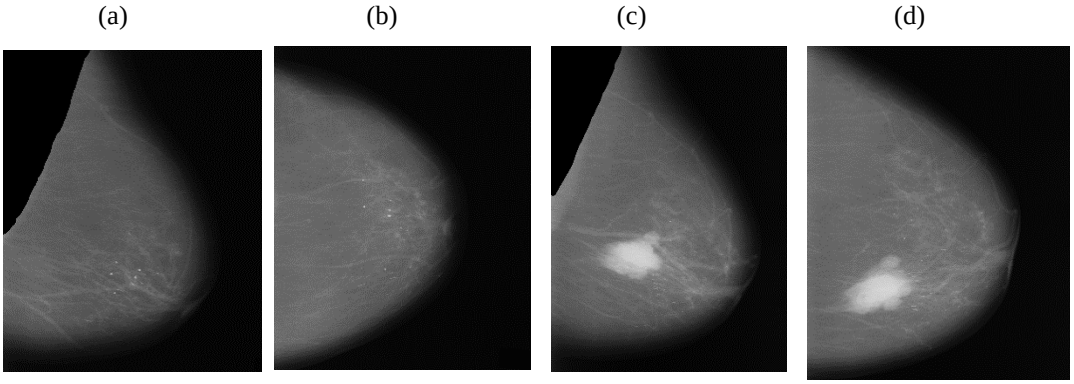

Figure 5.1 Input Images for Multichannel architecture (a) Left_MLO (b) Left_CC (c) Right_ MLO (d) Right_ CC

5.4 Contrast Enhancement

MBD classification is a function of the density of fibro glandular tissues inside the breast. Contrast enhancement helps to improve the visibility of fibro glandular tissues. Subsequently, it helps to improve the classification accuracy of deep learning models. In literature, there are many contrast enhancement methods recorded to enhance the quality of medical images. These methods are histogram equalization (HE), Adaptive histogram equalization (AHE), and Wavelet transform coefficients (WT) [126]. However, these recorded methods consist of an enormous processing time and are less effective in noise reduction. Another recorded method is the Unsharp masking method (USM) which enhances the local contrast inside the image by limiting the global contrast of the image. Still, this technique creates artifacts in the image. Due to this the

image looks artificial; hence it is not suitable for enhancement of the medical images.

Contrast to gain adjustment for the high-frequency component of the image is the basic principle behind adaptive contrast enhancement (ACE) but this consists of limitations in terms of high processing time [127].In MBD classification, local details are more important than global features and reduce processing time; the proposed architecture uses Contrast Limited Adaptive Histogram Equalization (CLAHE) algorithm for local contrast enhancement of fibro glandular tissues [128].

The first merit of this method helps to minimize the edge shadowing effect and noise produced in homogenous input digital mammograms. Secondly, small images known as tiles are used instead of the entire image to perform the CLAHE operation. Hence contrast enhancement of each tile histogram matches with exponential distribution or Rayleigh distribution. Furthermore, to reduce artificial induced boundaries neighbouring tiles are combined by bilinear interpolation.

The proposed CLAHE technique described below:

1. Initially, each input mammogram is divided into 8×8 non-overlapping contextual regions of equal sizes, and then a histogram of each contextual region is calculated.
2. The clip limit (β) is the threshold parameter used to alter the contrast of the image, which is calculated by Equation-5.1.

$$\beta = \frac{M \times N}{L}\left(1 + \frac{\propto}{100}\left(S_{max} - 1\right)\right) \tag{5.1}$$

3. Where β is the clip limit which is calculated as eight by different experiment, M×N is the number of pixels in each region, L is number of grayscales, α is a clip factor (0-100), and S_{max} is the maximum allowable slope which is set to be 4 for this experiment.
4. Each histogram is adjusted such that its height does not exceed more than the clip limit.
5. The transformation function described below, is used to modify the histogram.

$$t(r_k) = \sum_{j=0}^{k} p_r(r_j) \tag{5.2}$$

$$\text{Where} \quad p_r(r_j) = \frac{n_j}{n} \tag{5.3}$$

6. Equation-5.2 describes the probability function of input image gray scale value j, and n is total number of pixels in input mammogram image and n_j is the input pixel number of gray value j.
7. The neighboring tiles were combined using bilinear interpolation and the image grayscale values were altered according to the modified histograms.

In this method, the contrast factor is limited to 0.01to prevent over-saturation of the image, specifically inhomogeneous areas for optimized output. Furthermore, for contract enhancing transformations, the number of bins for the histogram building is limited to 64 over the uniform distribution. Figure-5.2 depicts the result of contrast enhancement of the CLAHE algorithm on input images.

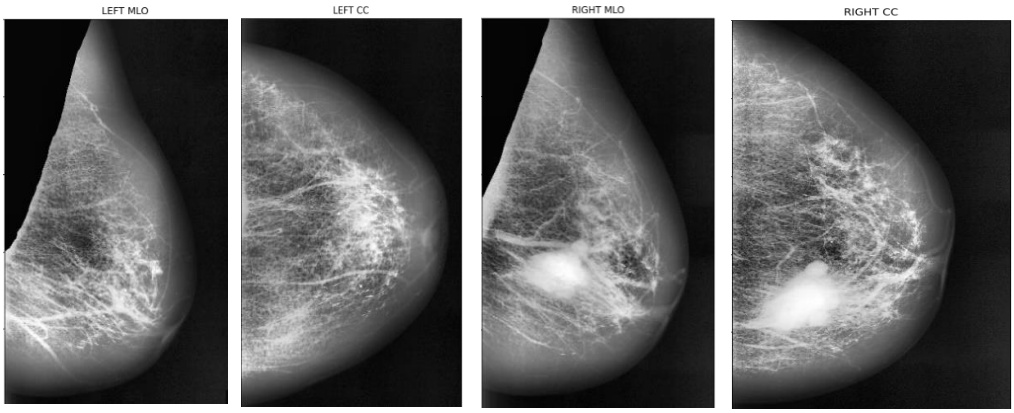

Figure- 5.2 Contrast enhancement of input images

5.5 Multi-Channel Model Development

This article proposes the feature learning ability of multi-channel Dense-Net architecture presented by Huang et al. [125] towards MBD classification. The proposed method uses four independent Dense-Net architecture as four-channel architecture known as multi-channel architecture. This architecture is competent in taking all four views of an individual patient for the classification of MBD.

5.5.1 Conversion of Gray Scale Image into RGB

The dense-Net model is pre-trained on RGB images, but the proposed work uses the grayscale image as the input image. To appear grayscale image as an RGB, performed

repetition of image array three times due to which the same image appears on the channels. Then, after duplication of the input image, all the input images are resized into 320×320×3. Figure-5.3 depicts the conversion of the grayscale image into a three-channel RGB.

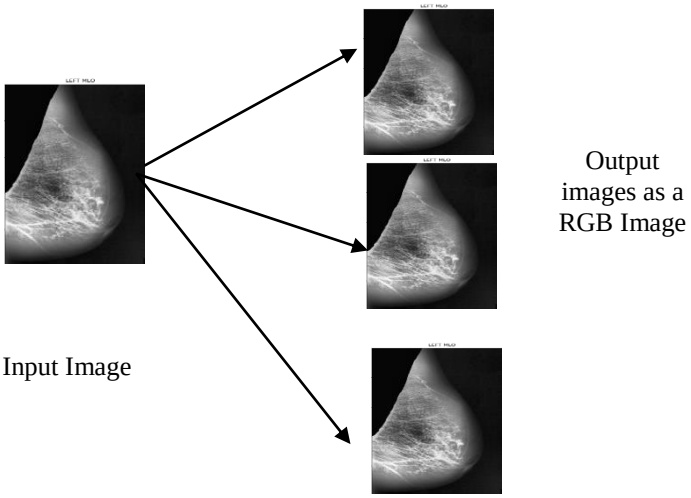

Figure- 5.3 Conversion of Grayscale image appear as a RGB

5.5.2 Input Convolutional Layer

The four input channels of the proposed architecture are marked as L_CC, L_MLO, R_CC, and R_MLO. The fundamental merit of this combination is that all four views of digital mammography are processed concurrently. Each input layer of Dense-Net architecture consists of a convolution layer of the kernel of 7×7 with a stride of 2. This convolution operation reduces the input size of the images to 112×112×3. Input image further passes through a pooling layer of 3×3 maximum pooling with stride 2×2. Thus, the input layer's convolution and pooling operation reduces the input image size to 56×56×3 and before passing to the dense blocks. Figure-5.4 depicts the proposed multi-channel architecture.

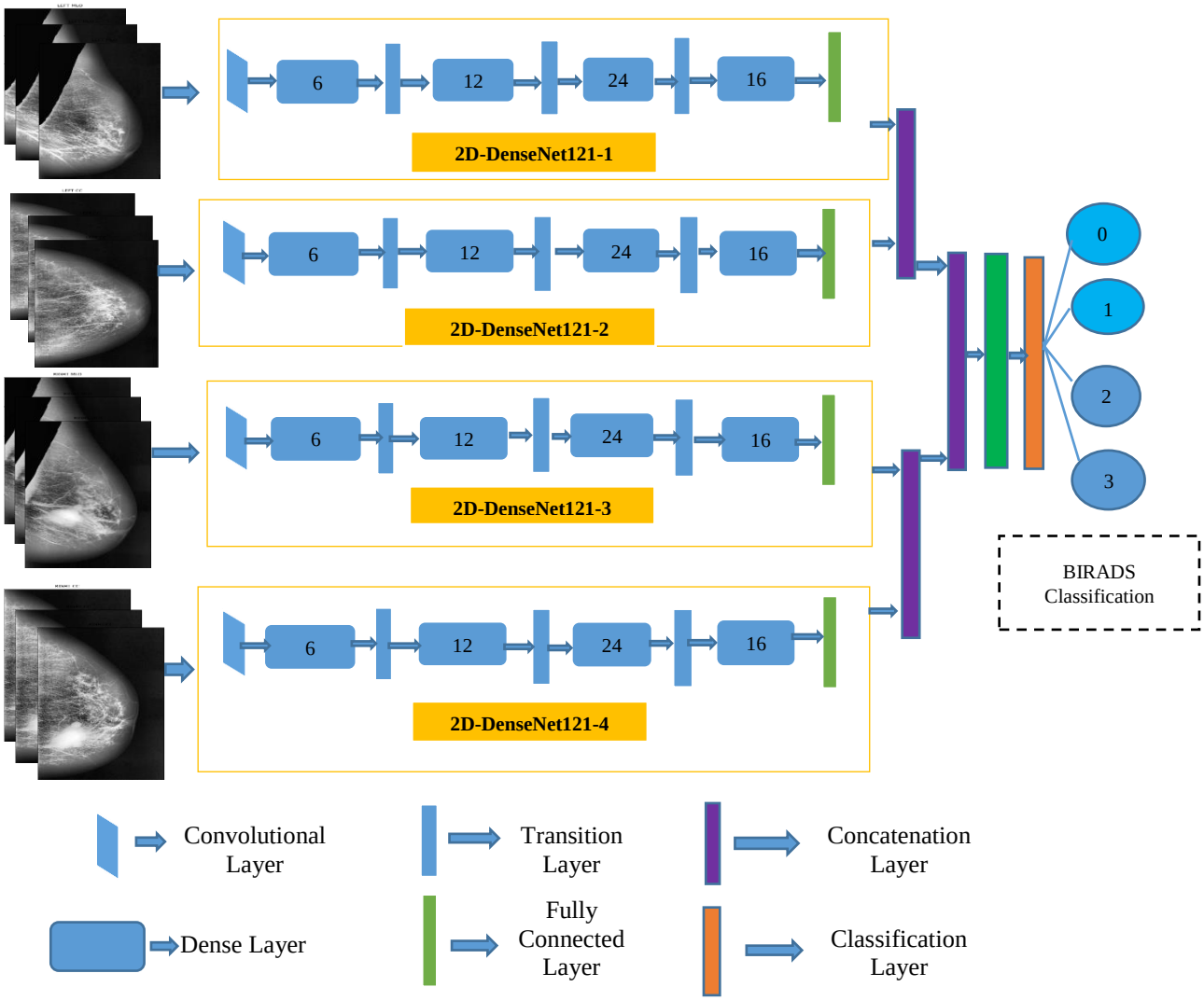

Figure- 5.4 Proposed multichannel Dense-Net Framework for BIRADS classification

5.5.3 Design of Dense-Net Neural Structure

The dense-Net architecture consists of different design variants like DenseNet121, DenseNet169, Dense-Net 201, and Dense-Net 264. The Dense-Net architecture's fundamental merit is the structure of dense layers precisely designed to take care of down sampling and feature concatenation. Therefore, out of four variants, the proposed architecture uses the Dense-Net121 network structure, consisting of a combination of dense block layers and transition layers. Thus, the proposed model uses 58 convolutional layers and a growth rate k=12, including four dense and two transition

layers. In addition, the proposed model consists of comparatively fewer parameters hence saves computational memory and reduce the over fitting problem.

5.5.4 Dense Block Layer

In four dense blocks, the individual layer is responsible for forming a k-characteristic map after convolution, which also maintains feature maps of each layer which that are of the same size. K is the convolution kernels which will extract all features from the layers. Parameter k is known as a hyper parameter in Dense-Net, which is the growth rate of the network. Each dense layer receives different inputs from previous layers to reduce the computation and enhance the efficiency of the dense block. The dense block uses the bottleneck layer (1×1 convolution layer between batch normalization, ReLU, and 3×3 convolution layer) internally.

5.5.5 Transition layer

This layer connects two adjacent dense block layers to reduce the feature map size. This block consists of a batch normalization layer and a 1× 1 convolution layer followed by a 2 × 2 average pooling layer. A combination of 4 dense blocks and transition layers converts the image size into 7×7×3, further provided to the output layer. Each layer connects to the previous stage as an input described by Equation-5.4:

$$X_l = H_l([x_0, x_1, \dots\dots, x_{l-1}]) \tag{5.4}$$

A nonlinear transformation function $H_l(.)$ is responsible for combining series output of batch normalization, ReLU, pooling and convolution operation. Figure-5.5 depicted the design architecture of dense layer.

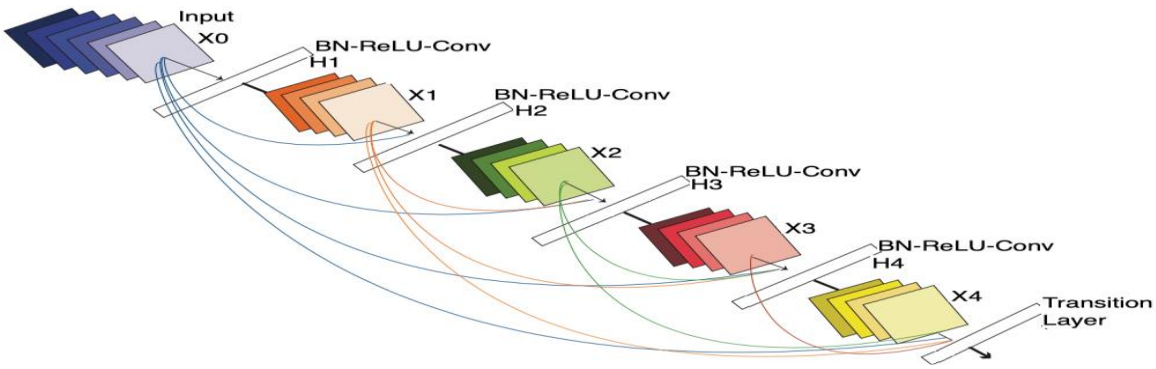

Figure- 5.5 Architecture of dense layer

5.5.6 Output Classification Layer

The output layer of the proposed architecture consists of a specific average pooling layer for each channel to extract meaningful features. Extracted features are flattened by the flatten layer and are given to the individual dense layer. MBD features received from four-channels are concatenated together with two concatenation blocks. Subsequently, the third concatenation block joins all features of the proposed method together. The three dense layers accept all the features collected together, and finally, the classification layer receives the output of three dense layers for classification.

The proposed method uses a SoftMax classifier to classify output into four classes as per BIRADS density class. Table-5.1 presents the specifications of the proposed method.

Table 5.1. Technical specification of proposed architecture

No. of channels	**04**	
Layers/Channel	**Output size/channel**	**Block description/Channel**
Convolution	112 by 112	Kernel 7×7 stride 2
Pooling	56 by 56	3×3 Max.Pooling, stride 2×2
'Dense block 1'	56 by 56	[1×1 Conv] ×6 [3×3 Conv] ×6
Transition 1	56×56 28×28	Batch normalization layer and a 1× 1 convolution layer followed by 2 × 2 average pooling layer'
'Dense Block 2'	28×28	1×1 Conv] ×12 [3×3 Conv] ×12
Transition 2	28×28 14×14	Batch normalization layer and a 1× 1 convolution layer followed by 2 × 2 average pooling layer'
'Dense Block 3'	14×14	1×1 Conv] ×24 [3×3 Conv] ×24
Transition layer 3	14×14 7×7	Batch normalization layer and a 1× 1 convolution layer followed by 2 × 2 average pooling layer'
'Dense Block 4'	7×7	1×1 Conv] ×16 [3×3 Conv] ×16
Classification layer	1×1	7×7 global average pool
	1000D fully connected, SoftMax	

5.6 Summary of Dense Net Architecture

After preprocessing and segmentation of pectoral muscle from a digital mammogram, the next task is to classify mammographic breast density per BIRADS classification. For this purpose, we proposed multichannel architecture. In this architecture, we have used the transfer learning concept of Dense-Net architecture, in which all the views of the single patient are processed simultaneously. Graphical abstract of multichannel architecture is depicted in Figure- 5.6

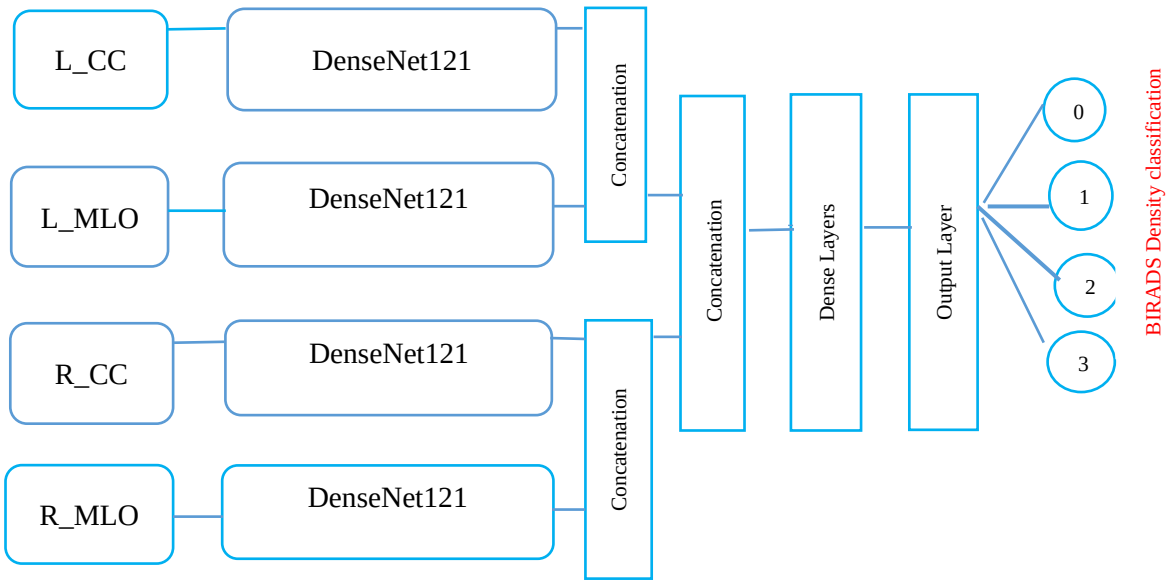

Figure- 5.6 Proposed Multichannel architecture for mammographic breast density classification

CHAPTER-6
RESULTS AND DISCUSSION

6.1 Overview

This chapter describes the results obtained by proposed algorithms to achieve proposed objectives. These results are further validated with existing state-of-art algorithms, and the outcome of the proposed algorithms are discussed. This chapter is further divided into two subsections:

1. Results analysis of segmentation of pectoral muscle by DFS algorithm.

2. Results analysis of Multichannel DenseNet architecture Towards MBD classification.

6.2 Results Analysis of Segmentation of Pectoral Muscle by DFS Algorithm

The proposed segmentation algorithm is applied over different BIRADS density classes separately with and without a Heuristic approach. For assessments, all sample images are classified into five different categories for each BIRADS density class. Subjective evaluation is performed on the basis that:

I. If the pectoral muscle in the original image is equal to the segmented portion in the output image, then it is well-segmented.

II. If a minor part of the pectoral muscle is remain, then it is acceptable, and

III. If a significant amount remains, then it is under-segmented.

IV. If the proposed algorithm removes pectoral muscle and some part of the breast, then it is over-segmented.

V. Finally, if the proposed algorithm does not perform any segmentation, it is called as no segmentation.

Evaluation of the proposed algorithm is presented in this section.

6.2.1 Subjective Assessment of Results

In medical imaging, manual segmentation by an expert radiologist is widely accepted as the gold standard for evaluation; hence, subjective evaluation of segmentation accuracy is done with the support of expert radiologists' ground truth. The output image of the DFS algorithm in each BIRADS class is compared with the Radiologist's ground truth. The subjective evaluation of the proposed algorithm is presented in Table- 6.1.

Table 6.1 Subjective assessment of the proposed algorithm

Segmentation Category	Subjective assessment criteria	BIRADS density class			
	% Matching with Radiologist ground truth	**BIRADSA**	**BIRADS B**	**BIRADS C**	**BIRADSD**
Correct segmented images	95-100	255	655	451	356
Acceptable range images	90-95	62	245	142	133
Under segmented images	< 90	28	99	70	44
Not Segmented images	Not able to segment	9	25	11	14
Over Segmented images	Images with the removal of the breast part	5	19	24	28
Segmentation Accuracy		**88.30%**	**86.28%**	**85.08%**	**85.04%**
Overall segmentation accuracy		**86.175%**			

The combined results of correct and acceptable images from segmented categories are added together to get total pre-processed images to perform subjective validation. Equation-6.1 calculates segmentation accuracy.

$$\% \text{ Segmentation Accuracy} = \frac{\text{Total pre-processed images}}{\text{Total input images}} \times 100 \qquad (6.1)$$

6.2.2 Objective Assessment of Results

The intersection over union (IOU) is the most effective and straightforward matrix used to validate segmentation results. The same procedure is used to determine the overlap with the gold standard by Jaccard coefficient and Dice similarity coefficient to perform the quantitative evaluation. Jaccard Index and Dice similarity coefficient is calculated by Equation-6.2 and 6.3.

$$(A, B) = \frac{|A \cap B|}{|A \cup B|} \tag{6.2}$$

$$\text{DSC} = \frac{2\,|A \cap B|}{|A| + |B|} \tag{6.3}$$

where A and B are the SET of ground truth image and sample image, both the coefficient ranges from 0 to 1, in which 1 shows perfect overlap, and 0 indicates no overlap. The objective analysis of the proposed algorithm is presented in Table 6.2.

Table 6.2 Objective evaluation of the proposed algorithm

	BIRADS-A		**BIRADS-B**		**BIRADS-C**		**BIRADS-D**	
Comparison parameters	**Jaccard Index**	**Dice similarity coefficient**	**Jaccard Index**	**Dice similarity coefficient**	**Jaccard Index**	**Dice similarity coefficient**	**Jaccard Index**	**Dice similarity coefficient**
Images >0.9	295	340	259	1019	641	682	515	549
Images between 0.8 to 0.9	49	11	762	06	44	07	35	09
Images between 0.8 to 0.5	07	00	05	01	04	00	06	02
Images <0.5	08	08	17	17	09	09	15	15
Mean value	**0.9346**	**0.9551**	**0.8801**	**0.9291**	**0.9647**	**0.9754**	**0.9467**	**0.9596**

Variation in Segmentation accuracy, Jaccard index, and dice similarity coefficient overall sample images are shown in Figure-6.1 and 6.2

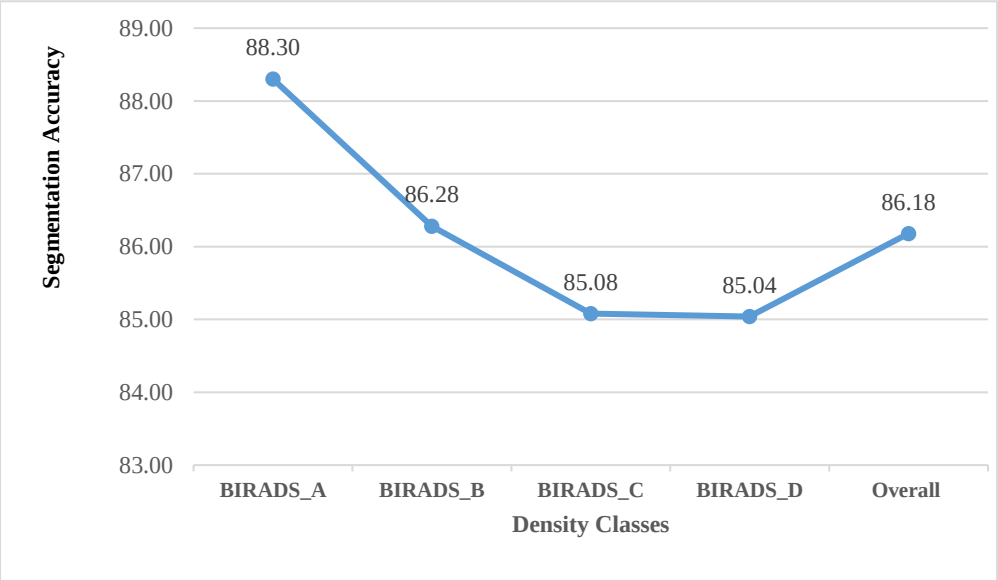

Figure- 6.1 Subjective assessment of the proposed algorithm

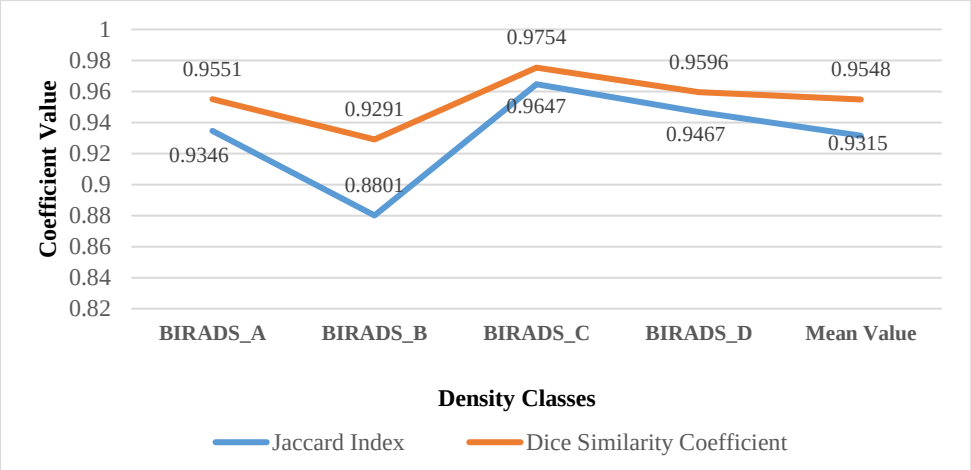

Figure- 6.2 Objective assessment of the proposed algorithm

Subjective and objective assessment of the proposed algorithm are depicted in figure-6.3

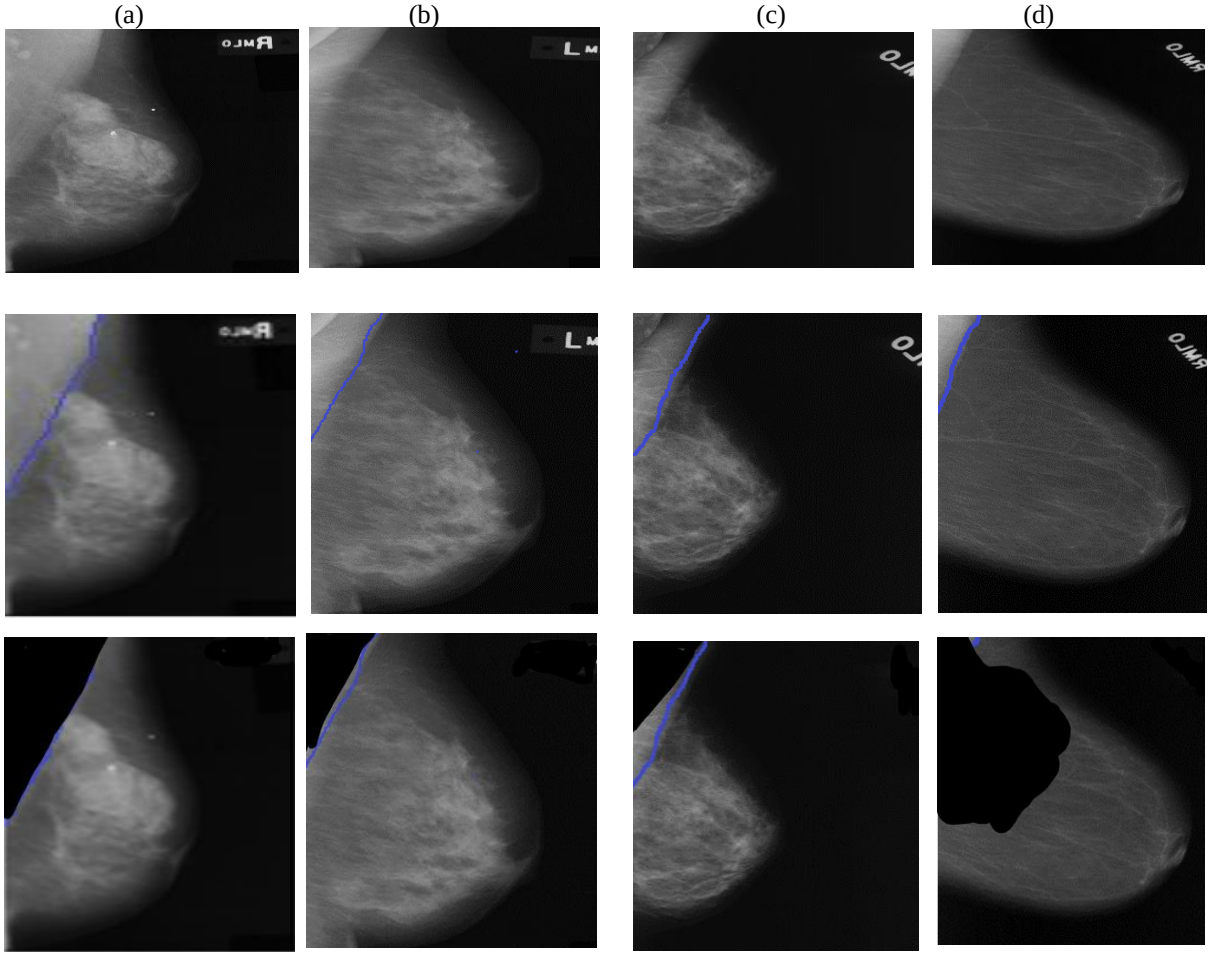

Figure- 6.3 Subjective and objective assessment of the proposed algorithm (a) Correct segmented input and output images (b) Acceptable segmented input and output images (c) Under segmented input and output images (d) Over segmented input and output images (below the images values of Jaccard and dice coefficient of each class is mentioned)

6.2.3. Ablation Experiment

This experiment is performed to understand the effect on the decision system or the Artificial Intelligence system after removing a particular component. The proposed algorithm with and without heuristic approach is applied over different density classes separately. Table-6.3 presents the results of this experiment.

Table 6.3 Ablation experiment results on different density class

BIRADS Density class	Segmented Accuracy		Jaccard Index		Dice Similarity Coefficient	
	Without Heuristic	With Heuristic	Without Heuristic	With Heuristic	Without Heuristic	With Heuristic
BIRADS_A	84.12%	88.30%	0.9132	0.9346	0.9421	0.9551
BRADS_B	83.48%	86.28%	0.8512	0.8801	0.9129	0.9291
BIRADS_C	81.22%	85.08%	0.9345	0.9647	0.9563	0.9754
BIRADS_D	81.15%	85.04%	0.9156	0.9467	0.9432	0.9596
Mean Value	82.49%	86.18%	0.9036	0.9315	0.9386	0.9548

This ablation experiment shows an enhancement of accuracy by 4% concerning the heuristic approach of DFS Algorithms. Figure- 6.4 depicted the results of the ablation experiment.

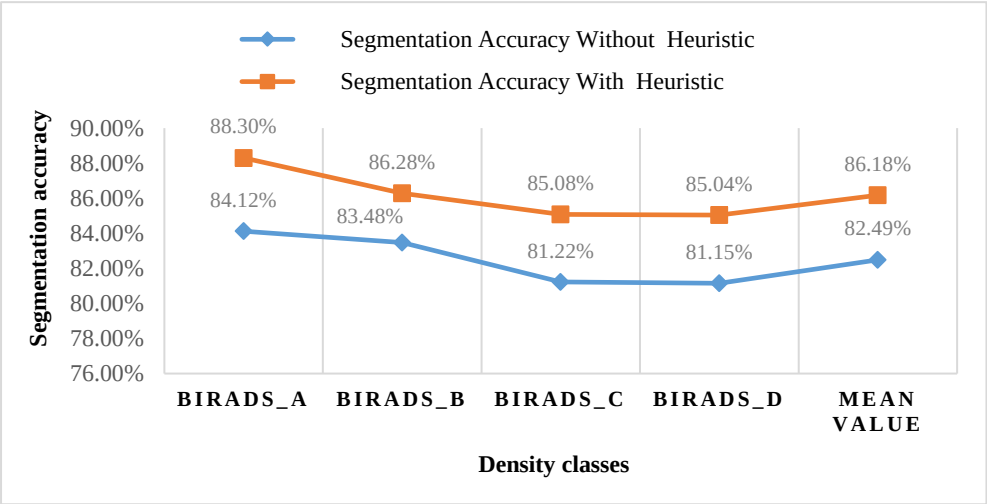

Figure- 6.4 Results of Ablation experiment

6.2.4 Comparative Study

Due to differences in used datasets and evaluation techniques, direct comparison is difficult for researchers. However, the rational comparison status of the proposed algorithm with existing methods is summarized in this section. Comparative results

presented in this section are divided into two subsections.

6.2.4.1. Subjective comparative study

A few researchers have evaluated the performance of their methods for pectoral muscle extraction qualitatively, where expert radiologists validate the segmentation accuracy. The proposed method is comparable with Mustra et al. [129], in which a fusion method is proposed for pectoral muscle removal. In this method, wavelet decomposition and bit depth reduction are used to eliminate pectoral muscle from the breast area. But in wavelet decomposition, the high-frequency component of the edge is missing, which further creates an issue to detect the accurate edge of pectoral muscle in comparison with the proposed algorithm. An initial seed selection is not dependent upon the pectoral muscle's edge, providing better pectoral muscle information for segmentation. The proposed method is also comparable with Marijeta et al. [130], in which (AGCWD) algorithm is used for image enhancement and a K-mean clustering algorithm for pectoral muscle removal. This approach recorded low segmentation accuracy due to the selection of clusters, which depends on the percentage of the image representing the pectoral muscle. This approach further leads to over-segmentation, i.e., some part of the breast also gets segmented along with the pectoral muscle. The proposed method acts superior to this method as no such selection of the cluster object is required in the proposed segmentation algorithm. A dynamic seed selection mechanism takes care of the over-segmentation cases hence provides better segmentation accuracy. The summary of the subjective comparative evaluation is presented in Table 6.4.

Table- 6.4 Comparison of the subjective evaluation

Authors/ Year	Method	No of Images/Dataset	Name of dataset	Segmentation accuracy
Raba et al. 2005 [131]	Adaptive histogram method and region growing algorithm	322	Mini-MIAS	86%
Mustra et al. 2009 [129]	Wavelet Decomposition	322	Mini-MIAS	85%

Rampun et al[56]	Canny Edge detection	100	DDSM	85.25%
Bora et al.[132]	Texture gradient-based approach	200	DDSM	81.28%
Proposed method	**Depth- first search with heuristic approach**	**2675**	**DDSM**	**86.32%**

In this Table -6.4, No. of images/ dataset column indicates total number of images used by other authors and their respective datasets.

6.2.4.2 Objective Comparative Study

Some of the researchers have evaluated the performance of their methods based on metrics such as the Jaccard index and Dice similarity coefficient to validate the results. The proposed algorithm is comparable with Rampun et al. [56], in which canny edge detection with five features is used to detect the edge of the pectoral muscle, and an active contour growing model is used for final suppression of pectoral muscle. However, the proposed approach over estimates the boundaries of pectoral muscle due to artifacts and noise, which requires further post-processing which increases time complexity. Compared with the proposed algorithm, such issues do not occur as artifacts are automatically removed before pectoral muscle segmentation takes place; hence there is no requirement of post-processing in the proposed method. Results of the proposed algorithm are also comparable with another recent research approach with Bora et al. [132], in which a texture gradient-based approach is used for pectoral muscle removal. This smooth curve of pectoral muscle is obtained with Euclidean distance regression and polynomial modeling techniques. The primary limitation of this method is that this method does not act effectively when the size of the pectoral muscle is small. Comparatively, the proposed method was superior to this method as it dynamically modified the initial seed when the pectoral muscle size is smaller.

The fundamental merit of U-net architecture is that it can learn local features more precisely. Therefore, different researchers have proposed this architecture in recent years [133-137] for semantic segmentation of pectoral muscle and recorded good

objective assessment in terms of dice similarity coefficient and Jaccard index. But in the case of pectoral muscle removal, this approach consisted of some limitations. Firstly, all the images are down sampled, which causes loss of some texture information; hence, direct comparison with the original image results is difficult as the size and original shape of the pectoral muscle change during down sampling. Another limitation of these approaches is that time complexity is higher due to the number of layers and hyper parameters. And finally, in the cases of deep learning models, when the number of images is less in quantity [134-135], then the stability of the proposed architecture is another serious concern. However, compared with all the above issues, the proposed algorithm is free from the problems mentioned above, providing better time complexity and easy design and implementation. Close rational comparative results of proposed methods with other such methods are summarized in Table- 6.5.

Table- 6.5 Comparison of the objective evaluation

Authors/ Year	**Proposed Method**	**No. of images Dataset/**	**Name of dataset**	**Segmentation Accuracy**	
				Jaccard Index	**Dice similarity Coefficient**
Rampun et al. 2017 [56]	Canny edge detection	100	DDSM	0.858	0.919
Wang et al. 2019 [72]	U-net architecture	2000	Private dataset	-	0.8879
Rampun et al. 2019 [137]	CNN	100/ BCDR	DDSM	0.969	0.988
Bora et al. 2016 [132]	Texture gradient-based approach	340	Private dataset	------	0.9675
Proposed method	**Depth- first search with heuristic approach**	**2675**	**DDSM**	**0.9315**	**0.9548**

6.2.4.3 Failure Assessment

Due to the diverse nature of mammograms, it is practically difficult for any segmentation algorithm to provide 100% segmentation accuracy. In this algorithm, few cases (13.82 %) are under under-Segmentation and no segmentation. However, the segmentation, in some cases, fails due to the following reasons.

1. Part of the inner breast is removed as a pectoral muscle, which causes over-segmentation, but that happens when the tissue inside the breast is also of very low pixel density.
2. It is challenging to identify a strongly connected component where superimposed boundaries between pectoral muscle and breast tissue.
3. Different markings on breast tissue, especially cancerous images in categories C and D, are difficult to segment with the proposed algorithm.
4. In some cases, when the gray level intensity of mammograms is less than 100, the algorithm fails to produce output due to improper image acquisition conditions.

6.2.4.4. Limitations of the study

This algorithm is proposed for breast density measurement, but cancer detection removal of pectoral muscle may create specific issues listed below.

1. Invasion of pectoral muscle in breast malignancy changes staging and breast cancer management; and hence removing pectoral muscle in these cases will not be feasible, specifically in deep-seated malignancy.

2. Evaluation of axillae is critical in breast malignancy for nodal involvement. In some cases, axillary lymph node palpation can be the first sign or symptom of breast lesions; in these cases, evaluation of pectoral muscle and axillae is mandatory.

6.2.5 Discussion

Identification and segmentation of the pectoral muscle from the digital mammogram are essential for advanced analysis of breast cancer due to the following details.

1. When the density of the pectoral muscle and tumor cells are similar to each other hence, the minor presence of pectoral muscle in MLO can increase the false

positive rate in computer-aided detection (CAD) of breast cancer.

2. The existence of pectoral muscle in a mammogram will reduce the classification score of the mammographic breast density [70].

This thesis proposes the novel dynamic seed selection mechanism and heuristic approach of the DFS algorithm to identify and segment of the pectoral muscle to address the issues mentioned earlier.

The proposed algorithm uses AGCWD [71] to enhance the contrast of the input image. This method is superior to other methods because exceptionally dark and light points are not affected by mid-tones due to the non-linear function of this algorithm. This algorithm also enhances the visibility at the breast border, which further helps to get a thin breast border compared to other enhancement methods listed in Section 4.1. Otsu multi-class thresholding is used to select the initial seed for the DFS algorithm to detect breast borders and identify the pectoral muscle. This algorithm's fundamental merit is that it provides a stable initial seed by optimizing the variance between the classes. Thus, the initial value of seed is not affected by the pectoral muscle or artifacts intensity [72].

The proposed algorithm is the first approach to apply the DFS algorithm for pectoral muscle removal. It is elemental merit of the DFS algorithm as compared to most of the state-of-algorithms and it does not rely on the assumption that pectoral muscle is an edge, straight line, or substantial gradient magnitude at the border of the pectoral muscle. Hence performs competently on different sizes, shapes, and textures of the pectoral muscle. However, some state-of-art algorithms found it challenging to segment the pectoral muscle of smaller size and contrast [73]. But, due to the heuristic approach's dynamic seed selection mechanism, DFS dynamically modifies the initial seed in the breast area. Ablation study reveals that the dynamic seed selection mechanism (heuristic method of the DFS algorithm) enhances overall segmentation accuracy by 4% on all comprehensive BIRADS density classes and avoids over-segmentation. To investigate the correctness of the proposed method, results are validated subjectively by expert radiologists and objectively by the Jaccard index and Dice-similarity coefficient. This method has recorded a mean of 86.18% segmented accuracy over the Radiologist's ground truth and 0.9315 and 0.9548 Jaccard index and

dice similarity coefficient on 2675 images of all BIRADS density classes.

6.3 Results Analysis of Multichannel DenseNet Architecture towards MBD Classification

Input images after preprocessing and segmentation of the pectoral muscle further given as input to the multichannel architecture. The experimentally proposed architecture is trained and tested on the Pytorch framework on Google Colaboratory, which is a free online cloud-based Jupiter notebook environment. A segmentation algorithm for pectoral muscle removal was implemented in python. Input image dataset for the proposed method is not sufficient to split into the train, validate, and test data set; hence, training and testing of the model is done in two phases. Fig.6.5 depicts the image data distribution during training (phase-I) and training and testing (phase-II).

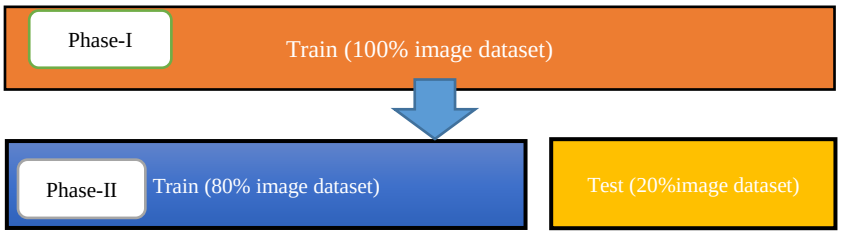

Figure- 6.5. The distribution of image data

6.3.1 Phase-I

The entire model is trained with stochastic gradient descent (SGD) algorithm using batch sizes 4 and 30 epoch on the entire dataset. SGD is an optimization algorithm that estimates the error gradient for the model's current state with an example of a training set, after this it updates the weights of the model using back propagation [34]. Eq-6.1. describes weight updating mechanism in SGD algorithm

$$w_{new=W_{old}} - n\nabla Qi(w_{new}) \quad (6.1)$$

Where w_{new} is new weight, W_{old} is weight at previous iteration n is learning rate and Qi weight gradient. The primary merit of this algorithm is that it updates parameters for each training example and performs one update at one time. Thus, SGD is faster and it can also learn online. The weight updating step size is the learning rate (n) of the

model. The learning rate is a configurable hyperparameter that controls the speed by which the model learns. The initial learning rate for this model is 0.1 (default value), further divided by ten at 50% and 75% of the total training epochs. The categorical cross-entropy act as a loss function in this model, which quantifies the difference between four probability distributions. This loss function works well with the SoftMax activation function in multi-class classification. Eq-6.2 describes mathematically the categorical cross-entropy is

$$C.E. = -\sum_i^c t_i \log(s_i) \tag{6.2}$$

Where $C.E.$ is cross entropy t_i and s_i ground truth and the CNN score for each class i in c.

Table-6.6. illustrated the setting of different hyper parameters used to obtain the optimized results of the proposed architecture.

Table- 6.6 Setting of hyper parameters used during Experiment

Hyper parameters	**Value**
Model	Multichannel-Dense Net
No. of Channel	04
Model Initial learning rate	0.1
Image size	320×320×3
Batch size	04
Target labels	Ground Truth
Data Augmentation	Not used
Loss function	Categorical cross-entropy
Optimization algorithm	Stochastic gradient decent
Validation parameter	Classification accuracy

During the training on the entire dataset, the best classification accuracy score was 96.35 % at 18 epochs with a loss factor of 0. 1344. Figure-6.6 depicts the training phase results on the dataset as a whole.

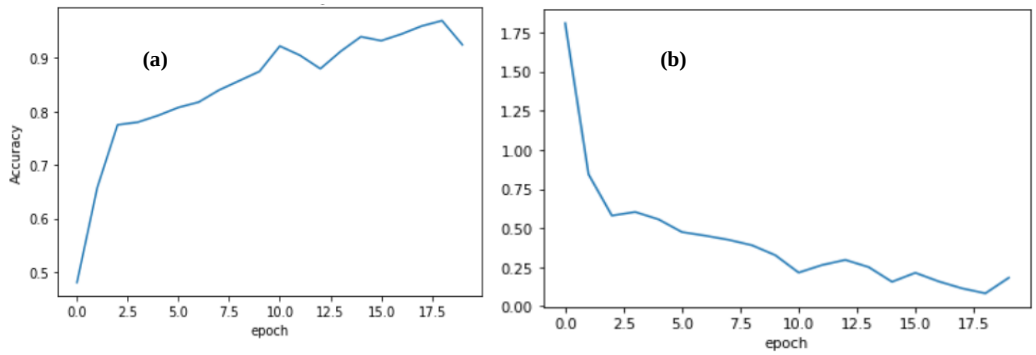

Figure- 6.6 Shows training phase performance of the model (a) Model accuracy (b) Model loss

6.3.2 Phase-II

After training the model on the entire dataset, validation of the proposed model performance is done by spitting the image dataset in a ratio of 80 % as training and 20% testing. During the testing phase, the proposed model performed significantly well on all the BIRADS density classes and recorded the best classification accuracy, 90.00%, with a validation loss of 0.3814. Fig.6.7 depicts the results of validation over the training model.

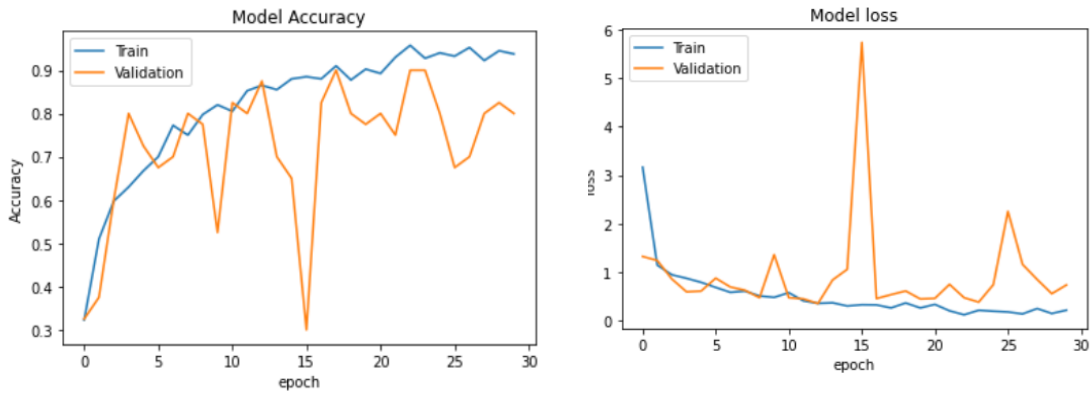

(a) (b)

Figure- 6.7 Validation results of proposed model in phase-II (a) Model accuracy (b) Model loss

6.3.3 Results Evaluation

The proposed multichannel Dense-Net architecture performance is analyzed from the confusion matrix of the model on the test dataset. Figure-6.8(a) shows the proposed architecture's heat map (confusion matrix) on the test. The heat map helps to analyze which category is correctly classified by the proposed architecture. The main diagonal darker version indicates a better classification rate. Although it is clear that the model

is working well in classes A, C, and D., there is some confusion in classifying category class B. Still, this model correctly classifies heterogeneous dense(C) and extremely dense (D), which is the essential bottleneck behind MBD classification. Fig.6.8 depicts the heat map and AUC curve of the proposed model.

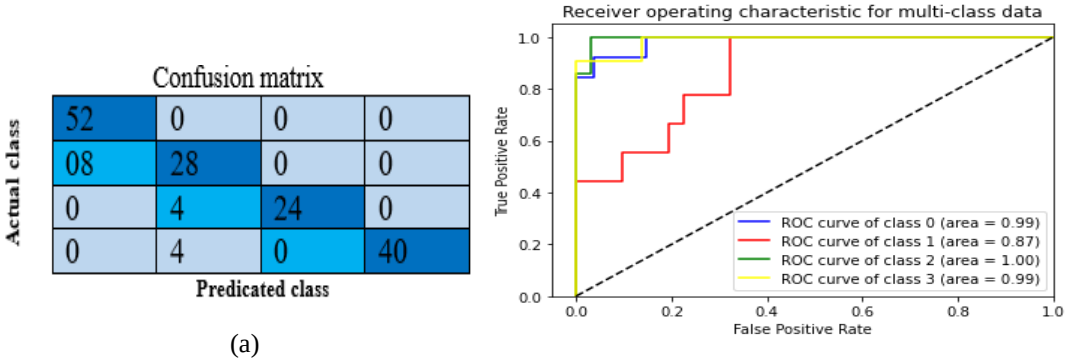

(a) (b)

Figure 6.8 The Heat map(a) and the ROC curve (b) of the proposed model

Evaluation of the classification performance of the proposed model is done in terms of precision, recall, F1-score, and classification accuracy. Among those parameters, precision is the ratio of the number of samples with positive predictions concerning the total number of correct positive samples. The recall is the ratio of correctly predicted samples to the whole samples, and the F1-score is the precision and recall weight. Finally, classification accuracy is the total correct predictions to the total number of samples. Equation (6.3)-(6.6) defines precision, recall, and F1-score, and classification accuracy, respectively:

$$Acc = \frac{N_A+N_B+N_C+N_C}{N_{All}} \tag{6.3}$$

$$F1 - score = \frac{2PR}{P+R} \tag{6.4}$$

Where N_{All} is the total number of images and $Na, Nb, Nc, and\ Nd$ signifies the number of images in BIRADS density classes A, B, C, and D.

$$P = \frac{N_t}{N_i} \times 100 \tag{6.5}$$

$$R = \frac{Nt}{Nf} \times 100 \tag{6.6}$$

Where, Nt is the correct number of predictions of a certain category, N_i is the all the number of predictions of a class and Nf indicates the actual number of the category.

Among them, P and R are precision and Recall, respectively.

The model accuracy is the ratio of the sum of the diagonal elements to all the elements. Thus, it acts as an indicator of the overall prediction of the model. In Table-6.7, illustrate the model's overall performance in detail and variation in precision rate, the recall rate, and the F1-score rate under different categories. The number of accurate positive samples for all four BIRADS density classes are 92%, 75.5%, 92.2%, and 94.7% of their respective totals. From the results shown in table-4, there is no confusion between classes A and C, B and C, and C and D. The results of the proposed algorithm results are consistent with the results evaluated by the radiologists. Which is a positive sign that indicates deep learning models are helpful for the classification of MBD.

Another graphical method used to analyzes the performance of computer-aided diagnostic systems is the receiver operating characteristic (ROC) shown in Figure-12(b). This curve analysis shows the performance of the model in terms of TP and FP. The AUC value refers to the area enclosed by the ROC curve in the [0, 1] interval and the X-axis. The greater the AUC value, the better the performance of the model. It also highlights the capability of the model to distinguish between the classes.Table-6.7 presents the performance parameters of the proposed architecture.

Table 6.7. Performance parameter of the proposed method

BIRADS Density Classes	Precision	Recall	F1-score	Overall classification Accuracy	Overall AUC
Predominantly fatty-class A	1	0.866	0.92	0.9006	0.9625
Fat with some fibro glandular tissue class B	0.77	0.77	0.755		
Heterogeneous dense-class C	0.857	1	0.922		
Extremely dense-class D	0.90	1	0.947		

Due to improved system architecture and hardware capability, the deep learning model can be an alternative for medical image classification. Still, the need for a larger dataset and vanishing gradient are the primary bottleneck issues to obtain state-of-art results from deep learning models [139].

6.3.4 Advantages of proposed method

This research article proposes multichannel Dense-Net architecture for MBD classification to investigate the performance of Dense-Net architecture on a smaller dataset. The proposed architecture has recorded good classification performance into four class classification. Furthermore, the visualization results show that the model can distinguish between all the BIRADS density classes, especially in "Scattered density" and "Heterogeneously dense category of BIRADS. Thus, this model can help the radiologists to classify the BIRADS density classes quickly. The main reasons for the excellent performance of this model are as follows:

- Instead of using raw images, the proposed architecture uses preprocessed images. Hence there are no high-density areas like pectoral muscle and tags on mammograms which is helpful to enhance the classification accuracy of the proposed model.
- The proposed method uses a contrast enhancement technique to improve the quality of training data.
- The model contains of four Dense-Net branches, which extract the features of mammograms from four views of the single patient so that the network can focus on a broader range of spatial information.
- Due to multichannel architecture, it is possible to process all the views of a single patient simultaneously.
- Finally, with multi-channel and multi-view architecture, it is possible to fusion all the features together; hence performance of the proposed model is found better than single view classification.

6.3.5 Comparison with state-of-art

As there are differences in used datasets and evaluation techniques, direct comparison is difficult for researchers. However, this section summarizes the proposed algorithm's comparison status with existing methods.

To study the inter-observer variation in MBD assessment, N. Kaiser et al. [92].proposed the novel multichannel VGG architecture. This approach uses a total of 8150 digital mammograms, divided into 600 cases. This method recorded 88% two-

class classification accuracy ((dense and non-dense) with an AUC of 0.954. Besides, the results are also compared with the 32 individual radiologist's panel's density ground truth. This study reveals that the deep learning approach performs better than average radiologists. Thus, we only need to refine the deep learning model for MBD classification. However, the fundamental limitation of this method is gradient flows from the final layer to the initial layer; hence vanishing gradient problem takes place, which increases training time and reduces the classification accuracy. In the proposed method, due to Dense-Net architecture, all the layers are directly connected in feed-forward nature, hence acting as an effective solution for vanishing gradient and reduce the training time. Thus, the results of the proposed algorithm outperform this method on a smaller dataset.

Another method directly comparable to the proposed method is the optimized lightweight deep learning architecture proposed by Peng Shi et al. [90]. The elemental focus of this method is to overcome the requirement of the larger dataset and vanishing gradient problem of the deep learning algorithm. This method combines three CNN layers, one dense layer, and an output layer to classify MBD. This architecture is tested on a 322 Mini-Mias dataset with different data augmentation techniques and recorded 83.6% classification accuracy. However, due to the smaller dataset, this architecture has limitations regarding moderate classification accuracy and low stability of the network. Therefore, the proposed method used the concept of transfer learning and multichannel architecture to overcome these limitations. As a result, the proposed model outperforms this method in classification accuracy on a smaller dataset. Table-6.8 provides the comparative status of the proposed method with other different current state-of-art methods.

Table- 6.8 Comparative status of the proposed method with current state-of-art methods

Author	Dataset	Proposed method	Classification accuracy
Nan Wu et al.[82]/2018	2,00,000	A deep convolutional network with 100 layers.	0.825 on Four views
Ciritsis et al.[86]/2019	20578	A deep convolutional network with 11 layers and performed analysis separately on CC and MLO views.	0.897 On CC views and 0.866 on MLO views.
N. Kaiser et	8150	A multichannel architecture with	0.88 on all four

al.[92]/2019		transfer learning by VGG-Net.	views
Peng Shi et al. [90]/2019	322	A light-weight deep learning architecture with 3 convolutional layers.	0.836 On MLO views.
Deng et al.[74]/2020	18157	A single channel architecture with transfer learning by Dense Net 121 combined with SE-Attention network.	0.9179 on all Four views
Lee et al. [140]/2021	2500 DDSM	Machine leaning approach for MBD classification(Decision tree, SVM, KNN)	AUC of 0.801,0.805,0.810 Respectively.
Mohamed et al.[141]/2018	22000	CNN architecture for classification of MBD	AUC=0.9225
Bovis et al.[142]/2002	377	Feed forward neural network	0.714 on four class and 0.967 on two class
Proposed method	800	A multichannel architecture with transfer learning with Dense Net 121	0.90 on Four views

6.4 Summary

The final experimental results shows that the proposed multi-channel model has achieved good performance with an accuracy of 96.67% during training and 90.06% during testing, and an average AUC of 0.9625. Obtained results are also validated qualitatively with the help of a radiologist expert in the field of MBD. Proposed architecture achieved state-of-art results with a fewer number of images and with less computation power.

Highlights of proposed research work

- Multi-channel Dense-Net architecture for mammographic breast density classification.
- Classifier performance is evaluated with 800 digital mammograms with different BIRADS density classes.
- Results are validated subjectively by expert's Radiologists and objectively by classification accuracy and AUC.

CHAPTER-7
CONCLUSION AND FUTURE PERSPECTIVES

7.1 Overview

In summary, the primary objective behind this study is to classify MBD as per BIRADS classification. This study proposes the novel approach of multi-channel architecture with Dense-Net 121 for the objective assessment of MBD and Depth-first search algorithm for segmentation of pectoral muscle. This section describes the conclusion and future perspectives of proposed research work.

7.2 Conclusion

Identification and segmentation of the pectoral muscle from the digital mammogram are essential for breast cancer detection and classification of mammographic breast density. Hence, the fundamental objective behind the research work is to remove artifacts, tags, and pectoral muscle using a novel seed selection mechanism and DFS algorithm with a novel heuristic approach towards better segmentation accuracy. Otsu-multi-class thresholding and DFS algorithm remove the artifacts and labels successfully from all the input mammograms. Further, to reduce the input mammogram's size, the breast skin-air interface of the breast is detected. A novel dynamic seed selection approach is used to identify the pectoral muscle from the breast area. Finally, the DFS algorithm with and without heuristic approach is used to segment pectoral muscle from 2675 digital mammograms. The DFS algorithm without the heuristic approach yielded a segmentation accuracy of 82.32%. A dynamic seed selection mechanism due to the heuristic approach of DFS enhances the overall segmentation accuracy up to 86.16% on all BIRADS density classes. The proposed algorithm works well on a wide range of mammograms with varying textures, sizes, and shapes. Discussion of the failure cases, which are infrequent ones, are provided, and the work to address failure cases is in progress. The proposed algorithm can be used in the pre-processing unit of breast cancer detection and MBD classification systems used during clinical practice.

The proposed framework uses the four views of a single patient to enhance feature learning ability through a multi-view approach. In this method, image contrast enhancement and pre-processing of the input image are performed to improve the quality of the training image data. All the input images are simultaneously processed through Multi-channel architecture to extract and fusion all the features together. Analysis of the results suggests that the proposed model successfully distinguishes between all the BIRADS density classes but is predominantly found superior in the two most distinctive and challenging BIRADS categories: "Scattered density" and "Heterogeneously dense. Classification accuracy of the proposed model is recorded at 96.67% during training and 90.06% during testing, and an average AUC of 0.9625. The proposed model consists of some limitations which are discussed in previous chapters and will be addressed in future work; with certain modifications, the proposed architecture is suitable to use in clinical workflow in breast cancer screening to avoid false recalls.

7.3 Future Perspectives

Due to the simplicity and encouraging results of the Depth-first search algorithm, this algorithm can improve in regards to some failed cases in categories of under-segmentation and no segmentation. Future work is under process to modify the proposed algorithm to address the above issues and be tested on different public and clinically proven datasets to address the proposed algorithm's generalization.

In case of multichannel dense-net architecture, it has improved the classification performance of BIRADS density classes, but there are still some issues that need to be addressed. Firstly, this study uses a smaller amount of image data, and no image enhancement strategies are used to expand the dataset. Hence, model performance, especially stability during validation, is affected due to a small number of image data. And the model found it a little confusing in classify classes A and B.

7.3.1 Future research directions

1. Therefore, in the future, the research direction will be to use data enhancement techniques to improve the model's performance and use the larger dataset to improve the stability of the model.
2. A comparative study with different deep learning approaches needs to be tested with enhanced datasets.
3. Finally, the proposed work address only one type of dataset; hence this approach does not address the robustness of the model. Future work will address the model's robustness by training the model with different vendor-specific image datasets. The proposed work will undoubtedly perform more precisely if we address the abovementioned issues.

DISSEMINATION OF WORK

Published Work in Conferences

1. Pawar, S., & Sharma, K. K. (2019). Refining healthcare in terms of diabetic care: Future area of scope for artificial intelligence. International Journal of Recent Technology and Engineering, 8(2 Special Issue 8), 888–893. https://doi.org/10.35940/ijrte.B1003.0882S819 (Scopus Indexed).
2. Sharma K.K., Pawar S.D., Bali B. (2020) Proactive Preventive and Evidence-Based Artificial Intelligene Models: Future Healthcare. In: Singh Tomar G., Chaudhari N.S., Barbosa J.L.V., Aghwariya M.K. (eds) International Conference on Intelligent Computing and Smart Communication 2019. Algorithms for Intelligent Systems. Springer, Singapore. https://doi.org/10.1007/978-981-15-0633-8_44.(Scopus Indexed).
3. Pawar, Shivaji and Sapate, Suhas and Sharma, Kamal, Machine Learning Approach towards Mammographic Breast Density Measurement for Breast Cancer Risk Prediction: An Overview (April 8, 2020). Proceedings of the 3rd International Conference on Advances in Science & Technology (ICAST) 2020, Available at SSRN: https://ssrn.com/abstract=3599187 or http://dx.doi.org/10.2139/ssrn.3599187.

Published Work in Book chapter

1. Pawar, S. D., Sharma, K. Kr., & Sapate, S. G. (2021). Advances in Machine Learning and Deep Learning Approaches for Mammographic *Techniques* (pp. 125–143). Chapman and Hall/CRC. https://doi.org/10.1201/9781003133681-8Breast Density Measurement for Breast Cancer Risk Prediction: An Overview. In *Design of Intelligent Applications Using Machine Learning and Deep Learning*. (Scopus Indexed)

Published Work in Journal

1. Pawar, S. D., Sharma, K. K., Sapate, S. G., & Yadav, G. Y. (2021). Segmentation of pectoral muscle from digital mammograms with depth-first search algorithm towards breast density classification. *Biocybernetics and Biomedical Engineering*, *41*(3), 1224–1241. https://doi.org/10.1016/j.bbe.2021.08.005. (Scopus/ WOS indexed).

Accepted Article in Conferences

2. Shivaji Pawar, Kamal Sharma and Suhas Sapate. Review on Pre-processing algorithms for Breast Density Classification using Digital Mammograms. International Conference on Innovations in Computer Science, Electronics and Electrical Engineering-2022) (Scopus Indexed)

Article Under review

1. Shivaji Pawar, Kamal Sharma and Suhas Sapate. Multi-channel Dense-Net Architecture for Classification of Mammographic Breast Density for Breast Cancer Detection. CMC journal

REFERENCES

1. Siegel RL, Miller KD, Fuchs HE, Jemal A. Cancer Statistics, 2021. CA Cancer J Clin2021; 71:7–33. https://doi.org/10.3322/caac.21654.

2. Sharma KK, Pawar SD, Bali B. Proactive Preventive and Evidence-Based Artificial Intelligence Models: Future Healthcare 2020:463–72. https://doi.org/10.1007/978-981-15-0633-8_44.

3. Zucca-Matthes, G., Urban, C., & Vallejo, A. (2016, February 1). Anatomy of the nipple and breast ducts. *Gland Surgery*. AME Publishing Company. https://doi.org/10.3978/j.issn.2227-684X.2015.05.10.

4. Prusty, R. K., Begum, S., Patil, A., Naik, D. D., Pimple, S., & Mishra, G. (2020). Knowledge of symptoms and risk factors of breast cancer among women: A community based study in a low socio-economic area of Mumbai, India. *BMC Women's Health*, *20*(1). https://doi.org/10.1186/s12905-020-00967-x.

5. Medich DC, Martel C. Medical Health Physics. Health Physics Society 2006 Summer School. Medical Physics Publishing. ISBN 1930524315 pp.25.

6. Sapate SG, Mahajan A, Talbar SN, Sable N, Desai S, Thakur M. Radiomics based detection and characterization of suspicious lesions on full field digital mammograms. Comput Methods Programs Biomed 2018; 163:1–20. https://doi.org/10.1016/j.cmpb.2018.05.017.

7. Ng, K.-H., & Lau, S. (2015). Vision 20/20: Mammographic breast density and its clinical applications. Medical Physics, 42(12), 7059–7077. doi:10.1118/1.4935141

8. N. F. Boyd, B. O'Sullivan, J. E. Campbell, E. Fishell, I. Simor, G. Cooke, and T. Germanson, "Mammographic signs as risk factors for breast cancer," Br. J. Cancer 45(2), 185–193 (1982).

9. Lau, S., Ng, K. H., & Aziz, Y. F. A. (2016). Volumetric breast density measurement: Sensitivity analysis of a relative physics approach. *British Journal of Radiology*, *89*(1066). https://doi.org/10.1259/bjr.20160258.

10. Wolfe, J. N. (1976). Risk for breast cancer development determined by mammographic parenchymal pattern. *Cancer*, *37*(5), 2486–2492. https://doi.org/10.1002/1097-0142(197605)37:5

11. Richard-Davis, G., Whittemore, B., Disher, A., Rice, V. M., Lenin, R. B., Dollins, C., Eswaran, H. (2018). Evaluation of Quanta Hologic Volumetric Computerized Breast Density Software in Comparison With Manual Interpretation in a Diverse Population. *Breast Cancer: Basic and Clinical Research*, *12*. https://doi.org/10.1177/1178223418759296.

12. HP C, MA H. Deep Learning for Mammographic Breast Density Assessment and Beyond. Radiology 2019; 290:59–60.

13. (ACR), Radiological Society of North America (RSNA) and American College of Radiology. "Mammography (Mammogram)". radiologyinfo.org.

14. Sapate, S., & Talbar, S. (2016). An overview of pectoral muscle extraction algorithms applied to digital mammograms. In Studies in Computational Intelligence (Vol. 651, pp. 19–54). Springer Verlag. https://doi.org/10.1007/978-3-319-33793-7_2.

15. Mohamed, A. A., Luo, Y., Peng, H., Jankowitz, R. C., & Wu, S. (2017). Understanding Clinical Mammographic Breast Density Assessment: A Deep Learning Perspective. Journal of Digital Imaging, 31(4), 387–392. Doi: 10.1007/s10278-017-0022-2.

16. N. Boyd, J. Byng, R. Jong, E. Fishell, L. Little, A. Miller, G. Lockwood, D. Tritchler, and M. Yaffe, “Quantitative classification of mammographic densities and breast cancer risk: Results from the Canadian national breast screening study,” J. Natl. Cancer Inst. 87, 670–675 (1995).

17. H. Lee-Han, G. Cooke, and N. F. Boyd, “Quantitative evaluation of mammographic densities: A comparison of methods of assessment,” Eur. J. Cancer Prev. 4(4), 285–292 (1995).

18. Sickles, E. A. (2007, February). Wolfe mammographic parenchymal patterns and breast cancer risk. *American Journal of Roentgenology*. https://doi.org/10.2214/AJR.06.0635

19. Boyd, N. F., Rommens, J. M., Vogt, K., Lee, V., Hopper, J. L., Yaffe, M. J., & Paterson, A. D. (2005, October). Mammographic breast density as an intermediate phenotype for breast cancer. *Lancet Oncology*. https://doi.org/10.1016/S1470-2045(05)70390-9.

20. Johansen Taber, K. A., Morisy, L. R., Osbahr, A. J., & Dickinson, B. D. (2010). Male breast cancer: Risk factors, diagnosis, and management (review). *Oncology Reports*. Spandidos Publications. https://doi.org/10.3892/or_00000962.

21. D'Orsi, C., Sickles, E., Mendelson, E., Morris, E. (2013). *ACR BI-RADS Atlas 5th Edition* (Vol. 53, pp. 1689–1699).

22. Byng, J. W., Boyd, N. F., Fishell, E., Jong, R. A., & Yaffe, M. J. (1994). The quantitative analysis of mammographic densities. *Physics in Medicine and Biology*, *39*(10), 1629–1638. https://doi.org/10.1088/0031-9155/39/10/008.

23. Byng, J. W., Yaffe, M. J., Jong, R. A., Shumak, R. S., Lockwood, G. A., Tritchler, D. L., & Boyd, N. F. (1998). Analysis of Mammographic Density and Breast Cancer Risk from Digitized Mammograms. *Radiographics*, *18*(6), 1587–1598. https://doi.org/10.1148/radiographics.18.6.9821201.

24. Yaffe, M. J. (1998). Breast cancer risk and measured mammographic density. *European Journal of Cancer Prevention*, *7*(SUPPL. 1). https://doi.org/10.1097/00008469-199802001-00010.

25. Lee-Han, H., Cooke, G., & Boyd, N. F. (1995). Quantitative evaluation of mammographic densities. *European Journal of Cancer Prevention*, *4*(4), 285–292. https://doi.org/10.1097/00008469-199508000-00003.

26. Ursin, G., Astrahan, M. A., Salane, M., Parisky, Y. R., Pearce, J. G., Daniels, J. R.Spicer, D. V. (1998). The detection of changes in mammographic densities. *Cancer Epidemiology Biomarkers and Prevention*, *7*(1), 43–47.

27. Heine, J. J., & Velthuizen, R. P. (2000). A statistical methodology for mammographic density detection. *Medical Physics*, *27*(12), 2644–2651. https://doi.org/10.1118/1.1323981.

28. Tagliafico, A., Tagliafico, G., Tosto, S., Chiesa, F., Martinoli, C., Derchi, L. E., & Calabrese, M. (2009). Mammographic density estimation: Comparison among BI-

RADS categories, a semi-automated software and a fully automated one. *Breast*, *18*(1), 35–40. https://doi.org/10.1016/j.breast.2008.09.005.

29. Hartman, R. Highnam, R. Warren, and V. Jackson, "Volumetric assessment of breast tissue composition from FFDM images," in Digital Mammography, edited by E. Krupinski (Springer, Berlin, Heidelberg, 2008), Vol. 5116, pp. 33–39.

30. Pawluczyk, O., Augustine, B. J., Yaffe, M. J., Rico, D., Yang, J., Mawdsley, G. E., & Boyd, N. F. (2003). A volumetric method for estimation of breast density on digitized screen-film mammograms. *Medical Physics*, *30*(3), 352–364. https://doi.org/10.1118/1.1539038.

31. Hartman, K., Highnam, R., Warren, R., & Jackson, V. (2008). Volumetric assessment of breast tissue composition from FFDM images. In *Lecture Notes in Computer Science (including subseries Lecture Notes in Artificial Intelligence and Lecture Notes in Bioinformatics)* (Vol. 5116 LNCS, pp. 33–39). https://doi.org/10.1007/978-3-540-70538-3_5.

32. Vucomp, Inc., Vucomp—Breast density. http://www.vucomp.com/products/breast-density.

33. Li, J., Szekely, L., Eriksson, L., Heddson, B., Sundbom, A., Czene, K., Humphreys, K. (2012). High-throughput mammographic-density measurement: a tool for risk prediction of breast cancer. *Breast Cancer Research*, *14*(4). https://doi.org/10.1186/bcr3238.

34. Nickson, C., Arzhaeva, Y., Aitken, Z., Elgindy, T., Buckley, M., Li, M., … Kavanagh, A. M. (2013). AutoDensity: An automated method to measure mammographic breast density that predicts breast cancer risk and screening outcomes. *Breast Cancer Research*, *15*(5). https://doi.org/10.1186/bcr3474.

35. RP, H., JM, B., & BJ, S. (1997). Mammographic image analysis. *European Journal of Radiology*, *24*(1), 20-32. Retrieved from http://www.ncbi.nlm.nih.gov/pubmed/9056146.

36. M. Brady, D. Gavaghan, A. Simpson, M. M. Parada, and R. Highnam, "diamond: A grid-enabled federated database of annotated mammograms," in Grid Computing:

Making the Global Infrastructure a Reality, edited by F. Berman, G. Fox, and A. G. Hey (John Wiley & Sons, Ltd., Chichester, 2003), pp. 923–943.

37. K. Hartman, R. Highnam, R. Warren, and V. Jackson, "Volumetric assessment of breast tissue composition from FFDM images," in Digital Mammography, edited by E. Krupinski (Springer, Berlin, Heidelberg, 2008), Vol. 5116, pp. 33–39.

38. Ducote, J. L., & Molloi, S. (2010). Quantification of breast density with dual energy mammography: An experimental feasibility study. *Medical Physics*, *37*(2), 793–801. https://doi.org/10.1118/1.3284975.

39. Sabee Molloi, Ding, H., & Molloi, S. (2012). Quantification of breast density with spectral mammography based on a scanned multi-slit photon-counting detector: A feasibility study. *Physics in Medicine and Biology*, *57*(15), 4719–4738. https://doi.org/10.1088/0031-9155/57/15/4719.

40. https://www.medgadget.com/2018/03/mammomat-revelation-mammography-system-with-automatic-breast-density-measurement.

41. https://www.siemens-healthineers.com/mammography/digital-mammography/mammomat-revelation#FEATURES_BENEFITS

42. Hardy, K. (2012). Breast Density Notification. *Radiology Today*, *13*(8), 30–33. Retrieved from http://search.ebscohost.com/login.aspx?direct=true&db=ccm&AN=108143041&site=ehost-live.

43. Sharma, K. Kr., Pawar, S. D., & Bali, B. (2020). Proactive Preventive and Evidence-Based Artificial Intelligene Models: Future Healthcare (pp. 463–472). https://doi.org/10.1007/978-981-15-0633-8_44.

44. Mohamed, A. A., Luo, Y., Peng, H., Jankowitz, R. C., & Wu, S. (2017). Understanding Clinical Mammographic Breast Density Assessment: A Deep Learning Perspective. Journal of Digital Imaging, 31(4), 387–392. Doi: 10.1007/s10278-017-0022-2.

45. Sak, M. A., Littrup, P. J., Duric, N., Mullooly, M., Sherman, M. E., & Gierach, G. L. (2015). Current and future methods for measuring breast density: a brief comparative

review. *Breast Cancer Management*, *4*(4), 209–221. https://doi.org/10.2217/bmt.15.13.

46. Pawar, S. D., Sharma, K. K., Sapate, S. G., & Yadav, G. Y. (2021). Segmentation of pectoral muscle from digital mammograms with depth-first search algorithm towards breast density classification. *Biocybernetics and Biomedical Engineering*, *41*(3), 1224–1241. https://doi.org/10.1016/j.bbe.2021.08.005.

47. Liu, L., Wang, J., & He, K. (2010). Breast density classification using histogram moments of multiple resolution mammograms. In *Proceedings - 2010 3rd International Conference on Biomedical Engineering and Informatics, BMEI 2010* (Vol. 1, pp. 146–149). https://doi.org/10.1109/BMEI.2010.5639662.

48. Liu, Q., Liu, L., Tan, Y., Wang, J., Ma, X., & Ni, H. (2011). Mammogram density estimation using sub-region classification. In Proceedings - 2011 4th International Conference on Biomedical Engineering and Informatics, BMEI 2011 (Vol. 1, pp. 356–359). https://doi.org/10.1109/BMEI.2011.6098327.

49. Keller, B. M., Nathan, D. L., Wang, Y., Zheng, Y., Gee, J. C., Conant, E. F., &Kontos, D. (2012). Estimation of breast percent density in raw and processed full field digital mammography images via adaptive fuzzy c-means clustering and support vector machine segmentation. Medical Physics, 39(8), 4903–4917. https://doi.org/10.1118/1.4736530.

50. Mustra, M., & Grgic, M. (2013). *Robust automatic breast and pectoral muscle segmentation from scanned mammograms. Signal Processing, 93(10), 2817–827.* doi:10.1016/j.sigpro.2012.07.026

51. Rampun, A., Morrow, P. J., Scotney, B. W., & Winder, J. (2017). Fully automated breast boundary and pectoral muscle segmentation in mammograms. Artificial Intelligence in Medicine, 79, 28–41. https://doi.org/10.1016/j.artmed.2017.06.001

52. Devi, S. S., & Vidivelli, S. (2018). Classification of breast tissue density in digital mammograms. In *Proceedings of 2017 International Conference on Innovations in Information, Embedded and Communication Systems, ICIIECS 2017* (Vol. 2018-January, pp. 1–7). Institute of Electrical and Electronics Engineers Inc. https://doi.org/10.1109/ICIIECS.2017.8276139.

53. Saidin, N., Ngah, U. K., Sakim, H. A. M., Siong, D. N., & Hoe, M. K. (2009). Density based breast segmentation for mammograms using graph cut techniques. In IEEE Region 10 Annual International Conference, Proceedings/TENCON. https://doi.org/10.1109/TENCON.2009.5396042.

54. Saltanat, N., Hossain, M. A., & Alam, M. S. (2010). An efficient pixel value based mapping scheme to delineate pectoral muscle from mammograms. In *Proceedings 2010 IEEE 5th International Conference on Bio-Inspired Computing: Theories and Applications, BIC-TA 2010* (pp. 1510–1517). https://doi.org/10.1109/BICTA.2010.5645272.

55. Maitra, I. K., Nag, S., & Bandyopadhyay, S. K. (2012). Technique for preprocessing of digital mammogram. *Computer Methods and Programs in Biomedicine*, *107*(2), 175–188. https://doi.org/10.1016/j.cmpb.2011.05.007.

56. Rampun, A., Morrow, P. J., Scotney, B. W., & Winder, J. (2017). Fully automated breast boundary and pectoral muscle segmentation in mammograms. *Artificial Intelligence in Medicine*, *79*, 28–41. https://doi.org/10.1016/j.artmed.2017.06.001.

57. Devi, S. S., & Vidivelli, S. (2018). Classification of breast tissue density in digital mammograms. In *Proceedings of 2017 International Conference on Innovations in Information, Embedded and Communication Systems, ICIIECS 2017* (Vol. 2018-January, pp. 1–7). Institute of Electrical and Electronics Engineers Inc. https://doi.org/10.1109/ICIIECS.2017.8276139.

58. Liu, Q., Liu, L., Tan, Y., Wang, J., Ma, X., & Ni, H. (2011). Mammogram density estimation using sub-region classification. In *Proceedings - 2011 4th International Conference on Biomedical Engineering and Informatics, BMEI 2011* (Vol. 1, pp. 356–359). https://doi.org/10.1109/BMEI.2011.6098327

59. Subashini, T. S., Ramalingam, V., & Palanivel, S. (2010). Automated assessment of breast tissue density in digital mammograms. *Computer Vision and Image Understanding*, *114*(1), 33–43. https://doi.org/10.1016/j.cviu.2009.09.009.

60. Bora, V. B., Kothari, A. G., & Keskar, A. G. (2016). Robust Automatic Pectoral Muscle Segmentation from Mammograms Using Texture Gradient and Euclidean Distance

Regression. *Journal of Digital Imaging*, *29*(1), 115–125. https://doi.org/10.1007/s10278-015-9813-5.

61. Ferrari, R. J., Rangayyan, R. M., Desautels, J. E. L., Borges, R. A., & Frère, A. F. (2004). Automatic Identification of the Pectoral Muscle in Mammograms. *IEEE Transactions on Medical Imaging*, *23*(2), 232–245. https://doi.org/10.1109/TMI.2003.823062.

62. Mustra, M., Bozek, J., & Grgic, M. (2009). Breast border extraction and pectoral muscle detection using wavelet decomposition. In *IEEE EUROCON 2009, EUROCON 2009* (pp. 1426–1433). https://doi.org/10.1109/EURCON.2009.5167827.

63. Kumar, I., H.S., B., Virmani, J., & Thakur, S. (2017). A classification framework for prediction of breast density using an ensemble of neural network classifiers. *Biocybernetics and Biomedical Engineering*, *37*(1), 217–228. https://doi.org/10.1016/j.bbe.2017.01.001.

64. Wang, K., Khan, N., Chan, A., Dunne, J., & Highnam, R. (2019). Deep Learning for Breast Region and Pectoral Muscle Segmentation in Digital Mammography. In *Lecture Notes in Computer Science (including subseries Lecture Notes in Artificial Intelligence and Lecture Notes in Bioinformatics)* (Vol. 11854 LNCS, pp. 78–91). Springer. https://doi.org/10.1007/978-3-030-34879-3_7.

65. Ali, M. J., Raza, B., Shahid, A. R., Mahmood, F., Yousuf, M. A., Dar, A. H., & Iqbal, U. (2020). Enhancing breast pectoral muscle segmentation performance by using skip connections in fully convolutional network. *International Journal of Imaging Systems and Technology*, *30*(4), 1108–1118. https://doi.org/10.1002/ima.22410.

66. Kim, Y. J., Yoo, E. Y., & Kim, K. G. (2021). Deep learning based pectoral muscle segmentation on Mammographic Image Analysis Society (MIAS) mammograms. *Precision and Future Medicine*, *5*(2), 77–82. https://doi.org/10.23838/pfm.2020.00170.

67. Guo, Y., Zhao, W., Li, S., Zhang, Y., & Lu, Y. (2020). Automatic segmentation of the pectoral muscle based on boundary identification and shape prediction. *Physics in Medicine and Biology*, *65*(4). https://doi.org/10.1088/1361-6560/ab652b.

68. Maitra, i. k., Nag, s., & Bandyopadhyay, s. k. (2013). Mammographic density estimation and classification using segmentation and progressive elimination method. *International Journal of Image and Graphics*, *13*(03), 1350013. https://doi.org/10.1142/s0219467813500137

69. Vikhe, P. S., & Thool, V. R. (2016). Intensity Based Automatic Boundary Identification of Pectoral Muscle in Mammograms. In *Procedia Computer Science* (Vol. 79, pp. 262–269). Elsevier B.V. https://doi.org/10.1016/j.procs.2016.03.034.

70. Taifi, K., Ahdid, R., Fakir, M., Elbalaoui, A., Safi, S., & Taifi, N. (2018). Automatic breast pectoral muscle segmentation on digital mammograms using morphological watersheds. In Proceedings - 2017 14th International Conference on Computer Graphics, Imaging and Visualization, CGiV 2017 (pp. 126–131). Institute of Electrical and Electronics Engineers Inc. https://doi.org/10.1109/CGiV.2017.24

71. Shen, R., Yan, K., Xiao, F., Chang, J., Jiang, C., & Zhou, K. (2018). Automatic Pectoral Muscle Region Segmentation in Mammograms Using Genetic Algorithm and Morphological Selection. Journal of Digital Imaging, 31(5), 680–691. https://doi.org/10.1007/s10278-018-0068-9

72. Wang K, Khan N, Chan A, Dunne J, Highnam R. Deep Learning for Breast Region and Pectoral Muscle Segmentation in Digital Mammography. Lect Notes Comput Sci (Including Subser Lect Notes Artif Intell Lect Notes Bioinformatics) 2019; 11854 LNCS: 78–91. https://doi.org/10.1007/978-3-030-34879-3_7.

73. Sapate, S., & Talbar, S. (2016). An overview of pectoral muscle extraction algorithms applied to digital mammograms. In *Studies in Computational Intelligence* (Vol. 651, pp. 19–54). Springer Verlag. https://doi.org/10.1007/978-3-319-33793-7_2

74. Deng, J., Ma, Y., Li, D. ao, Zhao, J., Liu, Y., & Zhang, H. (2020). Classification of breast density categories based on SE-Attention neural networks. *Computer Methods and Programs in Biomedicine*, *193*. https://doi.org/10.1016/j.cmpb.2020.105489.

75. Zhang, Y., Brady, M., & Smith, S. (2001). Segmentation of brain MR images through a hidden Markov random field model and the expectation-maximization

algorithm. *IEEE Transactions on Medical Imaging*, *20*(1), 45–57. https://doi.org/10.1109/42.906424.

76. Sivaramakrishna, R., Obuchowski, N. A., Chilcote, W. A., & Powell, K. A. (2001). Automatic segmentation of mammographic density. *Academic Radiology*, *8*(3), 250–256. https://doi.org/10.1016/S1076-6332(03)80534-2.

77. Ferrari, R. J., Rangayyan, R. M., Borges, R. A., & Frère, A. F. (2004). Segmentation of the fibro-glandular disc in mammograms using Gaussian mixture modelling. *Medical and Biological Engineering and Computing*, *42*(3), 378–387. https://doi.org/10.1007/BF02344714.

78. Torrent, A., Bardera, A., Oliver, A., Freixenet, J., Boada, I., Feixes, M., … Martí, J. (2008). Breast density segmentation: A comparison of clustering and region based techniques. In *Lecture Notes in Computer Science (including subseries Lecture Notes in Artificial Intelligence and Lecture Notes in Bioinformatics)* (Vol. 5116 LNCS, pp. 9–16). https://doi.org/10.1007/978-3-540-70538-3_2

79. Saidin, N., Ngah, U. K., Sakim, H. A. M., Siong, D. N., & Hoe, M. K. (2009). Density based breast segmentation for mammograms using graph cut techniques. In *IEEE Region 10 Annual International Conference, Proceedings/TENCON*. https://doi.org/10.1109/TENCON.2009.5396042.

80. Saidin, N., Ngah, U. K., Sakim, H. A. M., Siong, D. N., Hoe, M. K., & Shuaib, I. L. (2010). Density based breast segmentation for mammograms using graph cut and seed based region growing techniques. In *2nd International Conference on Computer Research and Development, ICCRD 2010* (pp. 246–250). https://doi.org/10.1109/ICCRD.2010.87

81. Keller, B. M., Nathan, D. L., Wang, Y., Zheng, Y., Gee, J. C., Conant, E. F., & Kontos, D. (2012). Estimation of breast percent density in raw and processed full field digital mammography images via adaptive fuzzy c-means clustering and support vector machine segmentation. *Medical Physics*, *39*(8), 4903–4917. https://doi.org/10.1118/1.4736530.

82. He, W., Harvey, S., Juette, A., Denton, E. R. E., & Zwiggelaar, R. (2016). Mammographic segmentation and density classification: A fractal inspired approach.

In *Lecture Notes in Computer Science (including subseries Lecture Notes in Artificial Intelligence and Lecture Notes in Bioinformatics)* (Vol. 9699, pp. 359–366). Springer Verlag. https://doi.org/10.1007/978-3-319-41546-8_45

83. Surajudeen, A., & Reyer, Z. (2017). Breast Density Segmentation based on Fusion of Super Pixels and Watershed Transform. *International Journal of Computer Applications*, *161*(12), 1–7. https://doi.org/10.5120/ijca2017913208.

84. Kamil, M. Y., & Salih, A. M. (2019). Mammography images segmentation via Fuzzy C-mean and K-mean. *International Journal of Intelligent Engineering and Systems*, *12*(1), 22–29. https://doi.org/10.22266/IJIES2019.0228.03.

85. Huang, G., Liu, Z., Van Der Maaten, L., & Weinberger, K. Q. (2017). Densely connected convolutional networks. In *Proceedings - 30th IEEE Conference on Computer Vision and Pattern Recognition, CVPR 2017* (Vol. 2017-January, pp. 2261–2269). Institute of Electrical and Electronics Engineers Inc. https://doi.org/10.1109/CVPR.2017.243.

86. Ciritsis, A., Rossi, C., De Martini, I. V., Eberhard, M., Marcon, M., Becker, A. S., Boss, A. (2019). Determination of mammographic breast density using a deep convolutional neural network. *British Journal of Radiology*, *92*(1093). https://doi.org/10.1259/bjr.20180691.

87. Wu, N., Geras, K. J., Shen, Y., Su, J., Kim, S. G., Kim, E., … Cho, K. (2018). Breast density classification with deep convolutional neural networks. In *ICASSP, IEEE International Conference on Acoustics, Speech and Signal Processing - Proceedings* (Vol. 2018-April, pp. 6682–6686). Institute of Electrical and Electronics Engineers Inc. https://doi.org/10.1109/ICASSP.2018.8462671.

88. Lizzi, F., Laruina, F., Oliva, P., Retico, A., & Fantacci, M. E. (2019). Residual convolutional neural networks to automatically extract significant breast density features. In *Communications in Computer and Information Science* (Vol. 1089, pp. 28–35). Springer Verlag. https://doi.org/10.1007/978-3-030-29930-9_3.

89. Mohamed, A. A., Berg, W. A., Peng, H., Luo, Y., Jankowitz, R. C., & Wu, S. (2018). A deep learning method for classifying mammographic breast density categories. *Medical Physics*, *45*(1), 314–321. https://doi.org/10.1002/mp.12683.

90. Shi, P., Wu, C., Zhong, J., & Wang, H. (2019). Deep learning from small dataset for bi-rads density classification of mammography images. In *Proceedings - 10th International Conference on Information Technology in Medicine and Education, ITME 2019* (pp. 102–109). Institute of Electrical and Electronics Engineers Inc. https://doi.org/10.1109/ITME.2019.00034.

91. Bengio Y. Learning deep architectures for AI. Found Trends Mach Learn 2009; 2:1–27. https://doi.org/10.1561/2200000006.

92. Kaiser, N., Fieselmann, A., Ritschl, L., Kappler, S., Ravikumar, N., Vesal, S., & Maier, A. (2019). Mammographic breast density classification using a deep neural network: assessment on the basis of inter-observer variability (p. 23). SPIE-Intl Soc Optical Eng. https://doi.org/10.1117/12.2513420.

93. Bovis, K. (2002). Classification of mammographic breast density using a combined classifier paradigm. *Medical Image Understanding and Analysis*, (c), 1–4. Retrieved from http://130.203.133.150/viewdoc/download?doi=10.1.1.19.1806&rep=rep1&type=pd.

94. Kallenberg, M., Petersen, K., Nielsen, M., Ng, A. Y., Diao, P., Igel, C., Lillholm, M. (2016). Unsupervised Deep Learning Applied to Breast Density Segmentation and Mammographic Risk Scoring. *IEEE Transactions on Medical Imaging*, *35*(5), 1322–1331. https://doi.org/10.1109/TMI.2016.2532122.

95. Gastounioti, A., Oustimov, A., Hsieh, M. K., Pantalone, L., Conant, E. F., &Kontos, D. (2018). Using Convolutional Neural Networks for Enhanced Capture of Breast Parenchymal Complexity Patterns Associated with Breast Cancer Risk. *Academic Radiology*, *25*(8), 977–984. https://doi.org/10.1016/j.acra.2017.12.025.

96. Yasar, H., Kutbay, U., &Hardalac, F. (2018). A new combined system using ANN and complex wavelet transform for tissue density classification in mammography images. In *2018 4th International Conference on Computer and Technology Applications, ICCTA 2018* (pp. 179–183). Institute of Electrical and Electronics Engineers Inc. https://doi.org/10.1109/CATA.2018.8398679.

97. Mohamed, A. A., Berg, W. A., Peng, H., Luo, Y., Jankowitz, R. C., & Wu, S. (2018). A deep learning method for classifying mammographic breast density categories. *Medical Physics*, *45*(1), 314–321. https://doi.org/10.1002/mp.12683.

98. Lee, J., & Nishikawa, R. M. (2018). Automated mammographic breast density estimation using a fully convolutional network: *Medical Physics*, *45*(3), 1178–1190. https://doi.org/10.1002/mp.12763.

99. Ciritsis, A., Rossi, C., De Martini, I. V., Eberhard, M., Marcon, M., Becker, A. S.Boss, A. (2019). Determination of mammographic breast density using a deep convolutional neural network. *British Journal of Radiology*, *92*(1093). https://doi.org/10.1259/bjr.20180691.

100. Yi, P. H., Lin, A., Wei, J., Yu, A. C., Sair, H. I., Hui, F. K., … Harvey, S. C. (2019). Deep-Learning-Based Semantic Labeling for 2D Mammography and Comparison of Complexity for Machine Learning Tasks. *Journal of Digital Imaging*. https://doi.org/10.1007/s10278-019-00244-w.

101. Hinton, B., Ma, L., Mahmoudzadeh, A. P., Malkov, S., Fan, B., Greenwood, H.,Shepherd, J. (2019). Deep learning networks find unique mammographic differences in previous negative mammograms between interval and screen-detected cancers: A case-case study. *Cancer Imaging*, *19*(1). https://doi.org/10.1186/s40644-019-0227-3.

102. Ha, R., Chang, P., Karcich, J., Mutasa, S., Pascual Van Sant, E., Liu, M. Z., &Jambawalikar, S. (2019). Convolutional Neural Network Based Breast Cancer Risk Stratification Using a Mammographic Dataset. *Academic Radiology*, *26*(4), 544–549. https://doi.org/10.1016/j.acra.2018.06.020.

103. Lizzi, F., Atzori, S., Aringhieri, G., Bosco, P., Marini, C., Retico, A., Fantacci, M. E. (2019). Residual convolutional neural networks for breast density classification. In *BIOINFORMATICS 2019 - 10th International Conference on Bioinformatics Models, Methods and Algorithms, Proceedings; Part of 12th International Joint Conference on Biomedical Engineering Systems and Technologies, BIOSTEC 2019* (pp. 258–263).

104. Maitra, I. K., Nag, S., &Bandyopadhyay. K. (2013). Mammographic density estimation and classification using segmentation and progressive elimination method. *International Journal of Image and Graphics*, *13*(03), 1350013. https://doi.org/10.1142/s0219467813500137.

105. Devi, S. S., & Vidivelli, S. (2018). Classification of breast tissue density in digital mammograms. In *Proceedings of 2017 International Conference on Innovations in Information, Embedded and Communication Systems, ICIIECS 2017* (Vol. 2018-January, pp. 1–7). Institute of Electrical and Electronics Engineers Inc. https://doi.org/10.1109/ICIIECS.2017.8276139.

106. Hartman, K., Highnam, R., Warren, R., & Jackson, V. (2008). Volumetric assessment of breast tissue composition from FFDM images. In *Lecture Notes in Computer Science (including subseries Lecture Notes in Artificial Intelligence and Lecture Notes in Bioinformatics)* (Vol. 5116 LNCS, pp. 33–39). https://doi.org/10.1007/978-3-540-70538-3_5

107. Lee-Han, H., Cooke, G., & Boyd, N. F. (1995). Quantitative evaluation of mammographic densities. *European Journal of Cancer Prevention*, *4*(4), 285–292. https://doi.org/10.1097/00008469-199508000-00003

108. Chan, H. P., & Helvie, M. A. (2019, January 1). Deep learning for mammographic breast density assessment and beyond. *Radiology*. Radiological Society of North America Inc. https://doi.org/10.1148/radiol.2018182116

109. [Dataset] M. Heath, K. Bowyer, D. Kopans RM and PKJ. The Digital Database for Screening Mammography. Fifth Int Work Digit Mammography, MJ Yaffe, Ed, Med Phys Publ 2001 2001:212–8.

110. Pawar, S. D., Sharma, K. K., Sapate, S. G., & Yadav, G. Y. (2021). Segmentation of pectoral muscle from digital mammograms with depth-first search algorithm towards breast density classification. *Biocybernetics and Biomedical Engineering*, *41*(3), 1224–1241. https://doi.org/10.1016/j.bbe.2021.08.005.

111. Maitra, I. K., Nag, S., & Bandyopadhyay, S. K. (2012). Technique for preprocessing of digital mammogram. *Computer Methods and Programs in Biomedicine*, *107*(2), 175–188. https://doi.org/10.1016/j.cmpb.2011.05.007.

112. Bt Ahmad, S. A., Taib, M. N., Khalid, N. E. A., & Taib, H. (2012). Analysis of image quality based on dentists' perception cognitive analysis and statistical measurements of intra-oral dental radiographs. In *2012 International Conference on Biomedical Engineering, ICoBE 2012* (pp. 379–384). https://doi.org/10.1109/ICoBE.2012.6179042.

113. Zeng, M., Li, Y., Meng, Q., Yang, T., & Liu, J. (2012). Improving histogram-based image contrast enhancement using gray-level information histogram with application to X-ray images. *Optik*, *123*(6), 511–520. https://doi.org/10.1016/j.ijleo.2011.05.017.

114. Öktem, H., Egiazarian, K., Niittylahti, J., & Lemmetti, J. (2003). An approach to adaptive enhancement of diagnostic X-ray images. *Eurasip Journal on Applied Signal Processing*, *2003*(5), 430–436. https://doi.org/10.1155/S1110865703211069.

115. Deng, G. (2011). A generalized unsharp masking algorithm. *IEEE Transactions on Image Processing*, *20*(5), 1249–1261. https://doi.org/10.1109/TIP.2010.2092441.

116. Chang, D. C., & Wu, W. R. (1998). Image contrast enhancement based on a histogram transformation of local standard deviation. *IEEE Transactions on Medical Imaging*, *17*(4), 518–531. https://doi.org/10.1109/42.730397.

117. Huang, S. C., Cheng, F. C., & Chiu, Y. S. (2013). Efficient contrast enhancement using adaptive gamma correction with weighting distribution. *IEEE Transactions on Image Processing*, *22*(3), 1032–1041. https://doi.org/10.1109/TIP.2012.2226047.

118. Slavković-Ilić, M., Gavrovska, A., Milivojević, M., Reljin, I., & Reljin, B. (2016). Breast region segmentation and pectoral muscle removal in mammograms. *Telfor Journal*, *8*(1), 50–55. https://doi.org/10.5937/telfor1601050S

119. Tarjan, R. (1972). Depth-first search and linear graph algorithms Connected Compon... *SIAM Journal on Computing*, *1*(2), 146–160.

120. Birdwell, R. L. (2009). Combined Screening With Ultrasound and Mammography vs Mammography Alone in Women at Elevated Risk of Breast Cancer. *Yearbook of Diagnostic Radiology*, *2009*, 43–45. https://doi.org/10.1016/s0098-1672(08)79266-x.

121. Melnikow MD MPH, J., Fenton MD MPH, J. J., Whitlock MD MPH, E. P., Miglioretti PhD, D. L., Weyrich MPH, M. S., Thompson MPH, J. H., & Shah, K.

(2016). Supplemental Screening for Breast Cancer in Women with Dense Breasts: A Systematic Review for the U.S. Preventive Services Task Force. *Annals of Internal Medicine*, *164*(4), 268.

122. Lee, J., & Nishikawa, R. M. (2018). Automated mammographic breast density estimation using a fully convolutional network: *Medical Physics*, *45*(3), 1178–1190. https://doi.org/10.1002/mp.12763.

123. Devi, S. S., & Vidivelli, S. (2018). Classification of breast tissue density in digital mammograms. In *Proceedings of 2017 International Conference on Innovations in Information, Embedded and Communication Systems, ICIIECS 2017* (Vol. 2018-January, pp. 1–7). Institute of Electrical and Electronics Engineers Inc. https://doi.org/10.1109/ICIIECS.2017.8276139.

124. Srivastava, R. K., Greff, K., & Schmidhuber, J. (2015). Training very deep networks. In *Advances in Neural Information Processing Systems* (Vol. 2015-January, pp. 2377–2385). Neural information processing systems foundation.

125. Huang, G., Liu, Z., Van Der Maaten, L., & Weinberger, K. Q. (2017). Densely connected convolutional networks. In *Proceedings - 30th IEEE Conference on Computer Vision and Pattern Recognition, CVPR 2017* (Vol. 2017-January, pp. 2261–2269). Institute of Electrical and Electronics Engineers Inc. https://doi.org/10.1109/CVPR.2017.243.

126. Bt Ahmad, S. A., Taib, M. N., Khalid, N. E. A., & Taib, H. (2012). Analysis of image quality based on dentists' perception cognitive analysis and statistical measurements of intra-oral dental radiographs. In *2012 International Conference on Biomedical Engineering, ICoBE 2012* (pp. 379–384). https://doi.org/10.1109/ICoBE.2012.6179042.

127. Chang, D. C., & Wu, W. R. (1998). Image contrast enhancement based on a histogram transformation of local standard deviation. *IEEE Transactions on Medical Imaging*, *17*(4), 518–531. https://doi.org/10.1109/42.730397

128. Maitra, I. K., Nag, S., & Bandyopadhyay, S. K. (2012). Technique for preprocessing of digital mammogram. *Computer Methods and Programs in Biomedicine*, *107*(2), 175–188. https://doi.org/10.1016/j.cmpb.2011.05.007.

129. Mustra, M., Bozek, J., & Grgic, M. (2009). Breast border extraction and pectoral muscle detection using wavelet decomposition. In *IEEE EUROCON 2009, EUROCON 2009* (pp. 1426–1433). https://doi.org/10.1109/EURCON.2009.5167827.

130. Huang, S. C., Cheng, F. C., & Chiu, Y. S. (2013). Efficient contrast enhancement using adaptive gamma correction with weighting distribution. *IEEE Transactions on Image Processing*, *22*(3), 1032–1041. https://doi.org/10.1109/TIP.2012.2226047.

131. Raba, D., Oliver, A., Martí, J., Peracaula, M., & Espunya, J. (2005). Breast segmentation with pectoral muscle suppression on digital mammograms. In *Lecture Notes in Computer Science* (Vol. 3523, pp. 471–478). Springer Verlag. https://doi.org/10.1007/11492542_58

132. Bora, V. B., Kothari, A. G., & Keskar, A. G. (2016). Robust Automatic Pectoral Muscle Segmentation from Mammograms Using Texture Gradient and Euclidean Distance Regression. *Journal of Digital Imaging*, *29*(1), 115–125. https://doi.org/10.1007/s10278-015-9813-5

133. Kumar, I., H.S., B., Virmani, J., & Thakur, S. (2017). A classification framework for prediction of breast density using an ensemble of neural network classifiers. *Biocybernetics and Biomedical Engineering*, *37*(1), 217–228. https://doi.org/10.1016/j.bbe.2017.01.001.

134. Wang, K., Khan, N., Chan, A., Dunne, J., & Highnam, R. (2019). Deep Learning for Breast Region and Pectoral Muscle Segmentation in Digital Mammography. In *Lecture Notes in Computer Science (including subseries Lecture Notes in Artificial Intelligence and Lecture Notes in Bioinformatics)* (Vol. 11854 LNCS, pp. 78–91). Springer. https://doi.org/10.1007/978-3-030-34879-3_7.

135. Ali, M. J., Raza, B., Shahid, A. R., Mahmood, F., Yousuf, M. A., Dar, A. H., & Iqbal, U. (2020). Enhancing breast pectoral muscle segmentation performance by using skip connections in fully convolutional network. *International Journal of Imaging Systems and Technology*, *30*(4), 1108–1118. https://doi.org/10.1002/ima.22410.

136. Kim, Y. J., Yoo, E. Y., & Kim, K. G. (2021). Deep learning based pectoral muscle segmentation on Mammographic Image Analysis Society (MIAS) mammograms. *Precision and Future Medicine*, *5*(2), 77–82. https://doi.org/10.23838/pfm.2020.00170.

137. Rampun, A., López-Linares, K., Morrow, P. J., Scotney, B. W., Wang, H., Ocaña, I. G., … Macía, I. (2019). Breast pectoral muscle segmentation in mammograms using a modified holistically-nested edge detection network. *Medical Image Analysis*, *57*, 1–17. https://doi.org/10.1016/j.media.2019.06.007.

138. Deng, J., Ma, Y., Li, D. ao, Zhao, J., Liu, Y., & Zhang, H. (2020). Classification of breast density categories based on SE-Attention neural networks. *Computer Methods and Programs in Biomedicine*, *193*. https://doi.org/10.1016/j.cmpb.2020.105489.

139. Wang H, Li JB, Wu L, Gao H. Mammography visual enhancement in CAD-based breast cancer diagnosis. *Clinical Imaging* 2013; 37:273–82. https://doi.org/10.1016/j.clinimag.2012.04.018.

140. LEE, Z. Y., GOH, Y. L. E., & LAI, C. (2021). Classification of mammographic breast density and its correlation with BI-RADS in elder women using machine learning approach. *Journal of Medical Imaging and Radiation Sciences*.

141. Mohamed, A. A., Berg, W. A., Peng, H., Luo, Y., Jankowitz, R. C., & Wu, S. (2018). A deep learning method for classifying mammographic breast density categories. *Medical Physics*, *45*(1), 314–321.

142. Bovis, K. (2002). Classification of mammographic breast density using a combined classifier paradigm. *Medical Image Understanding and Analysis*.